# Remotely sensing motion: The use of multiple bio-logging technologies to detect fine-scale, at-sea behaviour of breeding seabirds in a variable Southern Ocean environment

Stefan Schoombie

Thesis presented for the degree Doctor of Philosophy

FitzPatrick Institute of African Ornithology

DST/NRF Centre of Excellence

Department of Biological Sciences, Faculty of Science

University of Cape Town

March 2021

Supervised by Professor Peter G. Ryan

Co-supervised by Professor Rory P. Wilson

## Declaration

Work submitted in this thesis is original research performed through the FitzPatrick Institute at the University of Cape Town. I declare that I conducted the research myself, under normal input from supervisors, and have fully acknowledged where I received assistance with field work. The presented work has not been submitted to another institution in any form to obtain a degree.

Signed by candidate

Stefan Schoombie

Cape Town, March 2021

An adult Wandering Albatross equipped with multiple bio-loggers taking off on a foraging trip from Marion Island

# Table of contents

# Abstract

The at-sea behaviour of seabirds, such as albatrosses and petrels (order Procellariiformes), is difficult to study because they spend most of their time on the ocean and have extremely large ranges. In the early 2000s, behavioural studies of seabirds were dominated by diving patterns of diving birds or spatial studies from satellite telemetry. Recent advances in bio-logging technologies have opened up new avenues for studying the at-sea behaviour of far-ranging seabirds in their natural environment. Bio-logging devices are now small enough to be attached to flying seabirds where multiple sensors record data at infrasecond sampling rates. These data can be used to infer, *inter alia*, body posture, activity (e.g. flapping, take-off, landing, etc.), magnetic heading and spatial distribution at a resolution that was not previously possible. Bio-logging devices are battery powered and a tradeoff exists between the length of deployments and sampling frequencies, however not a lot of study has been done on what the effect of coarse sampling rates are on data quality. Together with the masses of data that are generated by bio-logging devices, analytical tools have also become available to extract useful metrics from the data.

This thesis utilized some of the latest bio-logging technology to study the at-sea behaviour of several procellariiforms, breeding on Marion, Gough and Nightingale Islands, from fine-scale data. After describing the loggers used and the methods of deployment in **Chapter 2**, I assess the effect that sampling rates have on metrics derived from GPS loggers in **Chapter 3**. This was done by sub-sampling GPS tracks recorded at 1-s sampling intervals, showing the effect that different sampling intervals have on metrics, including the total distance travelled and behavioural states derived from path length and turning angles. I show that for larger sampling intervals, the total distance travelled will be underestimated at varying degrees depending on flight sinuosity. By varying sampling rates when estimating behavioural states, I show that moderate (10–30 min) sampling intervals may produce better results. I explore the limitations of low-cost GPS loggers for fine-scale analyses and conclude that specialized loggers are most likely required when sampling at intervals < 1 s. In **Chapter 4** I use specialized loggers in the form of tri-axial magnetometer, and video loggers and describe two novel methods to extract roll angles of albatrosses during dynamic soaring flight. Animal body angles are normally extracted by using tri-axial accelerometer data, but their dynamic soaring flight mode inhibits the use of these methods. I show how magnetometer data are independent of dynamic movement and can be used to estimate roll angles of flying seabirds. This method is validated from bird-borne video footage where the horizon is used as a proxy for the bird's roll angle and I describe a method to automatically extract such angles using computer vision techniques. These new methods are then applied to data collected from Wandering Albatrosses *Diomedea exulans* in **Chapter 5**, showing how the birds vary their

roll angle in response to changing winds. Additionally, flapping flight was identified from patterns in the vertical axis (heave) of a tri-axial accelerometer and I show how Wandering Albatrosses may be flapping more than expected. By coupling flapping and roll angles I show that flapping, on occasion, occur at the upper turn of the dynamic soaring cycle, a period previous thought devoid of flaps. These results also suggest possible sexual differences, where males seem to flap more often than females and limit their take-offs to favourable wind conditions. Lastly, in **Chapter 6** I use the same methods as in the previous two chapters to compare the fine-scale flight of six Procellariiformes species breeding on Marion, Gough and Nightingale Islands. I show how these species have varied flight patterns where they respond differently to wind patterns, most likely driving their distribution and eventual foraging areas. As expected, smaller species seem to be more manoeuvrable allowing them to rapidly roll at extreme angles in strong winds while tolerating light winds by increasing the amount of time spent flapping. Breeding location also played a role as birds from the Tristan da Cunha archipelago flapped more often and flew in lighter winds than Marion Island birds.

In summary, **Chapter 7** discusses how, using a multisensor approach, bio-logging technology can be effectively used to study the fine-scale behaviour of flying seabirds. Each of the loggers have their own limitations and it is important to take these into account when analyzing the data. I describe two new methods for extracting roll angles from dynamic soaring seabirds and show how individuals from several species vary roll angle and flapping flight in response to changing winds. This thesis highlights the varying behavioural strategies that flying seabirds use in the Southern Ocean, showing that individual species and populations may respond differently to changing environmental conditions.

# Acknowledgements

Overwintering on Marion Island changed my life and I am extremely grateful for the opportunity and the privilege to have been immersed in the world of the albatross on and off for the past eight years. I thank God for the strength and perseverance to see this project through to the end. In particular I thank my wife, Janine Schoombie, for standing by me (often in the wind and rain), for help in the field, and for indulging my crazy thoughts before the morning coffee has kicked in. Thanks for embarking on these adventures with me, leaving the luxury of stability behind.

I thank Peter Ryan for taking me on as a student, helping me combine my passion for technology and nature in a constructive manner. Thank you for introducing me to Marion Island and all the fun (and tough) days in the field, not to mention the many hours of hacky-sack on the back of the Agulhas II. I am grateful for all the support and good friends I made through the FitzPatrick Institute.

Thanks to Rory Wilson for co-supervising parts of this thesis, for your endless enthusiasm of bio-loggers and for the privilege of visiting the SLAM lab at Swansea University. Here I entered the world of big data analysis by visualizing data on their big screen and I would like to thank everyone I interacted with at the lab for sharing your thoughts and experiences. In particular I would like to thank Emily Shepard, Hannah Williams and Mark Holton for their ideas on albatross flight and technical help with the loggers and software. I thank Yan Ropert-Coudert for supplying GPS loggers and for his constructive comments during the early phases of my thesis.

Out in the field, I would like to thank everyone who helped with deployments of the loggers on respective sub-Antarctic Islands throughout the study and my fellow M76 teammates. These were difficult data to collect and I am grateful for the many hours spent in harsh weather, or the willingness of helpers to quickly jump up from the breakfast table to retrieve a device. In particular, Christiaan Brink, Chris Jones, Dannielle Keys, Janine Schoombie, Kim Stevens, Makabongwe Sigqala, Melissa Schulze, Michelle Risi, Stephan Keys for deployments on Marion Island and Ben Dilley, Chris Jones, Delia Davies, Fabrice le Bouard, Jaimie Cleeland and Michelle Risi for deployments on Gough and/or Nightingale Islands. I thank Pierre Pistorius for the use of field equipment and for willingness to volunteer field assistants to help with deployments, and Maëlle Connan for allowing me time to work on my thesis while on Marion Island. Richard Phillips assisted with equipment used for deployments on Gough Island for which I am thankful. Otto Whitehead provided me with videos of albatrosses flying at sea and I am grateful for his enthusiasm and interest in my work.

On the technical side, my father, Kobus Schoombie introduced me to the world of electronics and mathematics, and I am ever grateful for his advice and support throughout my studies. Also, my close friend, Japie van der Westhuizen, who was involved in the early development of the bird-borne cameras that was pivotal to this research. Stefan Lotz helped me with mathematical filters used on the accelerometer data.

Logistic support was provided by the Department of Environment, Forestry and Fisheries while staying on Marion Island and funding was provided by the FitzPatrick Institute Centre of Excellence and the South African National Antarctic Programme, through the National Research Foundation. Behind the scenes Hilary Buchanan, Anthea Links, Gonzalo Aguilar and Janine Dunlop provided invaluable administrative support.

Returning from Marion Island mid-COVID in 2020 was challenging and I am particularly grateful for the support received from my parents, Dalene and Kobus Schoombie and in-laws, Karen and Neels Versteegh during this time, providing me with space to see out the last months of work. I thank all my friends and family for their continued support and the willingness to listen to endless Marion stories.

I thank the reviewers for their comprehensive and constructive feedback on the thesis, ultimately improving the quality of my work.

# Chapter 1: General introduction

The constraints imposed by body size have long been studied in animals under the general term of allometry (Gould 1966), which underpins many of the general relationships in ecology (Dial et al. 2008). Birds are particularly useful to study these relationships, as their morphologies are easy to predict with allometric scaling (Dial et al. 2008) and they show strong allometric scaling in a host of morphological and physiological parameters (e.g. wing area, heart rate, eye size etc.; Warham 1977; Brooke et al. 1999; Shaffer et al. 2001b). Where general trends are well known, exceptions to these trends are particularly interesting to study and although flapping flight scales with body size (Pennycuick 1982), the distances travelled by soaring birds seem to be largely independent of body size (Spear and Ainley 1997; Watanabe 2016). Flying animals are also interesting to study as they appear to have similar efficiencies regardless of body size (Bale et al. 2014). Animals may have functional limitations that scale with body size, but can compensate for these by behavioural adaptations (Dial et al. 2008). Scaling effects of behaviour seem to be very complex and although allometric relationships are well studied, the allometry of behaviour and movement are not (Dial et al. 2008; Hebblewhite and Haydon 2010).

## Seabirds as central place foragers

While breeding, seabirds are central place foragers that have to find food within commuting range of their nests. The albatrosses and petrels (Procellariiformes) are among the most extreme central place foragers as they can travel at great speeds and remain away from their nests for up to 3–4 weeks while incubating eggs. This allows them to cover immense distances between incubation shifts (Phillips et al. 2008; Weimerskirch et al. 2014), and some species undertake long foraging trips lasing 2–4 weeks even while provisioning chicks (Weimerskirch 1998; Einoder et al. 2011; Cleeland et al. 2014; Schoombie et al. 2018). These long foraging trips during chick-rearing are thought to be self-provisioning trips, when parents recover body condition, and are usually alternated with several shorter chick-provisioning trips (Weimerskirch 1998). Coupled with their fast and fuel-efficient flight, these seabirds can cover vast distances during each trip, and thus exploit food resources thousands of kilometres from their breeding islands (Weimerskirch et al. 2014). These incredible flying feats are achieved by albatrosses and petrels largely independent of body sizes (Figure 1.1 and Supplementary Table S1.1). Seabird distribution and foraging behaviour may not be related to their body size, but rather to variations in foraging strategies (Weimerskirch et al. 2005). Studying their behaviour (and individual variation) together with environmental variables is crucial for conservation of biodiversity in the Southern

Ocean (Cooke 2008), where they function as top-predators and potential indicators of ecosystem health (Boyd et al. 2006).

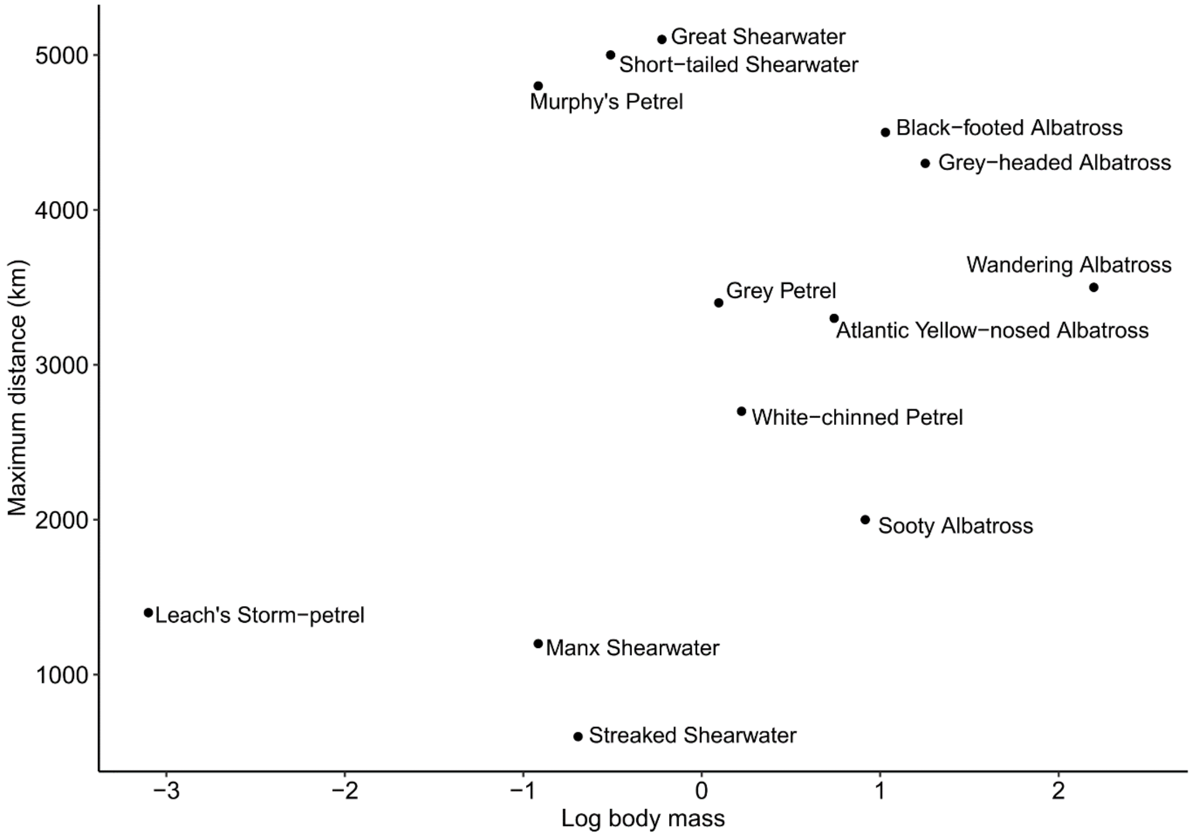

**Figure 1.1:** Maximum distance travelled from nesting grounds by breeding albatrosses and petrels in relation to body size. Supplementary Table S1.1 shows the data sources of the values.

## Seabird flight

Seabirds can be grouped by the proportion of time they spend performing different modes of flight: soaring, gliding, flapping, or a combination of gliding and flapping (Spear and Ainley 1997; Ainley et al. 2015). Soaring seabirds are sometimes split into dynamic and thermal soaring groups (Watanabe 2016), with thermal soaring largely restricted to the tropical Fregatidae (Pennycuick 1983; Weimerskirch et al. 2016). In oceanic areas with high wind speeds, birds can take advantage of the winds (and wind-induced waves) to soar at low altitudes at high speeds (Pennycuick 1982; Sachs 2005; Richardson 2011; Weimerskirch et al. 2012). Thus, when referring to procellariiforms in the Southern Ocean, I am assuming soaring birds to be gliding or dynamic soaring. Variations in flight type among procellariiforms are mainly attributed to their wing shape and wing loading, which influence their gliding and flapping speeds (Pennycuick 1987). Larger species generally glide more, and flap less than smaller species that flap more with intermittent gliding (Pennycuick 1982).

Wing loading (body weight divided by wing area) of procellariiforms decrease with decreasing body weight (Suryan et al. 2008), with the exception of diving petrels, which are highly adapted to propel themselves underwater by flapping (Warham 1977). Birds with high wing loading are better adapted for soaring flight, but often require flapping during take-off (Sato et al. 2009; Williams et al. 2020a). Flapping typically is the most energy expensive period of a soaring bird's flight (Weimerskirch et al. 2000; Sakamoto et al. 2013). As a result, albatrosses attempt to maximise their flight in periods of favourable winds (Clay et al. 2020), when they can achieve energy efficient flight in the form of dynamic soaring (Pennycuick 1982) which extracts energy from the wind gradient above the surface of the ocean through a series of upwind and downwind turns (Pennycuick 1982; Sachs 2005; Richardson 2011; Sachs et al. 2012).

## Wind-driven behaviour

Animal behaviour is the response of the individual to its environment and thus it is crucial to consider environmental conditions when studying animal behaviour (Fritz et al. 2003; Shepard et al. 2008). Wind is one of the main drivers of pelagic seabird behaviour, and wind patterns significantly alter the behaviour of albatrosses and petrels (Wakefield et al. 2009; Weimerskirch et al. 2012; Safi et al. 2013). Albatrosses and most petrels use a dynamic soaring flight mode (Pennycuick 1982; Weimerskirch et al. 2000; Richardson 2011; Sachs et al. 2012) with heart rates during flight close to resting heart-rates, at least for the larger species (Weimerskirch et al. 2000; Shaffer et al. 2001b). However, taking-off is energy expensive for large albatrosses and they appear to take longer to recover from increased heart-rates after take-off (Weimerskirch et al. 2000; Sakamoto et al. 2013) than large terrestrial soaring *Gyps* vultures (Duriez et al. 2014). Albatrosses seemingly save energy by taking off in favourable wind conditions (Clay et al. 2020) avoiding light winds or strong tail winds (Kroeger et al. 2020).

Dynamic soaring seabirds may take advantage of favourable winds to decrease flying costs, but their ability to compensate for wind can influence their flight efficiency (Tarroux et al. 2016). Seabirds seemingly have knowledge of the wind fields within their foraging ranges (Ventura et al. 2020) and can also use wind drift to their advantage by adjusting their heading so that their flight paths are directed straight to their nesting grounds (Goto et al. 2017; Yoda 2019). The winds experienced by dynamic soaring seabirds have the potential to shape their distribution (Frankish et al. 2020) and migratory routes (González-Solís et al. 2009). However, individual variation also occurs and birds may target specific foraging areas while flying in unfavourable winds (Dell'Ariccia et al. 2018; Frankish et al. 2020), especially when providing for offspring (Elliott et al. 2014; Frankish et al. 2020). Much of what we know about this fascinating behaviour has been learned in the last few decades through the development of bio-logging technologies.

## Bio-logging

Since the development of the first animal-borne data loggers in the 1960s, technological advances have revolutionized the way we study the behaviour of free-living animals (Kooyman 2004). Bio-logging refers to the use of animal borne loggers/transmitters to collect data on animal movement (Ropert-Coudert and Wilson 2005; Rutz and Hays 2009) and their surroundings (Boyd et al. 2004), which in turn can be used to study physiological or behavioural aspects of the animals (Ropert-Coudert and Wilson 2005; Cooke 2008). Some studies refer to the use of transmitting devices as “biotelemetry” (Kooyman 2004), however for simplicity, here “bio-logging” refers to both loggers and transmitters. Bio-logging enables researchers to study the behaviour of free-living animals, in their natural environment (Cooke et al. 2004; Cooke 2008), in the absence of human observers (Bograd et al. 2010). This is particularly useful where animals are difficult to access or when direct observation is impossible (Rutz and Hays 2009), such as far-ranging seabirds that spend most of their time away from land.

Most of the first bio-logging devices used to study animal behaviour were simple mechanical time-depth recorders, used to recording the diving behaviour of aquatic animals for at most one hour at a time (Kooyman 2004; Ropert-Coudert and Wilson 2005; Wilson and Vandenabeele 2012). These loggers were improved during the early 1980s by reducing the size and increasing the sampling time to more than 20 days, making it possible to obtain data from flying-diving seabirds (Naito 2004). With the introduction of microprocessors in the 1980s, the development of bio-logging devices changed considerably, as these devices were much smaller and able to log several variables at the same time (Kooyman 2004; Naito 2004; Wilson and Vandenabeele 2012). Together with better processing power, the development of solid-state electronic memory also improved bio-logging capabilities by allowing more data to be recorded on smaller devices at higher resolutions (Ropert-Coudert and Wilson 2005; Wilson and Vandenabeele 2012). Bio-logging devices also started to record data from animal’s environment, allowing researchers to study the environmental conditions where certain behaviours are observed (Ropert-Coudert and Wilson 2005).

Since the early 2000s, bio-logging devices have become increasingly complex, with the ability to record many different variables at the same time (Ropert-Coudert and Wilson 2005), and record at extremely high frequencies (> 300 times per second; Wilmers et al. 2015). A common combination in recent studies is that of GPS-accelerometer loggers, which can be used to derive energy expenditure or behaviour of an animal at known locations

(Wilmers et al. 2015). In addition to data loggers recording movement, visual observation is also possible for a range of seabirds through the use of animal-borne cameras (Marshall 1998; Rutz et al. 2007). This is perhaps the best way to study animal behaviour, but the method is limited by depth and duration when the subject is under water (Davis et al. 1999; Ropert-Coudert and Wilson 2005), and short battery life remains a problem for small animal-borne cameras (Thiebot et al. 2017). Video cameras are mostly used to calibrate other loggers such as accelerometers that are used to infer behaviours (Watanabe and Takahashi 2013; Pagano et al. 2017), although they also have revealed previously unobserved behaviours (Handley and Pistorius 2016) and animal interactions (Tremblay et al. 2014). Other bio-logging devices enable researchers to record parameters that cannot be observed visually, such as heart and breathing rates or skin humidity (Weimerskirch et al. 2000; Ropert-Coudert and Wilson 2005; Ponganis 2007).

In last two decades the use of accelerometers to infer animal behaviour (Shepard et al. 2008) has increased tremendously, allowing researchers to study behavioural patterns in unprecedented detail (Brown et al. 2013). Initially, accelerometers and animal-borne cameras were mostly used on diving animals, such as marine mammals or penguins, where device mass is less of an issue (Yoda et al. 1999, 2001; Cooke et al. 2004; Shepard et al. 2008). But more recently, accelerometers have been used to study the behaviour of a range of flying and flying-diving birds (Ropert-Coudert et al. 2004; Kato et al. 2006; Sato et al. 2008, 2009; Williams et al. 2015; Sherub et al. 2017; Leos-Barajas et al. 2017) down to species as small as Alpine Swifts *Tachymarptis melba* weighing ~100 g (Liechti et al. 2013). Some of the most recent advances in accelerometer technology include the transmission of data from Southern Elephant Seals *Mirounga leonina* through the Argos satellite system (Cox et al. 2018) or the use of real-time machine learning to record specific behaviours of Black-tailed Gulls *Larus crassirostris* (Korpela et al. 2020).

## Thesis aims, overview and outline

I aim to test the efficacy of several bio-logging technologies to study the fine-scale behaviour of free-ranging albatrosses and petrels in the Southern Ocean. I will discuss the effect of sampling rates on GPS-derived metrics and detail new methods to extract body angles from video loggers and inertial measurement units on dynamic soaring seabirds. Furthermore, I will test the idea that flight behaviour drives distribution ranges of soaring seabirds in the Southern Ocean and how this relates to changing winds.

In this thesis I use some of the latest in bio-logging technology, including inertial measurement units and bird-borne video cameras, combined with GPS tracking, to study the fine-scale at-sea behaviour of albatrosses and petrels across a range of body sizes. Remote-sensed wind estimates are used to show the fine-scale responses of these seabirds to local wind conditions, and how they take advantage of predictable wind fields to structure their foraging trips while breeding.

**Chapter 2** describes the various loggers used in this thesis, as well as the methods used to attach them to the study species.

In **Chapter 3**, I describe the effect of sampling rates on metrics and behavioural states inferred from low-cost GPS loggers by sub-sampling 1-s GPS tracks from a range of albatrosses and petrels. The sub-sampled tracks are compared to the original tracks to estimate the error associated with metrics commonly used in seabird tracking studies, at varying sampling intervals. GPS tracks are subjected to measurement error (fine-scale) and interpolation error (coarse-scale). I expect that:

1- Movement paths estimated from successive GPS locations will vary with sampling rates.
2- Behavioural states derived from path length and turning angles of successive location estimates will vary with sampling rates.

**Chapter 4** shows how a multisensor approach can be used to collect behavioural data from dynamic soaring seabirds at infrasecond rates and describes two novel methods of extracting roll angles from video and magnetometer data. Animal posture can be estimated from tri-axial accelerometer data with relative ease. However, dynamic soaring seabirds are subjected to increased centripetal acceleration during flight, which precludes the use of accelerometers when estimating posture during flight. I expect that:

1- A camera attached to a dynamic soaring seabird's back will allow estimates of roll angles relative to the horizon.
2- Because seabirds do not seem to pitch regularly during routine flight (i.e. not during prey encounter), tri-axial magnetometers may be suitable to estimate roll and yaw angles of dynamic soaring seabirds without additional postural data from accelerometers.

In **Chapter 5**, the methods developed in Chapter 4 are applied to Wandering Albatrosses breeding on Marion Island. Wandering Albatrosses are well studied, as their surface-nesting behaviour makes them easy to access and their large size makes them ideal candidates to carry multiple devices. Multiple bio-logging devices were deployed from 2016-2020 on Wandering Albatrosses incubating eggs or brooding small chicks. Data from these loggers were used to estimate fine-scale flight behaviour, which included the proportion of flapping flight and variations in roll angles within the dynamic soaring cycle. I hypothesize that:

1- Wandering Albatrosses will vary their roll angles in response to wind speed and direction.
2- Flapping rate of Wandering Albatrosses will decrease with increased wind speeds.
3- The behavioural responses to changing winds will be different between sexes of dimorphic Wandering Albatrosses.

**Chapter 6** uses the same approach as Chapter 5 to compare the fine-scale behavioural responses of a suite of albatrosses and petrels to varying winds by examining their flapping rates and roll angles. Despite having a wide range of body sizes, these species all have large ranges in the Southern Ocean. Although my sample sizes are small, I hypothesize that:

1- The fine-scale flight behaviour of all studied species will be affected by the wind.
2- The varying ability of species to adjust their fine-scale flight behaviour to changing winds may drive their distribution.

Finally, **Chapter 7** is a synthesis of the previous chapters discussing the broader context of the results, possible limitations of the technology used, and makes recommendations for future research.

The data chapters (Chapters 3–6) are written in the format of individual journal articles, leading to some repetition in text.

# Supplementary material

**Table S1.1:** An example of maximum foraging ranges of breeding albatrosses and petrels ranging from small to large body sizes. See Oppel et al. (2018) for a comprehensive list of seabird body sizes and ranges.

| **Species** | **Sample size (*n*)** | **Maximum range (km)** | **Mass (kg)** | **Reference** |
|---|---|---|---|---|
| Leach's Storm-petrel<br>*Oceanodroma leucorhoa* | 133 | 1400 | 0.045 | (Hedd et al. 2018) |
| Murphy's Petrel<br>*Pterodroma ultima* | 18 | 4800 | 0.4 | (Clay et al. 2019) |
| Manx Shearwater<br>*Puffinus puffinus* | 287 | 1200 | 0.4 | (Oppel et al. 2018) |
| Streaked Shearwater<br>*Calonectris leucomelas* | 21 | 600 | 0.5 | (Shiomi et al. 2012) |
| Short-tailed Shearwater<br>*Puffinus tenuirostris* | 27 | 5000 | 0.6 | (Cleeland et al. 2014) |
| Great Shearwater<br>*Ardenna gravis* | 20 | 5100 | 0.8 | (Schoombie et al. 2018) |
| Grey Petrel<br>*Procellaria cinerea* | 2 | 3400 | 1.1 | Present study |
| White-chinned Petrel<br>*Procellaria aequinoctialis* | 56 | 2700 | 1.25 | (Phillips et al. 2006; Rollinson et al. 2018; Frankish et al. 2020) |
| Atlantic Yellow-nosed Albatross<br>*Thalassarche chlororhynchos* | 11 | 3300 | 2.1 | Present study |
| Sooty Albatross<br>*Phoebetria fusca* | 70 | 2000 | 2.5 | (Schoombie et al. 2017) |
| Black-footed Albatross<br>*Phoebastria nigripes* | 20 | 4500 | 2.8 | (Fernández et al. 2001) |
| Grey-headed Albatross<br>*Thalassarche chrysostoma* | 98 | 4300 | 3.5 | (Oppel et al. 2018) |
| Wandering Albatross<br>*Diomedea exulans* | > 600 | 3500 | 9 | (Weimerskirch et al. 2014) |

# Chapter 2: Loggers and attachment methods

## Bio-loggers

In this chapter I describe the loggers used throughout the thesis, where each subsequent chapter lists the respective loggers used. Where devices were encased in plastic housings, the electronic units were removed and sealed in heat-shrink tubing or 3D-printed casings, for waterproofing and to reduce mass. These methods followed previous studies of logger deployment on Marion and Gough Islands (Nel et al. 2001; Schoombie et al. 2017, 2018; Reisinger et al. 2018; Rollinson et al. 2018; Carpenter-Kling et al. 2020)

## Global positioning system (GPS)

The development of satellite tracking technology is ongoing and newer devices are now able to process data from several satellite systems (in addition to the conventional GPS system) and are referred to as global navigation satellite system (GNSS) devices (Tomkiewicz et al. 2010). The loggers I used only logged location estimates from GPS satellites and for simplicity, when referring to satellite tracking, I use the term GPS.

GPS loggers used were one of the following models:

- i-gotU GT-120 and GT-600(Mobile Action Technology, Inc. 2013, Taiwan)
- CatTraQ/CatLog (Catnip Technologies, Ltd 2013, Hong Kong)

These were near identical GPS units, with a *SiRFstarIII* chipset and a ceramic patch antenna with a maximum update rate of 1 Hz.

## Video loggers

I used custom built video loggers which were miniature video cameras recording video in high-definition resolution (1280 x 720 pixels) at 24 frames·s$^{-1}$, controlled by an ATmega32U4 micro controller (Microchip Technology, USA). This allowed me to program the cameras to record at specific intervals for predefined periods of time.

## Inertial measurement units (IMUs)

These were Daily Diary (DD) loggers which are multichannel loggers recording data at infrasecond rates (Wilson et al. 2008). For my thesis I used data recorded at 40 Hz which included three accelerometer channels and three magnetometer channels. The tri-axial accelerometer and magnetometers consist of transducers mounted perpendicular to each other and allows measurements in three dimensions referred to as the X, Y, and Z planes. The DD loggers were calibrated prior to deployment, as close as possible to the deployment site, to account for hard- and soft-iron offsets in the magnetometry data (following Bidder et al. 2015; Williams et al. 2017).

## Device dimensions

The GPS loggers were 42 x 26 x 10 mm with a 380 mAh battery, weighing 15.7 g. For smaller petrels, a 200 mAh battery was used reducing the mass to 12.7 g. The video loggers were 77 x 34 x 18 mm and weighed 48 g, including 3D-printed housing and 800 mAh battery. Daily Diary loggers were 30 x 25 x 10 mm and weighed 25–27 g including waterproofing and a 750 mAh battery. Three of the DD devices deployed on Wandering Albatrosses in 2016 had pitot tubes attached to the loggers and were placed in streamlined 3D-printed housing, increasing the height to a maximum of ~40 mm. The combined device mass (including attachment tape and waterproofing) was well below 3% of body mass for albatrosses (Tickell 2000) and did not exceed 5% of mass for smaller petrels. It has to be noted that a 3-5% body mass threshold may differ between species (Vandenabeele et al. 2012). Albatrosses are large birds and although it could not be explicitly tested, there was no indication that the devices had any adverse effects on the birds. The added mass of devices may have an effect on the performance of smaller petrels and the results from these individuals have to be considered with this in mind.

## Deployment methods

The birds were caught by hand or by using a crook (modified hook attached to a ~2 m pole; Figure 2.1a), while on or next to their nests. The loggers were deployed by attaching them to contour feathers on the backs of the birds in a straight line (to minimize drag; Figure 2.1b) using waterproof Tesa tape (Beiersdorf), which allows safe removal without damaging the feathers (Wilson et al. 1997). A subset of individuals (see Chapter 5) had GPS and video loggers attached to back feathers, while DD loggers were attached to their central tail feathers.

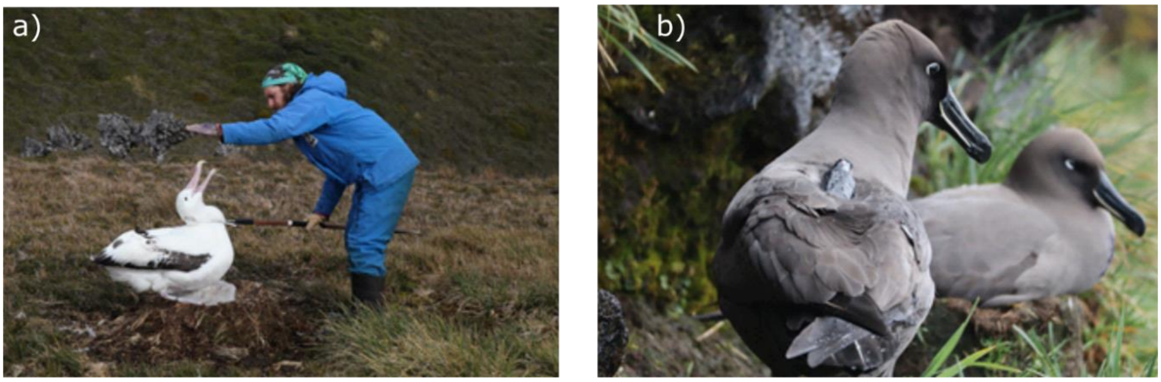

**Figure 2.1**: Deployment methods showing **a)** capture of a Wandering Albatross using a crook (photo credit PG Ryan) and **b)** bio-loggers attached to the back of an albatross.

All of the work presented in this thesis is my own, but I have to acknowledge the help of several field biologists who's dedicated field work made this project possible. Ben Dilley and

Delia Davies collected 1-s GPS tracks and DD data from several species on Gough and Nightingale Islands between 2014 and 2017. Christiaan Brink and Kim Stevens collected video and DD data from Marion Island albatrosses in 2017. Jaimie Cleeland and Fabrice le Bouard collected video and DD data from albatrosses breeding on Gough Island in 2017. Christopher Jones and Michelle Risi collected video and DD data from albatrosses on Marion Island in 2017 and Gough Island in 2018. Janine Schoombie, Makabongwe Sigqala and Melissa Schulze assisted me with DD and video deployments on a range of Marion Island species in 2020.

# Chapter 3: The efficiency of detecting seabird behaviour from movement patterns: the effect of sampling frequency on the inference of movement metrics in Procellariiformes

## Abstract

The use of satellite tracking allows researchers to study the movement of far-ranging animals such as seabirds anywhere on the planet. Recent technological advances have resulted in low-cost GPS loggers that are small enough to be used on a range of seabirds, producing accurate location estimates (± 5 m) at sampling intervals as low as 1 s. However, tradeoffs between battery life and sampling frequency result in studies using GPS loggers on flying seabirds yielding locational data at a wide range of sampling intervals. The effect of sampling interval on the metrics derived from these data have largely been ignored. GPS data have two main errors associated with them, depending on sampling intervals. Very frequent sampling, coupled with limited movement, can result in measurement error (associated with device accuracy) overestimating movement, but a much more pervasive problem results from sampling at long intervals, which grossly underestimates path lengths. In this chapter I use fine-scale (1-s sampling interval) GPS data from a range of albatrosses and petrels to study the effect of sampling interval on metrics derived from the data. The GPS tracks were sub-sampled at increasing intervals to show the effect on path length (i.e. ground speed), turning angles, total distance travelled, as well as inferred behavioural states. I show that distances are overestimated (4% on average, but up to 20%) at the shortest sampling intervals (1–5 s) and underestimated at longer intervals. The latter error is greater for more sinuous flights (underestimated by on average 40% when sampling > 1-min intervals) as opposed to straight flight (11%). Although sampling sizes were small, the error rates seemingly varied with species where species with more sinuous flight modes had larger error. Sampling intervals also played a large role when inferring behavioural states (e.g. foraging, commuting) from path length and turning angles, with the most stable results obtained from moderate sampling intervals (10–30 min). Location estimates from low-cost GPS loggers are appropriate to study the large-scale movements of seabirds when using coarse sampling intervals, but it is inevitable that the actual flight distances are underestimated. When inferring behavioural states from path lengths and turning angles, moderate sampling intervals (10–30 min) may provide more stable models, but the accuracy of the states will depend on the time period associated with specific behaviours. Sampling rates have to be considered when comparing behaviours derived using varying sampling intervals.

# Introduction

Satellite tracking is the simplest form of telemetry and can be used to determine the location of an animal anywhere on the planet, as long as the device is not obstructed (i.e. under water or dense tree cover; Cooke et al. 2004). This is especially useful for marine organisms that can't easily be tracked with other technologies, such as VHF radio tags (Hooker et al. 2002). From the mid-1990s, seabirds were most often tracked with platform terminal transmitters (PTTs) using Argos satellites to triangulate bird locations every 1–3 hours to a precision of a few kilometres (Tremblay et al. 2009). In the last two decades the use of global positioning system (GPS) devices are preferred to PTTs as they are more accurate (± 5 m; Fritz et al. 2003; Ryan et al. 2004; Forin-Wiart et al. 2015; Morris et al. 2017), can record locations more frequently (Cooke 2008; Hebblewhite and Haydon 2010) and can be used in conjunction with Argos or GSM systems (Global System for Mobile Communications) to transmit data, eliminating the need for device retrieval (Tomkiewicz et al. 2010; Orben et al. 2018). In the past, studies using GPS/PTT devices to track animals suffered from low sample sizes as a result of high device costs, device failures and loss (Hebblewhite and Haydon 2010). However, recent technological advances and increased demand in the electronics consumer sector (Wilson and Vandenabeele 2012) have driven reductions in device costs and increased reliability.

Although GPS loggers can acquire data at infrasecond rates (Bouten et al. 2013; Dewhirst et al. 2016), low-cost GPS loggers typically contain a *SIRFstarIII* chipset with a maximum update rate of 1 Hz (Morris and Conner 2017). However, most seabird tracking studies use even less frequent sampling intervals, mainly to conserve battery life but also to prevent spurious movement estimates arising from positional errors (Ryan et al. 2004; Dewhirst et al. 2016). Battery life is particularly important for far-ranging seabirds that undertake foraging trips lasting many days as the logger mass (and consequently battery size) is constrained by the size of the bird. Empirical studies suggest that procellariiforms behaviour is adversely affected if a logger weighs > 2–3% of the bird's mass (Phillips et al. 2003). Most studies of seabird movements using GPS loggers prioritize battery life rather than frequent sampling rates to ensure data for a full foraging trip (e.g. Reisinger et al. 2018). In practice, when comparing behaviours derived from several sampling scales, the coarser scale should be used for all data (Johnson et al. 2017). However, reducing location-based sampling intervals can limit the inferences that can be made from the data. Coarse sampling rates may be appropriate to study large-scale distribution of animals, but such rates might be less useful when inferring habitat selection or animal behavior from the same data (Johnson et al. 2017; Mitchell et al. 2019).

When studying animal behaviour from tracking data, the objective of the research should dictate the sampling rate and not the other way around (Halsey et al. 2009a). This can be problematic as high sampling rates are impractical for behaviours that stretch over extended periods (e.g. distance travelled during a foraging trip). However, location estimates at coarse sampling rates might not be applicable to the temporal scale of particular behaviours, and behavioural states identified from location-based data might vary with sampling intervals (Postlethwaite and Dennis 2013). Advances in microelectronic technology have reduced the size of GPS loggers allowing for smaller seabird species to be studied using this technology (Cagnacci et al. 2010), but again the effective lifespan of these loggers is limited by battery mass.

We know that seabird behaviour at sea is scale dependent (Spear and Ainley 1997; Fauchald et al. 2000; Fritz et al. 2003) and that sampling rates may have significant effects on estimating metrics derived from GPS locations, such as ground speed (Tarroux et al. 2016). However, few studies have examined the effect of sampling frequency on detected movement rates (Ryan et al. 2004; Johnson and Ganskopp 2008) and to my knowledge, none of these studies have included flying seabirds (Hebblewhite and Haydon 2010). The study of seabird movement using GPS locations has increased dramatically in recent years and studies collating large data sets from various sources are becoming more popular (Birdlife International 2004; Dias et al. 2017; Reisinger et al. 2018; Carneiro et al. 2020; Ropert-Coudert et al. 2020). However, a wide range of sampling intervals are used in these tracking studies. For example, albatross foraging behaviour have been studied using fine-scale tracking data with sampling rates < 10 s (Weimerskirch et al. 2007; Nevitt et al. 2008), intermediate rates (1–15 min; Torres et al. 2011) as well as coarse sampling rates > 15-min (Wakefield et al. 2009; Pereira et al. 2018; Reisinger et al. 2018; Clay et al. 2020). Studies with varying sampling intervals in their data usually sub-sample the data to the coarsest rate (Reisinger et al. 2018) or analyse data with similar rates separately (Clay et al. 2020), but the explicit effect of sampling rates on the inferred metrics are rarely acknowledged, let alone assessed.

Two main errors occur when using GPS data to infer movement patterns depending on sampling frequency: measurement error and interpolation error (Ranacher et al. 2016a & b). Measurement error occurs at high sampling rates resulting in overestimation of distances measured while interpolation error occurs at coarse sampling rates with large gaps between points (Ranacher et al. 2016a & b). This chapter determines errors associated with low-cost GPS loggers used in seabird studies, explores how these errors change with varying sampling intervals and describes best practice to address ecological questions using GPS data.

# Methods

## Field sampling

Data from several albatross and petrel species breeding on Gough (40° 20′ S, 9° 50′ W), Nightingale (37° 25′ S, 12° 28′ W; Tristan da Cunha archipelago), and Marion Islands (46° 50′ S, 37° 50′ E) were collected between 2014 and 2020 using CatTraQ (Catnip Technologies, Ltd 2013) or i-gotU (Mobile Action Technology, Inc. 2013) GPS loggers recording positions every second (except for one bird with a 2-s sampling interval; Table 3.1). Details of logger attachment methods can be found in Chapter 2. The GPS loggers were programmed to start a few days after deployment to maximize the likelihood of obtaining at-sea points, or loggers were deployed on individuals that had just been relieved by their partner at their nest.

**Table 3.1:** Fine-scale GPS tracking data acquired from albatross and petrel species from three Southern Ocean breeding islands, listed in order of descending body mass.

| Species | Breeding island | Year | Number of individuals | Sampling rate (s) | Logging duration (mean hours ± SD) |
|---|---|---|---|---|---|
| *Diomedea exulans* | Marion | 2018 | 4 | 1 | 8 ± 6 |
| | | 2020 | 4 | 1 | 25 ± 15 |
| *Diomedea dabbenena* | Gough | 2014 | 2 | 1 & 2 | 15 ± 0 |
| *Thalassarche chrysostoma* | Marion | 2019 | 1 | 1 | 8 |
| *Phoebetria fusca* | Marion | 2019 | 2 | 1 | 25 ± 1 |
| *Thalassarche chlororhynchos* | Gough | 2014 | 2 | 1 | 13 ± 6 |
| | Nightingale | 2014 | 2 | 1 | 15 ± 0 |
| *Procellaria cinereal* | Gough | 2016 | 2 | 1 | 12 ± 2 |
| *Ardenna gravis* | Gough | 2016 | 1 | 1 | 15 |
| | Nightingale | 2016 | 5 | 1 | 17 ± 1 |
| *Pterodroma incerta* | Gough | 2014 | 1 | 1 | 13 |
| *Pterodroma mollis* | Gough | 2016 | 2 | 1 | 15 ± 0 |

Point speed measurements recorded by GPS units are very accurate and independent of measurement error and can be used as a reference distance when interpolation error is negligible (as is the case at a 1-s sampling interval; Safi et al. 2013; Ranacher et al. 2016b). To test if this is the case for the loggers used in this study, 10 GPS loggers were placed in a stationary position with an unobstructed view of the sky and away from any structures on Marion Island. The loggers were placed outside on 19 July (3 loggers, ID S1–S3) and 21 July 2019 (7 loggers, ID S4–S10) and left to record until they ran out of battery power (~12 hours later). The mean ± SD total distance as well as the point speed recorded by the stationary loggers was calculated to the nearest metre. A Welch two-sample *t*-test was used to test for significant differences between speed and location derived distances reported by the stationary GPS loggers. Speed and distance were both log-transformed to conform to a normal distribution.

## Data analysis

### Track preparation

The GPS data were cleaned prior to analysis by removing points with duplicate date and time values as well as on-land points (22412 points ~2% of total). The cleaned data were converted to trajectories (referred to as tracks) using the R package *adehabitatLT* (Calenge 2006). It is expected that sinuosity of foraging trips will increase with trip duration and thus I split the tracks into individual flights to account for variation in foraging trips. The tracks were divided into individual flights where the average speed over 10 s were < 10 km·h$^{-1}$ (non-flying periods) for at least 60 s and the non-flying periods were removed from the data. A straightness index (SI) was calculated for each flight by dividing the great-circle distance between the first and last points of the flight by the total distance travelled during the flight (i.e. values close to 1 represent a straight flight; Figure 3.1a). Flights with a straightness index <= 0.75 were classified as sinuous flights and > 0.75 were straight flights. This threshold value was chosen by filtering the flights in a stepwise fashion, reducing the threshold value and looking at the rate at which flights were excluded at a given threshold (Figure 3.1b). Although sinuous flights are often associated with foraging flights, I did not differentiate between commuting and foraging here as the sampling rates will affect the outcome of behavioural state estimations (see below).

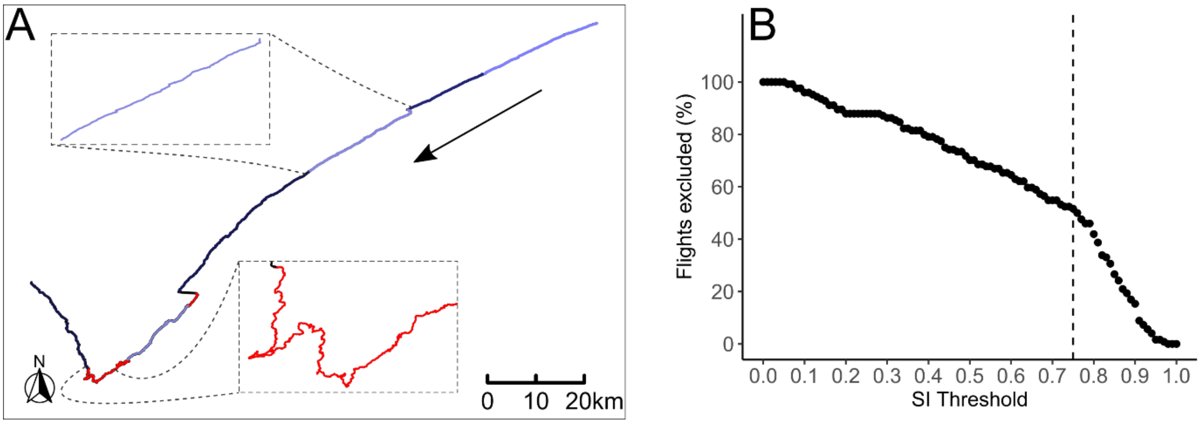

**Figure 3.1: a)** Example of classifying a 1-s track as straight (alternating shades of blue) or sinuous (red lines) flight as chosen by a straightness index (SI) threshold identified in **b)**. The track is from an Atlantic Petrel with data for ~11 hours of a foraging trip and the arrow shows direction of flight.

### *Sub-sampling*

To determine the effect of sampling rate on seabird GPS trajectories, individual flights were sub-sampled (re-discretized) at 1-s time intervals ($k$; sub-sampled flight denoted as $F_k$) and compared to a reference flight ($F_o$). Sub-sampling was done using the *redisltraj* function from the *adehabitatLT* package (Calenge 2006), with $k$ up to 3600 s (1 hr). Thus, only flights that were > 1 hr were used for the analysis. $F_o$ was equal to $F_1$ except for distance estimates between points, where point speed was used as a proxy for distance in $F_o$, while great circle distance between location estimates were used in $F_k$. Point speeds proved to be more accurate (see Results) when determining path lengths at short intervals where path lengths from distance between consecutive points were subject to measurement error. Speed between sub-sampled points was calculated as the distance divided by the sampling interval $k$. The raw tracks were set to record location at 1-s intervals, but ~10% (see Results) of points had 2-s sampling intervals and these points were linearly interpolated to obtain a uniform 1-s track for the reference track $F_o$. I acknowledge that hermite/cubic splines or Bézier curves are suggested to be better options when interpolating seabird tracks (Tremblay et al. 2006), but it did not make any difference at such short (2-s) intervals. The total distance of $F_k$ was divided by that of $F_o$ to get the proportional distance at different sampling intervals ($\mathrm{PD}_k$), where PD values > 1 indicated an overestimation and < 1 an underestimation of distance. This process is shown in Figure 3.2 where sub-sampling of a simulated track has a PD value of 1.12 (i.e. 12% overestimation of distance) at 1-s interval and a PD value of 0.98 (i.e. 2% underestimation of distance) at a 3-s interval.

Point errors (PE) were calculated for each point at varying sampling rates (Figure 3.3) for distance ($\mathrm{PE}_{dist}$), speed ($\mathrm{PE}_{speed}$), and relative turning angle ($\mathrm{PE}_{angle}$). This was done as the metrics associated with individual points are important when state-space models are used to estimate behavioural states. Figure 3.3. shows this process for two consecutive time steps where a simulated track is sub-sampled at a 3-s interval. $\mathrm{PE}_{dist}$ is calculated by subtracting the total distance between the sub-sampled points from the total distance of the reference track falling between the sub-sampled points. It is important here to note that the distances of the reference track are derived from the point speeds as described above. $\mathrm{PE}_{speed}$ was calculated in a similar way where the speed (total distance divided by time) between sub-sampled points were subtracted from the average point speeds of the reference track between the sub-sampled points. Lastly, $\mathrm{PE}_{angle}$ was the relative angle between sub-sampled points subtracted from the mean relative angles of the reference track between sub-sampled points (absolute values).

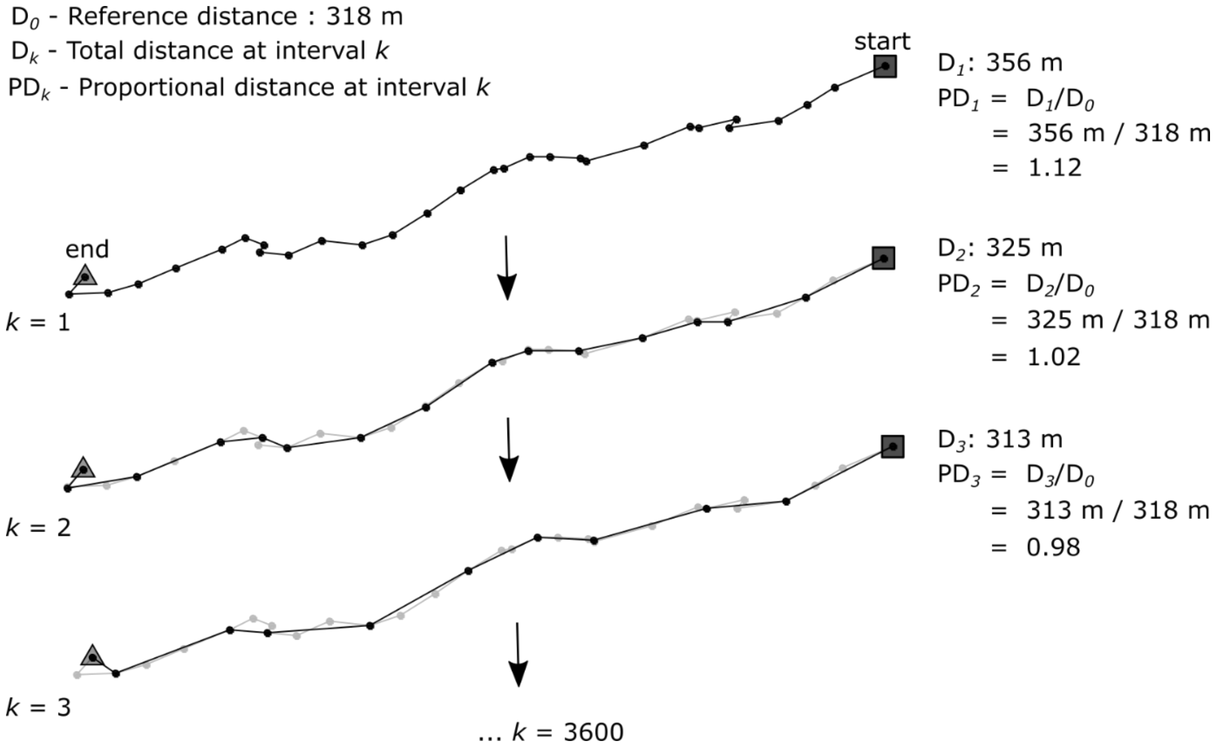

**Figure 3.2:** Steps followed when sub-sampling a flight to determine the proportional distance at varying sampling intervals ($PD_k$). Shown here is a hypothetical 30 s flight with sub-sampled points in black and reference track at 1-s interval as shaded points.

To show the effect that the above errors might have on analysis of seabird behaviour from tracking data, a state-space model was used on an example track at varying sampling intervals. Unfortunately, I could only record a full foraging trip with 1-s sampling interval from one individual (Wandering Albatross) and the rest of the tracks did not have enough points to extract behavioural states at coarse sampling rates. The track was rediscretized at 10-s increments, starting at 10 s and ending at 3600 s. Each sub-sampled point was assigned one of three states (rest, forage or commute) as a function of speed (distance over time) and relative turning angle, using the *depmix* function from the *depmixS4* R package (Visser and Speekenbrink 2010). Resting states had low speed and turning angle, foraging had intermediate speed and large turning angles, and commuting had high speed and low turning angles. To estimate the difference between sampling rates, the percentage of points belonging to each state was calculated and kernel density estimates were calculated for each state at respective sampling intervals. The kernel density estimates were produced with the *kernelUD* function (R package *adehabitatHR*) and the smoothing factor *h* was chosen using the "*href*" method which is based on the standard deviation of the x and y coordinates (Kie 2013). The 50% distribution kernels produced for each sampling interval were compared using the *kerneloverlapHR* function with the "VI" method. A linear mixed-effects model was used to test for differences in means of sinuosity between species, where individual birds were added as a random effect. Values are reported as means ± SD unless otherwise stated. All analyses were performed within the R software environment (R Development Core Team 2018).

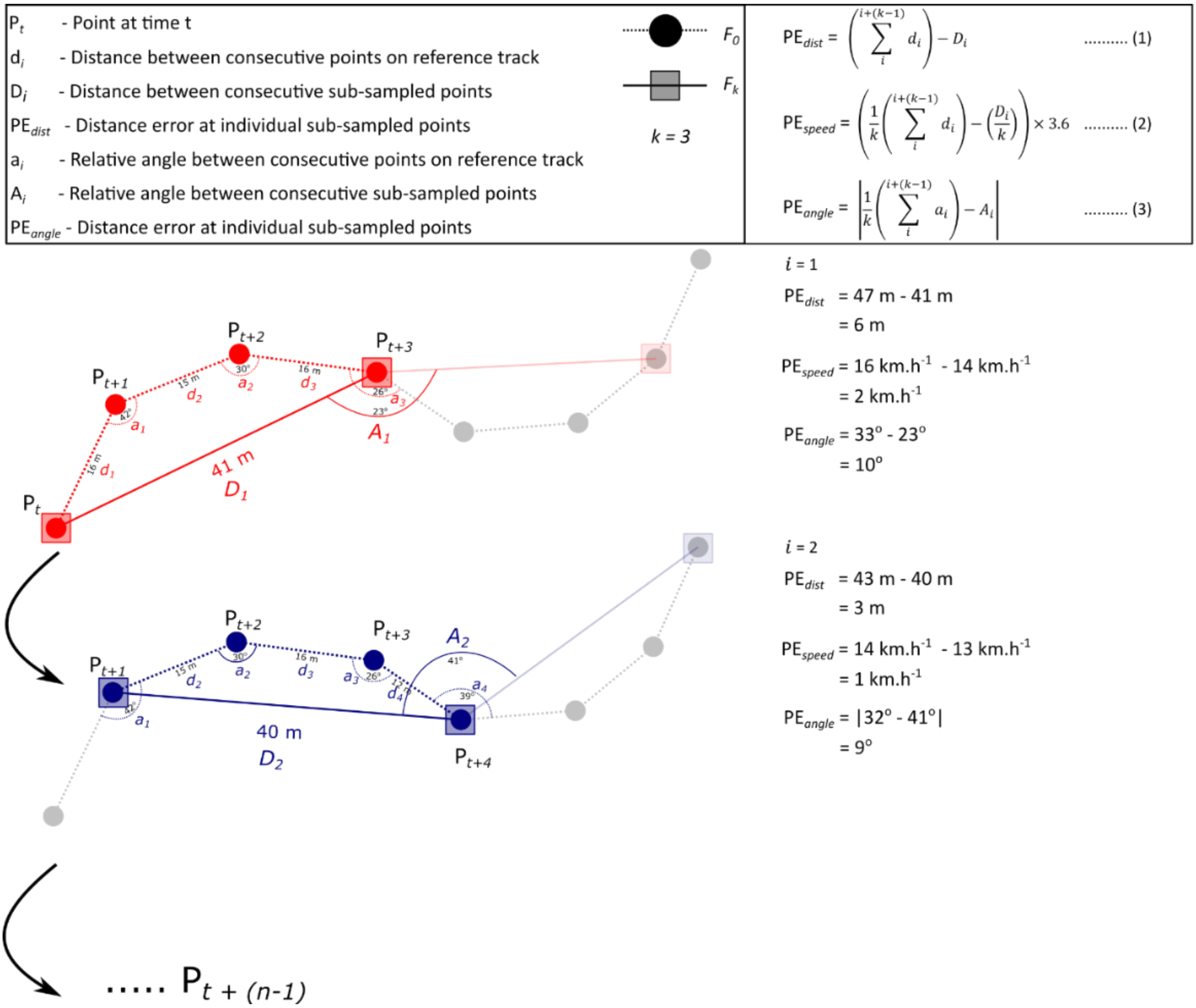

**Figure 3.3:** Example of how point error estimates were calculated for two time steps at a sampling interval of $k$ = 3 s. The reference track ($F_0$) is shown as dotted lines and circles with sub-sampled track ($F_3$) as solid lines and squares.

# Results

## Stationary loggers

The ten static GPS loggers produced 380 248 points that were used to determine the error of the units. The loggers performed well, maintaining the 1-s sampling interval for 98% ($n$ = 374 265) of the time and the rest (2%, $n$ = 5983) at 2-s intervals. The loggers erroneously recorded movement only on a few occasions (0.5%, *n* = 1969 points; Figure 3.4). The cumulative distance error (522 ± 618 m) was significantly larger than error from point speeds (156 ± 210 m; $t_{18}$ = 2.44, *p* = 0.025). Similarly, the mean error per second (0.018 ± 0.021 m) was higher than point speed error (0.006 ± 0.007 m; $t_{18}$ = 2.144, *p* = 0.046). The maximum recorded errors were 51 m and 3 m from distance and speed estimates respectively (Figure 3.4).

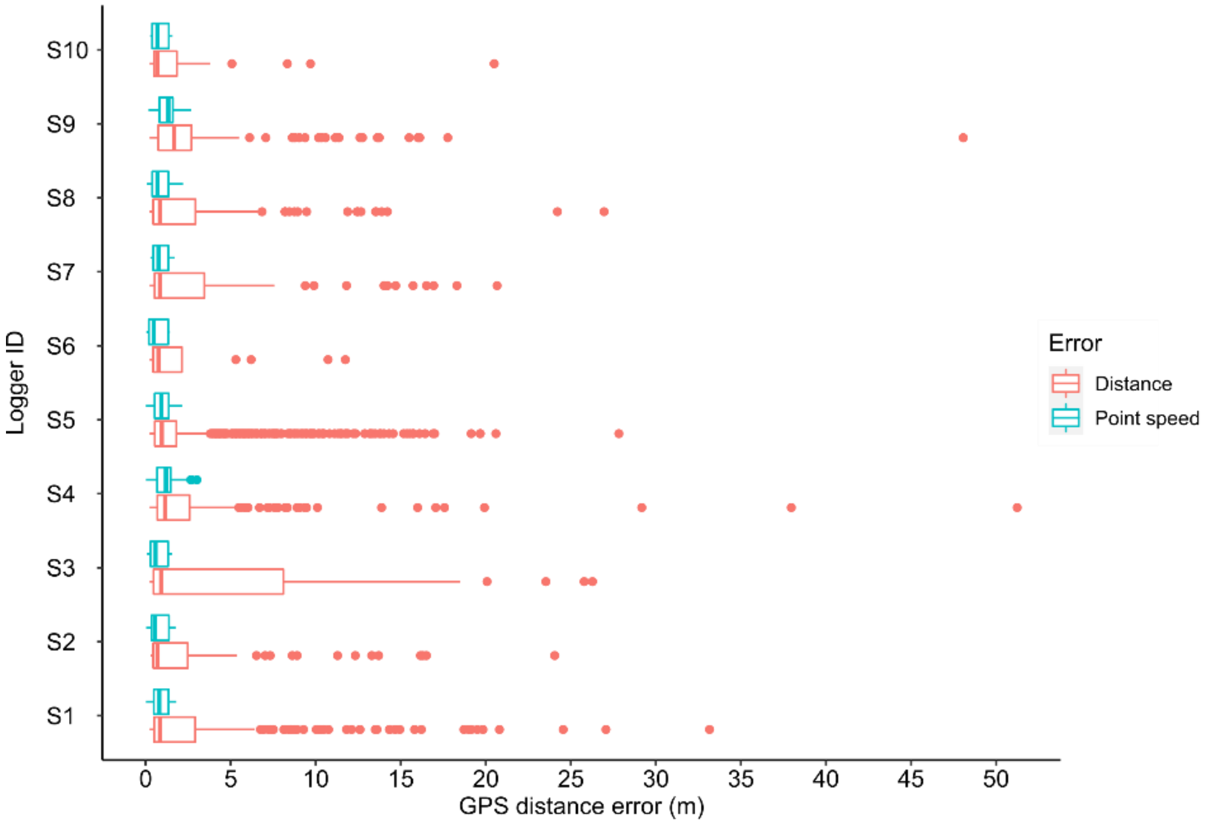

**Figure 3.4:** Boxplots of error associated with stationary low-cost GPS loggers recording position and point speed at 1-s intervals for ~12 hours on Marion Island. Values are from points where the distance between points were > 0 m (*n* = 1969 points), indicating erroneous location estimates. Boxplots are shown for error derived from distance (red) and point speed (blue).

## Tracked birds

Useful data were obtained from 28 individuals from nine different species: 27 birds generated 1 591 743 points at 1-s intervals and one bird 28 201 points at 2-s intervals (Table 3.1, Figure 3.5). Overall, the devices performed well, maintaining a 1-s sampling interval 89.7% of the time (1 427 284 points) and 99.6% of points (1 584 986) falling within a 2-s interval. Data gaps > 2 s were rare, and usually occurred at the start and/or end of a track. One individual, that was tracked for a complete foraging trip (2.8 days), had several isolated

~250 s data gaps most likely caused by interference from additional loggers deployed with the GPS. A total of 429 individual flights were isolated with 124 of those lasting more than 1 hour, providing a total of 293 hours of flight for the sub-sampling analysis. Of the 124 flights, 64 (143 flight hours) were classified as 'straight' and 60 (150 flight hours) as sinuous flight.

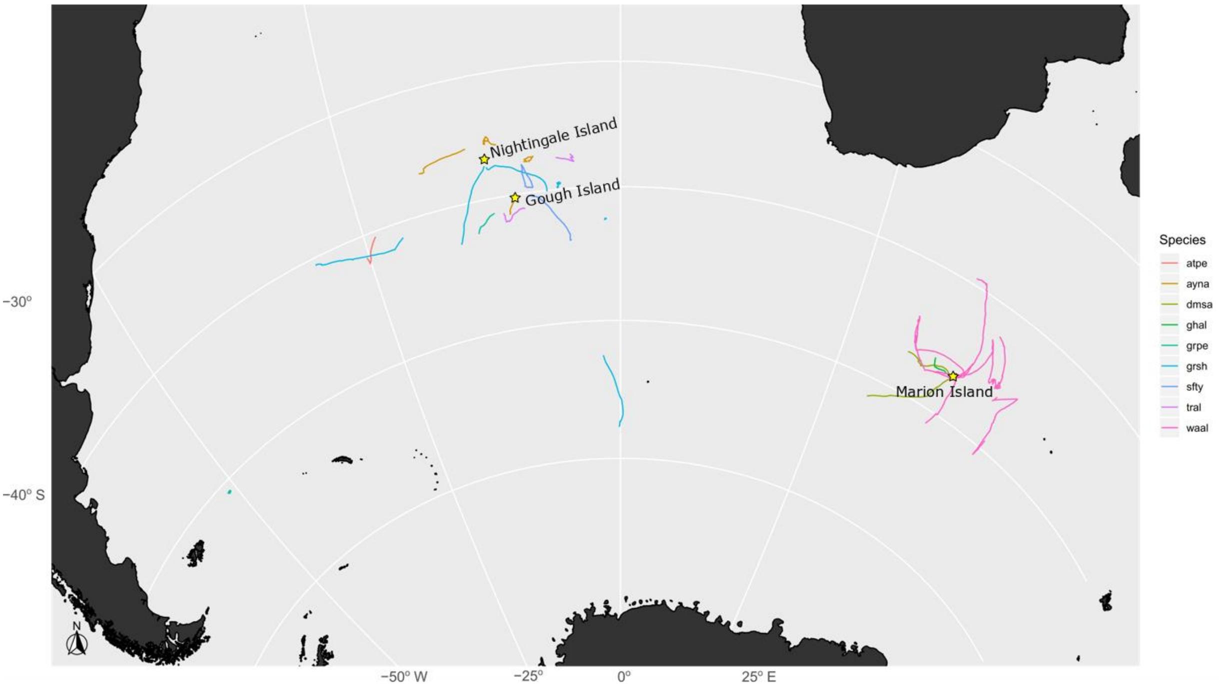

**Figure 3.5:** All GPS tracks for Procellariiformes tracked at 1-s sampling intervals from Marion, Gough and Nightingale Islands.

### *Sub-sampling*

On average, the total distance of sub-sampled flights was overestimated ($PD > 1$) up to $k = 6$ s for both sinuous (9% overestimate) and straight (4%) flight types, after which it was underestimated ($PD < 1$; Figure 3.6). From $k = 6$ s to 30 s the degree of underestimation increased rapidly, after which it levelled out around $k = 60$ s for both flight types, but the error for sinuous flights continued to steadily increase as $k$ increased up to 3600 s (Figure 3.6). The average underestimate for $k > 60$ s for straight flights (10%; $PD = 0.90 \pm 0.04$) was much less than that of sinuous flights (38%; $PD = 0.62 \pm 0.05$). Individual variability in PD also was much greater for sinuous flights than for straight flights (Figure 3.7a) and although sample sizes were small it is possible that species specific flight patterns may also influence the error rates (Figure 3.7b). The flight of Atlantic Yellow-nosed Albatrosses *Thalassarche chlororhynchos* was significantly more sinuous than any of the other species (Figure 3.7b; $t_{19} = 2.7$, $p = 0.014$). This might simply reflect a high proportion of sinuous foraging tracks, but two of the four Yellow-nosed Albatross tracks seemed to be commuting flights

(Supplementary Figure S3.1) and the low sinuosity is possibly as a result of erratic fine-scale movement during cruising flight.

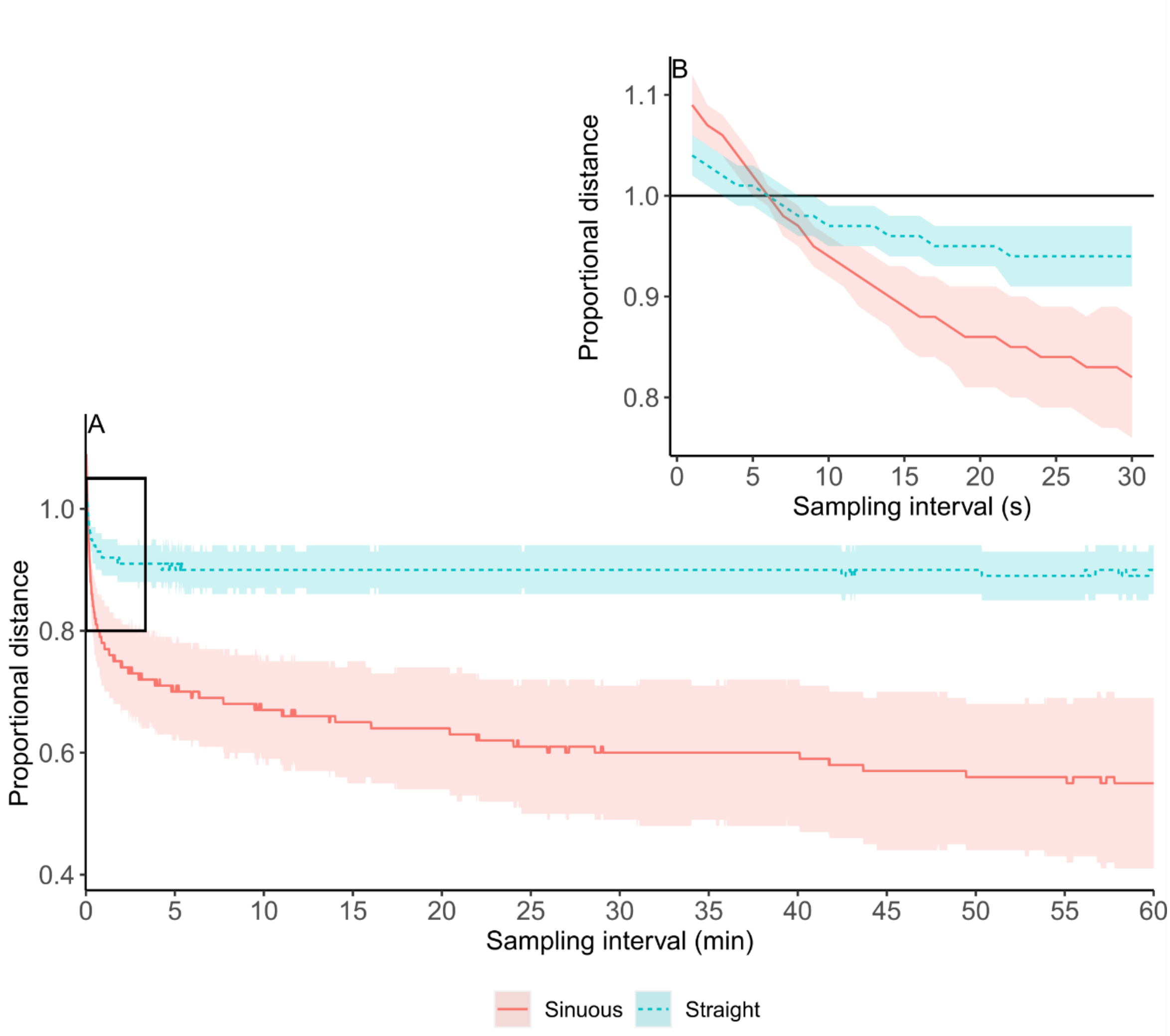

**Figure 3.6: a)** Proportional distance estimates for straight (blue dashed) and sinuous flights (red solid) at increasing sampling intervals. **b)** Zoomed in portion showing the same curves as in a), but only up to 30-s interval. Shaded regions indicate ± 1 SD of means.

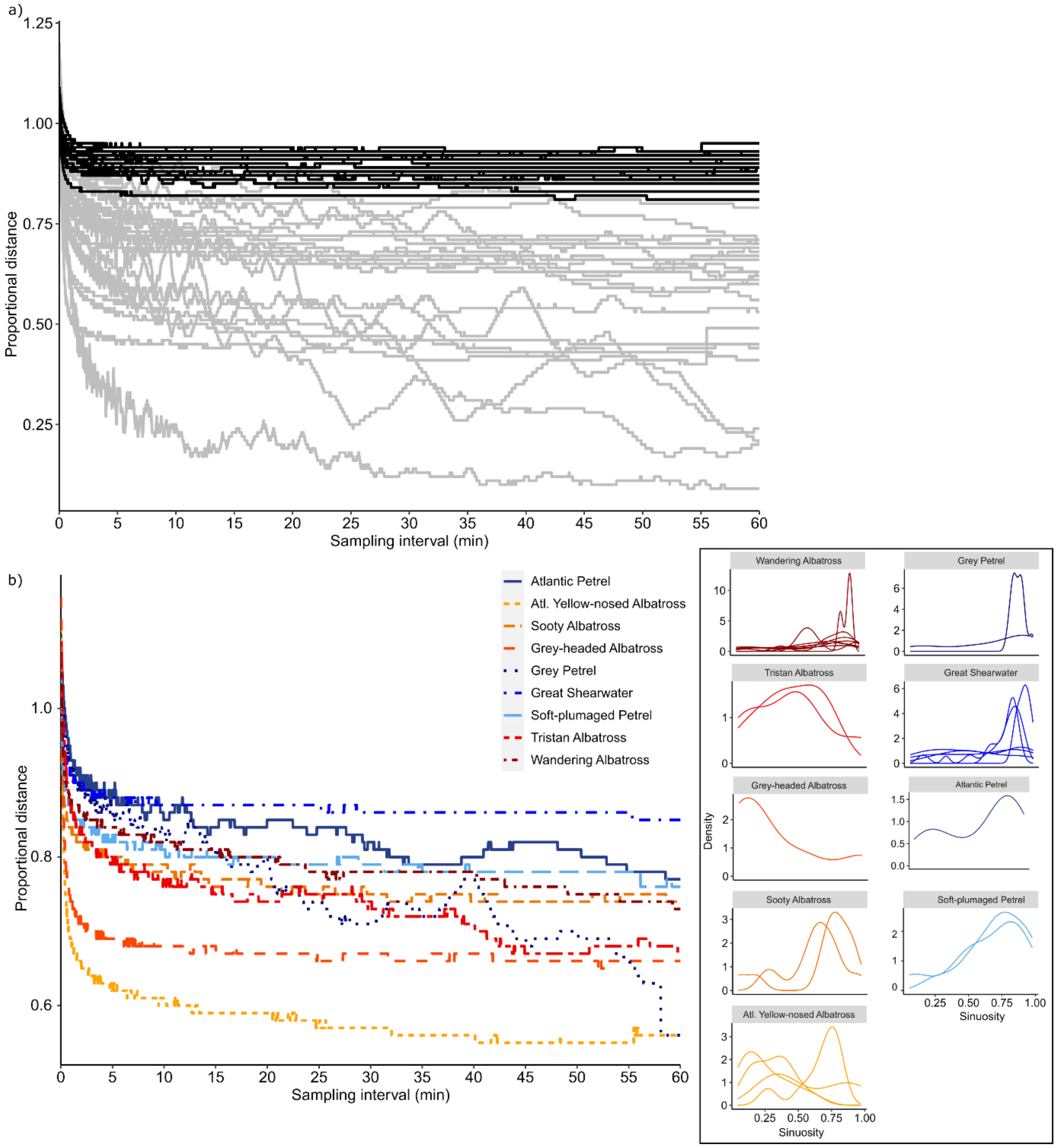

**Figure 3.7:** Proportional distance estimates of flying seabirds tracked at 1-s sampling interval. Curves are means for **a)** each individual separated into straight (black) and sinuous (grey) flights and **b)** averages for each species. The inset in **b)** shows the frequency of flight sinuosity for individuals from respective species.

The average distance error for individual points ($PE_{dist}$) was < 5 m up to $k = 9$ s for sinuous flights and $k = 11$ s for straight flights, with a steeper slope for sinuous flights ending at a value of 15.2 ± 9.8 km for $F_{3600}$ compared to a value of 4.7 ± 2.0 km for straight flights (Figure 3.8). The average speed error for individual points ($PE_{speed}$) curves were similar to the PD curves in Figure 3.6 (seeing that the speed was derived from distance), with a maximum PE$_{speed}$ of 12 ± 5 km·h$^{-1}$ for sinuous flights and 8 ± 2 km·h$^{-1}$ for straight flights at $F_{3600}$ (Figure 3.9). The average relative angle error for individual points (PE$_{angle}$) increased sharply up to $k$ = 10 s (where it reached a maximum value for straight flight; 22 ± 4°), after which it decreased up to $k$ = 120 staying steady for straight flight but increasing steadily for sinuous flights with a maximum value of 57 ± 38° at $F_{3600}$ (Figure 3.10).

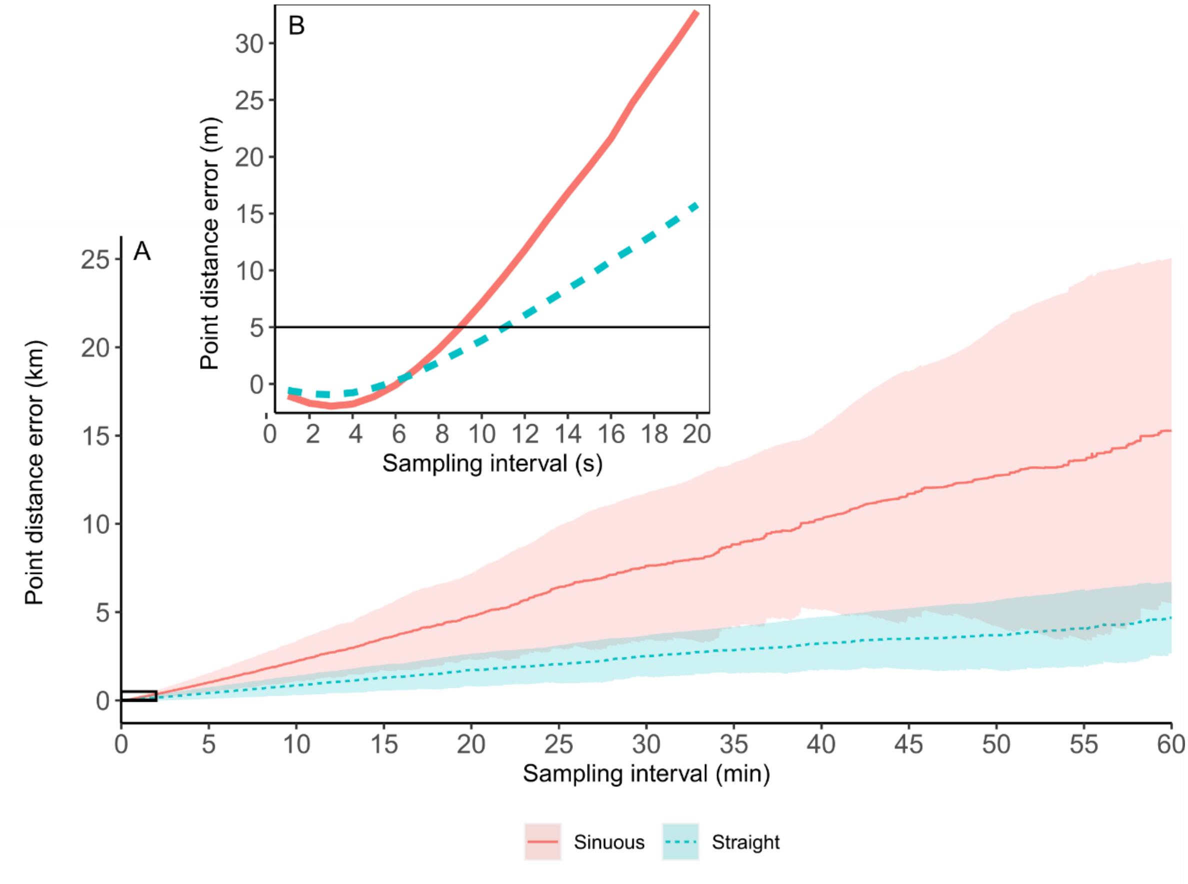

**Figure 3.8: a)** Mean ± SD point distance error (*PE$_{dist}$*) estimates for sinuous (red solid line) and straight (blue dashed) flights of all tracked birds. **b)** Zoomed in section of a) with means only and a solid line shown at an error of 5 m, within the positional error margins of the GPS loggers used.

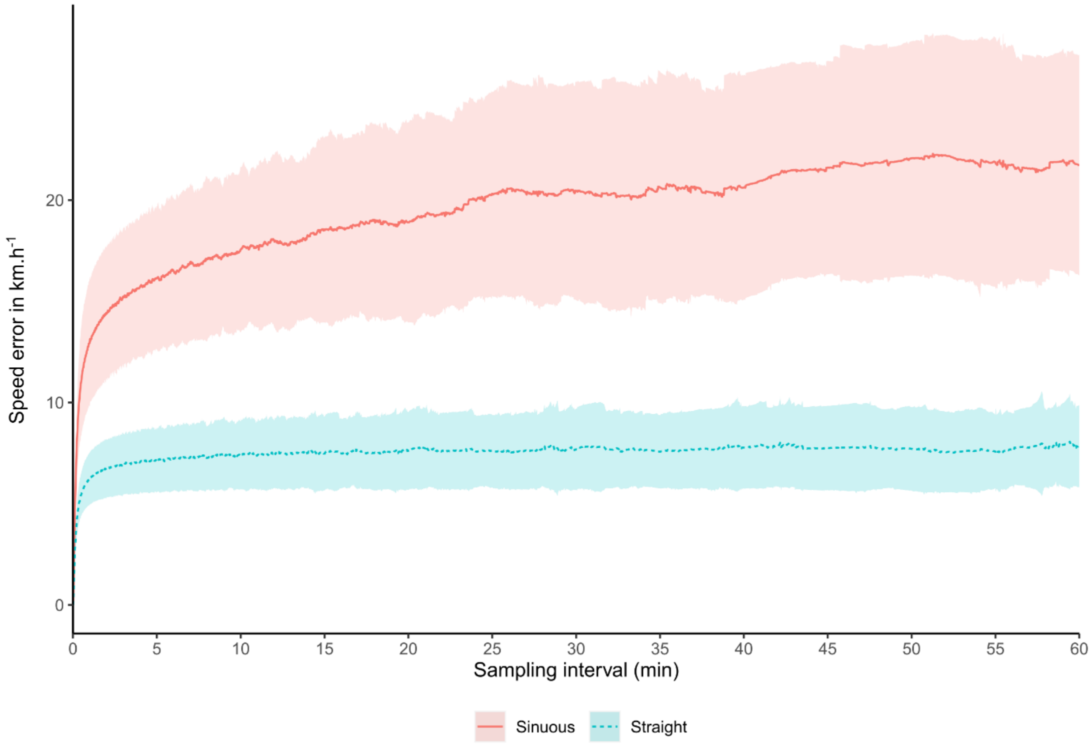

**Figure 3.9:** Mean ± SD point speed error ($PE_{speed}$) for flights at varying sampling intervals.

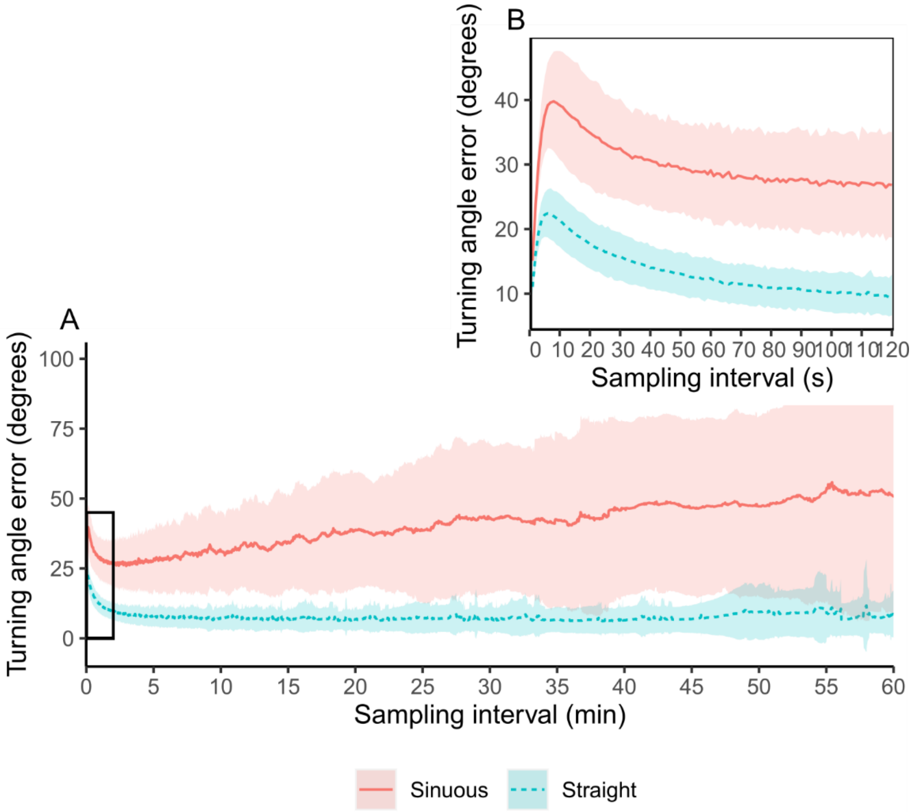

**Figure 3.10: a)** Mean ± SD point error for turning angles ($PE_{angle}$) of flights at varying sampling intervals. **b)** Zoomed in section of a).

State-space modelling, where speed and turning angle were used to determine states, had variable results depending on the value of *k* (Figure 3.11). At high sampling rates (< 300 s) the states were overrepresented by commuting and foraging states, with little distinction between the two (Figure 3.11a). At moderate sampling rates (10–30 min intervals) the states became more distinct and areas associated with each behaviour could be clearly seen (Figure 3.11b-c). At coarse the lowest sampling rate (1 hr), the states were still distinct, but seemingly different from those identified from moderate sampling rates (Figure 3.11d). The same trends were found from the kernel density estimation of foraging states at varying sampling intervals where the states identified at moderate sampling rates were most stable, while fine (< 5 min) and coarse sampling rates (1 hr) had lower overlap with the rest of the points (Figure 3.12). These stable periods are not necessarily more accurate reflections of behavioural states, but rather shows smearing of behaviours in space as sampling intervals become coarser, thus changing from specific foraging sites to general foraging areas. The rapid change up to 5 mins (Figure 3.12b) suggests the derived states may change perspective dramatically at these finer sampling intervals. The reason for these variations becomes clear from Figure 3.13, where the variation in speed and relative angle at different *k* values are shown. At lower sampling rates speed has a bimodal distribution, but this distribution flattens out as sampling interval increases, making it more difficult to distinguish different states.

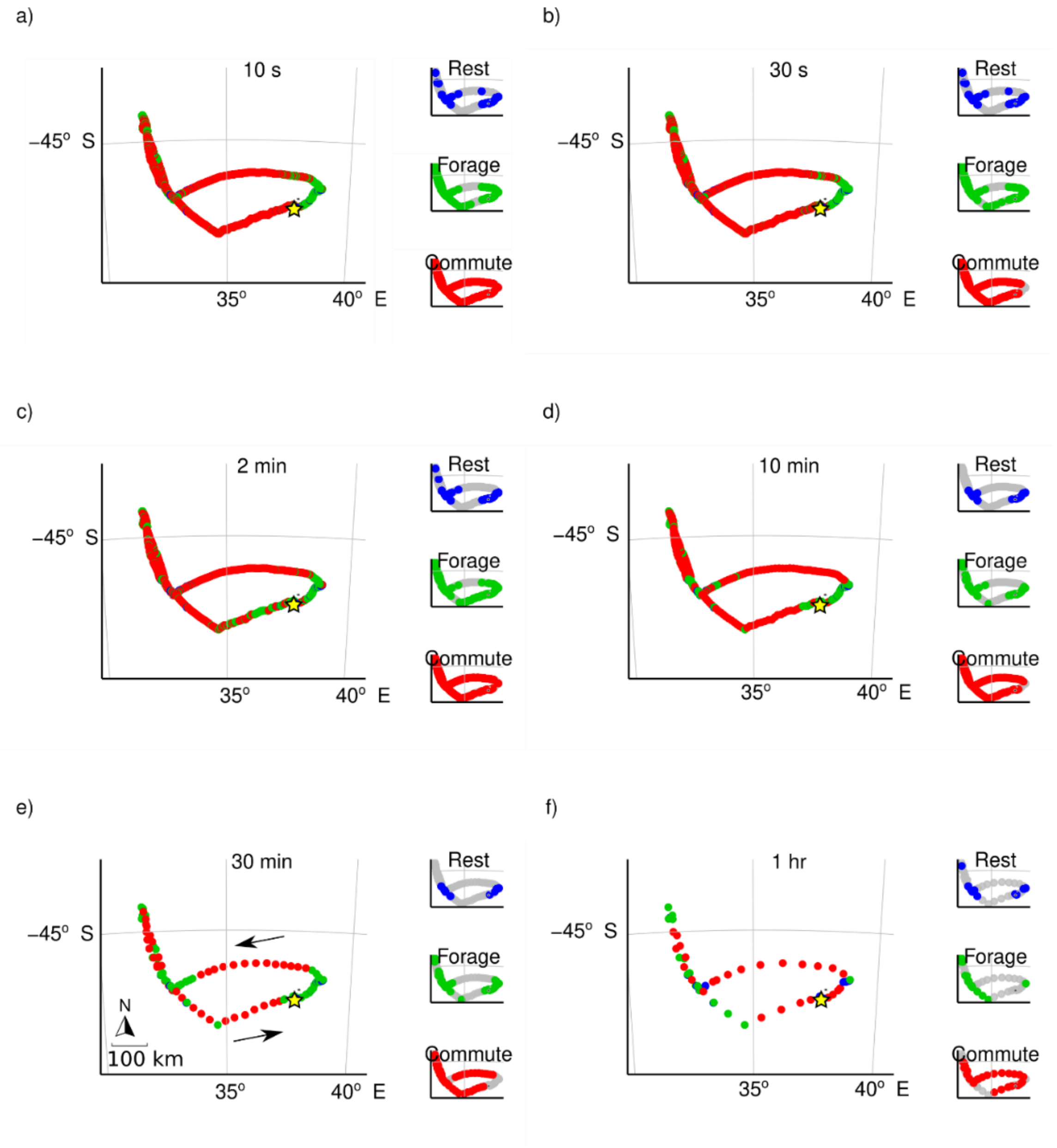

**Figure 3.11:** Example of the same state-space model run on a foraging trip (~37 hr) of a Wandering Albatross at different sampling intervals (10-s, 10-min, 30-min, and 1-hr), estimating commuting (red), foraging (green) and resting (blue) states.

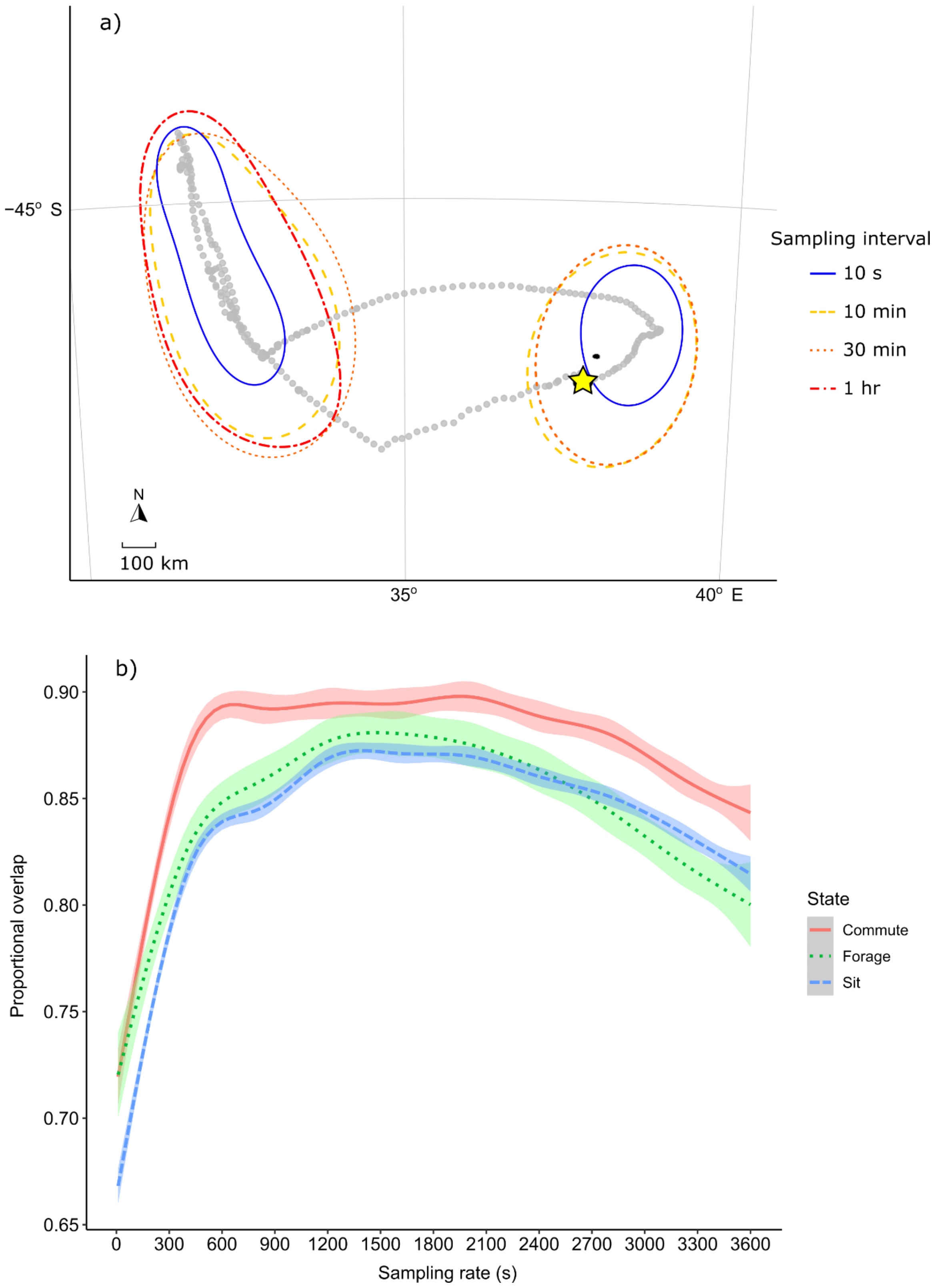

**Figure 3.12:** Effect of sampling rate on identification of behaviour states using a state-space model. **a)** Shows kernel density estimates of points identified as "foraging" at four different sampling rates. **b)** Shows the proportional overlap of kernel density estimates of respective behavioural states at varying sampling intervals.

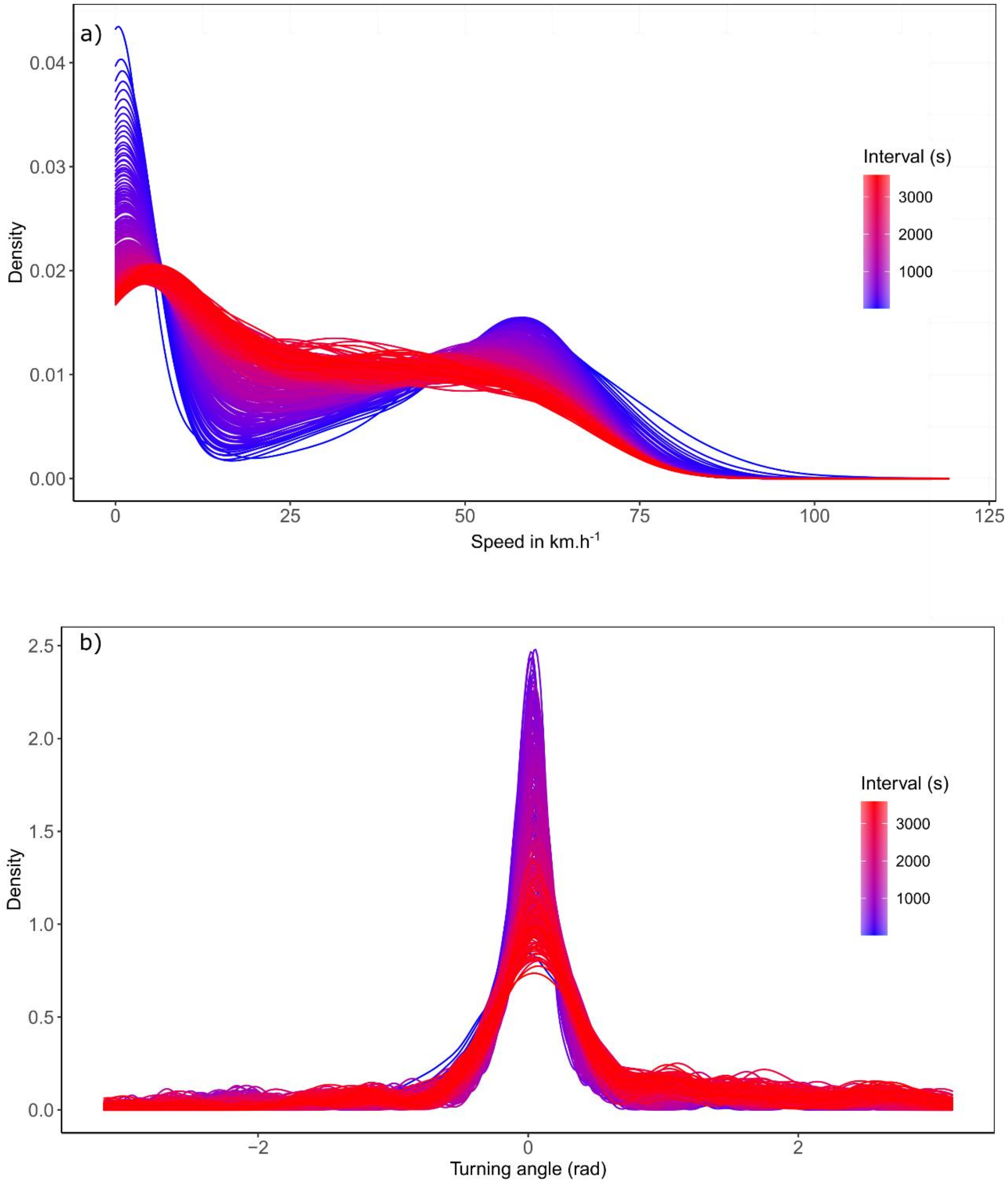

**Figure 3.13:** Density plots of **a)** speed and **b)** turning angle at varying sampling intervals for a complete foraging trip performed by a Wandering Albatross tracked with a 1-s sampling interval.

# Discussion

The results show the effect that sampling interval has on information obtained from GPS tracking data in flying seabird behavioural studies. Although the sample sizes were small, data from a wide range of species (varying in size and breeding location) were obtained and analysed to highlight the various factors that should be considered when interpreting GPS tracking data.

## Device performance

As noted by Forin-Wiart et al. (2015), the low-cost GPS loggers used in this and many other seabird tracking studies performed well compared to commercial devices at all sampling intervals. The manufacturer specifications for the *SiRFstarIII* chipset claim it can obtain GPS fixes at a maximum rate of 1 Hz with 2.5 m horizontal position accuracy. However, in practice the accuracy and fix acquisition rate of GPS loggers can be affected by many factors. Several studies have detailed the efficacy of low-cost GPS loggers in varying environmental conditions and generally the horizontal positional accuracy is closer to 5 m, depending on obstruction above the GPS (e.g. tree cover) and position of the antenna (Vazquez-Prokopec et al. 2009; Forin-Wiart et al. 2015; Morris and Conner 2017). The fix success rate of low-cost GPS loggers is often close to 100% (Morris and Conner 2017), which was the case for the stationary loggers tested in my study, but loggers deployed on seabirds had a lower fix success rate (90%). Weather conditions in the sub-Antarctic are harsh and could affect the fix rate, and some loggers were deployed with additional loggers (cameras, IMUs), which might have interfered with their ability to obtain fixes. Most GPS loggers record information regarding fix quality (Morris and Conner 2017), but downloading these data is not the default setting and it is often not downloaded (as was the case in my study). Additionally, at very high sampling rates (~1 Hz), track paths estimated from low cost GPS loggers are subject to measurement error (Ranacher et al. 2016a), where error associated with their accuracy (usually ± 5 m) compounds, resulting in inflated distances between points. However, point speed values recorded by the GPS loggers is derived from Doppler shift and are not implicated in the measurement error (Ranacher et al. 2016b). My results confirm that the error associated with point speed is much lower than distance error in stationary loggers. Point speeds can thus be used as a proxy for distance at 1-s sampling rates to create reference tracks with lower error rates.

## Fine-scale use

When estimating travel distances of flying seabirds from successive GPS locations, sampling intervals > 10 s will likely result in underestimation of the distances. For example, a Great

Shearwater *Ardenna gravis* tracked with a 1-hr sampling interval on a three week foraging trip may report a total distance of 11 000 km, but the actual distance may be closer to 12 100 km (10% underestimate) or even up to 15 400 km when the flight is extremely sinuous (40% underestimate). In reality, longer foraging trips may have large portions of commuting where flight may be straighter (Weimerskirch et al. 2007) and at hourly intervals total distance travelled will most likely be underestimated somewhere between 10–40%.

When estimating path length from successive GPS locations, sampling intervals > 60 s will likely result in path length errors of up to 5 km (at 1 hr intervals). Sinuous (often foraging) flights could have a much larger error, up to 15 km for path lengths at hourly intervals. When sampling at high frequencies (< 60 s intervals) the error becomes smaller, but only at rates < 10 s does it reach errors that are within the accuracy range of the loggers (i.e. path length error < 5 m). However, when sampling at rates < 6 s, the path lengths and total distance will likely be overestimated by up to 4% and 9% for straight and sinuous flights respectively due to measurement error. To avoid overestimation at these small sampling intervals, point speeds can be used as a proxy for speed to reduce the error.

Points speed and heading recorded by GPS loggers are measured using Doppler shifts and previous studies have shown speed to be within 0.01 $m\cdot s^{-1}$ of actual speed on straight paths and within 0.02 $m\cdot s^{-1}$ on curved paths (Townshend et al. 2008), while heading is accurate to 0.01° according to manufacture specifications. However, these are only useful at very high sampling rates and because they are instantaneous measurements, could provide values that are not representative of the overall movement (especially for heading). This will likely be the case for dynamic soaring seabirds that constantly change speed and heading during flight (Pennycuick 1982; Sachs 2005; Richardson 2011). However, Safi et al. (2013) suggested that point speed and heading estimates might be more informative than using successive locations, even at coarse sampling rates. These authors also suggested using short bursts of 1-s sampling rates where point speed measurements could not be recorded by loggers. My results suggest that this might be a plausible solution as measurement error only becomes a problem when compounded over many hours. In short bursts the measurement error of high frequency (~1 Hz) data should be small enough to be comparable with point speed measurements (see Figure 3.8). Other options include varying sampling rates according to external triggers or power availability (Bouten et al. 2013; Sherub et al. 2017). However, this has to be done with caution, because my results suggest that estimating speed from successive locations at high sampling intervals could overestimate speed and result in large errors in turning angle. Measurement error could result in erroneous conclusions from tracking studies and it might be beneficial to exclude points that are very close to each other in time (Ryan et al. 2004; Hurford 2009). Where fine-scale tracks are needed, specialized loggers that incorporate satellites from several systems and record raw signal data are better to obtain the required accuracy (Sachs et al. 2012; Sachs 2016). Alternatively, dead-reckoning complemented with intermittent GPS locations could produce tracks with high accuracy (Dewhirst et al. 2016), as has been done with Humpback Whales *Megaptera novaeangliae* (Wensveen et al. 2015). However, dead-reckoning for dynamic soaring seabirds will be challenging as they constantly change their heading and may be subjected to wind drift (Tarroux et al. 2016; Yoda 2019) that will not be easy to estimate without matching high resolution wind data.

### Inferring behaviour

Although sample sizes were small, there seemed to be differences in error rates of different species. Most notably, Atlantic Yellow-nosed Albatrosses had extremely tortuous fine-scale flight patterns, with their flights significantly more sinuous than other species. Two of the Yellow-nosed Albatross tracks were not obviously related to foraging as the overall tracks were relatively straight, but the fine-scale movement was tortuous. These tortuous tracks may be the result of flying in lower wind speeds where albatrosses perform longer soaring cycles (see Chapter 6). In contrast, Great Shearwaters performed very straight commuting flights with lower errors in total distance travelled. These shearwaters perform long foraging trips during incubation and alternate long and short trips during chick-rearing periods (Ronconi et al. 2018; Schoombie et al. 2018). These extraordinary chick-rearing trips often have high travelling speeds while commuting between foraging areas where the birds travel up to~14 000 km (Schoombie et al. 2018). However the total distance reported by Schoombie et al. (2018) is most likely an underestimate as they used hourly GPS sampling rates and the actual distance is probably closer to at least 15 000–17 000 km (10–20% underestimate) when accounting for sampling rates.

Body size did not have a marked effect on error rates as the largest (Wandering Albatross) and smallest species (Soft-plumaged Petrel *Pterodroma mollis*) had similar proportional distance curves (Figure 3.7b). However, Wandering Albatrosses had the largest sample size ($n$ = 8) while only two Soft-plumaged Petrels were sampled. The behaviour of the birds (i.e. foraging vs commuting) undoubtedly contributes to observed differences (or lack thereof) between species. Nonetheless, studies comparing several species of seabirds using coarse GPS sampling intervals (e.g. Wakefield et al. 2009) might be at risk of comparing behaviours that are not directly comparable as tracks from different species may be affected differently by sampling interval. Determining the effects of sampling intervals by having a subset of loggers with higher sampling rates might be beneficial for individual studies, as shown by Tarroux et al. (2016).

When using location data to infer behavioural states, error in relative turning angles can completely change the inferred behaviours (Hurford 2009; Postlethwaite and Dennis 2013). Errors in turning angle are very sensitive to sampling interval of GPS tracks. Particularly interesting is the steep increase in error from $k$ = 1–10 s with a local maximum at $k$ = 10 s for both sinuous and straight flights. Turning rates are often used in flying seabird studies to differentiate foraging, commuting and resting periods (e.g. Thiebault et al. 2013; Bennison et al. 2017; Clay et al. 2020). The large variation of inferred behaviour at high sampling frequencies (< 300 s intervals) is most likely as a result of larger error in turning rate at these frequencies. The inference of behaviour might again become unreliable at low sampling rates > 30 min intervals, as the error in path length increases. High levels of uncertainty in predictor variables (i.e. speed and turning angles) may significantly impact models using such predictors to infer behavioural states of seabirds and different conclusions can be drawn from the same track at varying sampling intervals (Postlethwaite and Dennis 2013). Location only data could be useful to infer behavioural changes or identify foraging areas at broad scales but inferring fine-scale behaviour using coarse location data will likely result in erroneous conclusions. Behaviour coupled with distribution can provide informed distribution maps (Shepard et al. 2008), but behaviour derived from location estimates are probably not informative enough and a multi-sensor approach might be more beneficial (Williams et al. 2020b). For example, fine-scale GPS locations (5-s interval) in conjunction with cameras showed fine-scale behaviour of Cape Gannets *Morus capensis* (Tremblay et al. 2014).

In some cases the need for fine-scale data can be overemphasized (Hebblewhite and Haydon 2010). When fine-scale data are not necessary to answer a certain research question, it might better to use coarse sampling rates (i.e. hourly fixes) and reduce logger mass by using smaller batteries, consequently reducing the load the study species has to carry. Where fine-scale data are required, using loggers with higher accuracy, or a multi-sensor approach might be better. This chapter is restricted to soaring seabirds, but the results may be applicable to other flying seabirds or even terrestrial animals where GPS path lengths are used to derive metrics and infer behaviour.

# Supplementary material

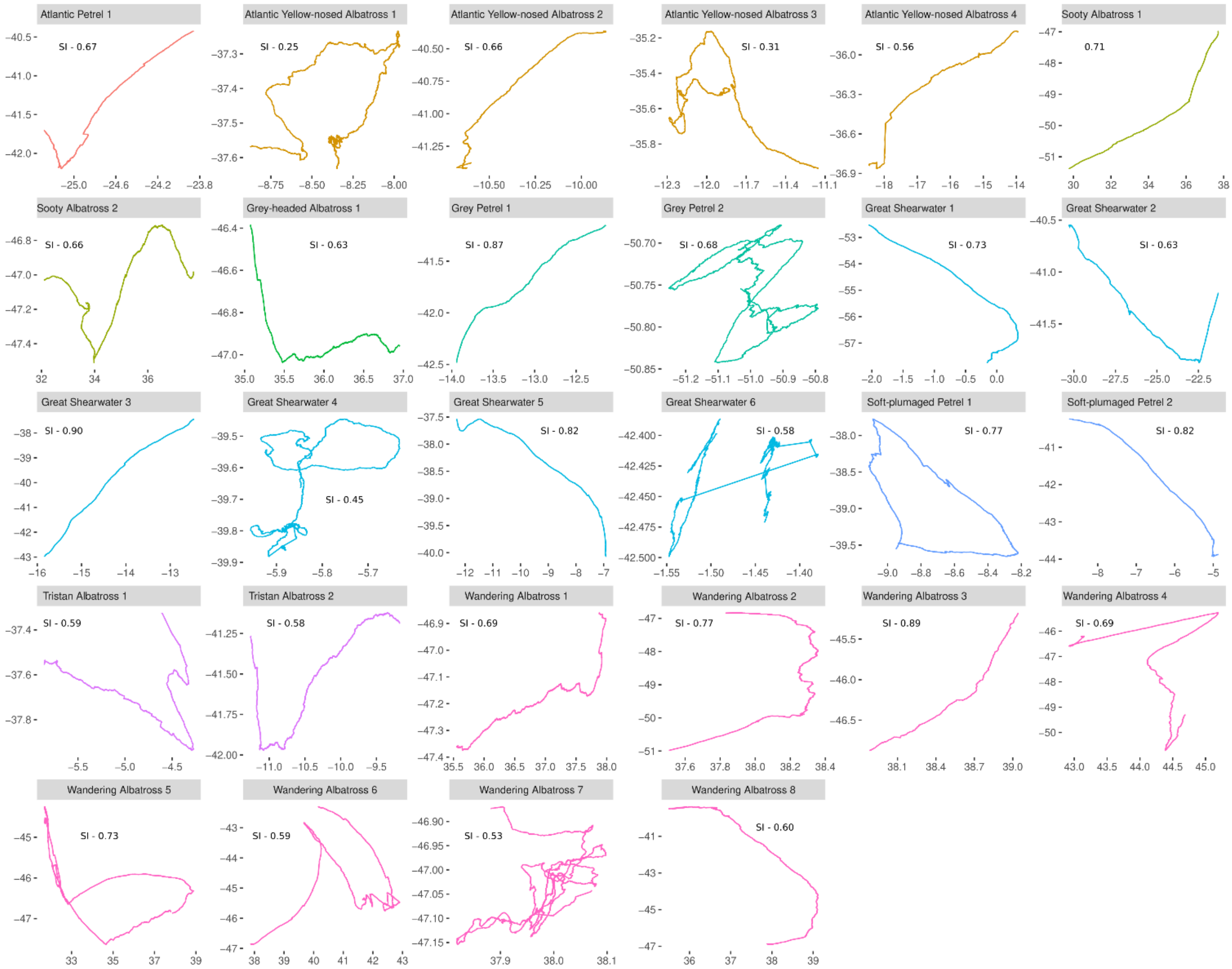

**Figure S3.1**: Tracking data from individual albatrosses and petrels tracked with GPS loggers at 1-s sampling intervals. The raw tracks are shown for individual birds with the mean sinuosity index of flights (SI) shown for each track.

# Chapter 4: Estimating body angles from bird-borne video cameras and tri-axial magnetometers

*Note: Parts of this chapter have been published in a peer reviewed journal as –*

*Schoombie, S., Schoombie, J., Brink, C.W., Stevens, K.L., Jones, C.W., Risi, M.M., & Ryan, P.G. (2019). Automated extraction of bank angles from bird-borne video footage using open-source software. Journal of Field Ornithology, 90, 361-372.*

## Abstract

Advances in bio-logging technology allows us to study the behaviour of free-ranging animals at unprecedented fine-scale resolution. The posture of animals is commonly described on a three-axis system, represented by yaw (rotation around the vertical axis), pitch (around the transverse axis), and roll (around the longitudinal axis), which can be detected by inertial measurement units (IMUs). Commonly used IMUs include tri-axial accelerometers to estimate pitch and roll angles (bank angles), and tri-axial magnetometers to estimate yaw angles (heading). More recently, bird-borne video cameras have also been used to estimate roll angle of flying seabirds, but video loggers have high power consumption, short recording duration and analysis of their datasets can be time-consuming. Many large seabirds use dynamic soaring flight to travel large distances with minimal energy expenditure. However, this flight mode has high centripetal acceleration, which obscures posture derived from accelerometers, limiting their use for studying body angles of dynamic soaring seabirds. Tri-axial magnetometers are not influenced by acceleration and might provide a more efficient means of estimating the posture of animals that typically experience high centripetal acceleration. I propose a new method to estimate yaw ($\varphi$) and roll ($\phi$) angles for dynamic soaring seabirds using tri-axial magnetometer data. This method relies on coarse positional data and the assumption that the birds do not have a large pitch ($\theta$) angle during routine flight. Using a directional cosine matrix, the reference magnetic field vector (from the World Magnetic Model 2020) is rotated around a point, measured by the magnetometer on the body axis of a bird. By assuming $\theta = 0$, the resultant matrix can be solved to produce estimates of angles $\varphi$ and $\phi$. The magnetometer-derived roll angles are validated by comparison to roll angles from bird-borne video loggers. To reduce the processing time for video analysis, I describe a new technique using open-source software to automatically extract bank angles from bird-borne video footage. These methods were field-tested by deploying a combination of bio-logging devices on three albatross species breeding on Marion Island. Comparison of magnetometer-derived angles with control data showed that the method worked well in most instances, with lower accuracy when the actual heading was

closer to magnetic north or south. Accurate estimates of seabird body angles could allow for the estimation of fine-scale tracks through dead-reckoning, while roll angles provide insight into dynamic soaring flight and how the birds react to different environmental conditions (e.g. wind). The magnetometer method has potential for use on other species where centripetal acceleration prevents the use of accelerometers to estimate body angles.

## Introduction

When studying animal behaviour, direct observation is considered among the most important and useful techniques (Ropert-Coudert and Wilson 2005; Hebblewhite and Haydon 2010). However, direct observation is not always possible, and this is particularly so for marine animals such as seabirds that are inaccessible to human observers for most of their life-cycle (Ropert-Coudert and Wilson 2005; Rutz and Hays 2009; Bograd et al. 2010). The inaccessible nature of these animals has given rise to the field of bio-logging, which uses miniaturised loggers/transmitters to provide information about an animal's movement and behaviour (Boyd et al. 2004; Kooyman 2004). In recent years, the increased demand for consumer electronics has resulted in ever smaller and more efficient electronic devices, leading to an increase in bio-logging studies across multiple taxa (Ropert-Coudert and Wilson 2005; Wilmers et al. 2015), opening up new doors to study the behaviour of free-ranging animals in their natural habitat.

Albatrosses are amongst the largest flying birds (Tickell 2000), making them ideal candidates for carrying a wide range of bio-logging devices that allow glimpses into their at-sea behaviour. Like most procellariiforms, albatrosses rely on wind-driven dynamic soaring as a means of low-energy flight (Pennycuick 1982; Weimerskirch et al. 2000, 2012; Sachs 2005; Richardson 2011; Sachs et al. 2012). Dynamic soaring has recently been described, in increasing detail, for Wandering Albatrosses as a series of sequential cycles consisting of four elements generally lasting 10–15 s: 1) a windward climb, 2) a turn, 3) a leeward descent, and 4) a turn to restart the windward climb (Figure 4.1; Richardson 2011, Sachs et al. 2012). More frequent cycles could increase the ground speed of the bird, but are limited by, *inter alia*, the angle of bank, physical strength of the bird and the wind speed (Richardson 2011). Albatrosses mainly fly with cross-winds (Alerstam et al. 1993; Weimerskirch et al. 2000; Sachs 2005; Richardson 2011), and to maintain a relatively straight flight path (despite the effects of wind drift), albatrosses can bank slightly during climbing and descent phases of dynamic soaring, lowering the required bank angles in the turns and consequently reducing the aerodynamic forces experienced by the bird (Richardson 2011). Wind patterns are seemingly predictable to Wandering Albatrosses at a large scale, as breeding birds regularly perform clockwise looping trips when travelling south from their breeding islands and anti-clockwise loops when travelling north from their islands (Weimerskirch et al. 2000). Understanding the fine-scale flight patterns of albatrosses could help predict behavioural changes as a result of their changing environment.

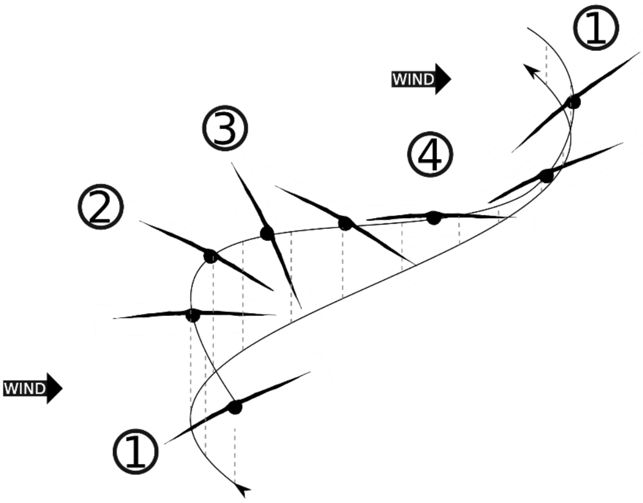

**Figure 4.1:** Illustration of a typical dynamic soaring cycle showing the four characteristic elements. 1) a windward climb, 2) a turn, 3) a leeward descent, and 4) a turn to restart the windward climb.

Inertial measurement units (IMUs) have been widely used in bio-logging technology (Rutz and Hays 2009; Wilson and Vandenabeele 2012) and mostly include a combination of accelerometers, magnetometers, and gyroscopes, with the former utilized most often (Bograd et al. 2010; Wilmers et al. 2015). Gyroscopes are generally seldom used due to their high power consumption and sensitivity to environmental conditions (Ettinger et al. 2002; Williams et al. 2017), while magnetometers produce complex data that are often perceived as difficult to use (Williams et al. 2017). Alternatively, recent advances in video camera technology (Rutz and Troscianko 2013) have resulted in animal-borne cameras now being readily available to researchers. This allows direct observation of behaviour from the perspective of the animal in its natural environment (Moll et al. 2007). Up until the late 2000s, animal-borne cameras were mainly limited to large marine animals (Moll et al. 2007), but these devices are now small enough to use on flying birds (Rutz et al. 2007; Tremblay et al. 2014; Yamamoto et al. 2017). However, cameras also have high power consumption and record much less data compared to IMUs using a similar power source.

Dynamic soaring flight imposes limitations on the use of accelerometers and, as a result, accelerometers are not used to study flight behaviour to the same extent as for animals moving on land or in water (Williams et al. 2015, 2017). Tri-axial accelerometers measure instantaneous acceleration in three different axes (Wilson et al. 2008). A stationary accelerometer will be subjected to an acceleration of 9.81 $m \cdot s^{-2}$ (or 1 $g$), as a result of gravity, and the proportion of the 1 $g$ measured on each of the three orthogonal axes of the accelerometer can be used to derive its posture (Shepard et al. 2008; Wilson et al. 2008). The static acceleration component of a moving accelerometer can be estimated by calculating the rolling mean of each accelerometer axis (Shepard et al. 2008). During flight, many seabirds are often subjected to varying centripetal acceleration as a result of their dynamic soaring flight mode (Sachs et al. 2012). Increased centripetal acceleration results in an inflated measurement of acceleration in the heave axis of the bird, which adds to the static acceleration, and consequently hinders the estimation of posture from accelerometer data (Williams et al. 2015, 2017). Accelerometers are thus applicable to study the posture of slow-moving/stationary animals, or to study short bursts of high energy movement, such as rapid jaw movement when catching prey or individual flaps of flying birds (Shepard et al. 2008). In certain instances, tri-axial magnetometers may be better suited to estimate body angles of flying seabirds, as their measurements are not influenced by dynamic acceleration (Williams et al. 2015, 2017). Nowadays, inexpensive magnetometers are sensitive enough to measure the Earth's magnetic field and tri-axial magnetometers can be interpreted in a similar way as accelerometers to infer posture (Shepard et al. 2008; Williams et al. 2017). However, the Earth's magnetic field is not constant, changing in intensity and direction depending on time and location. Fortunately, in recent years, a collaboration between the United States National Geospatial-Intelligence Agency (NGA) and the United Kingdom Defence Geographic Centre (DGC) has produced a world magnetic model (WMM), which provides estimates of the magnetic field around the earth (NCEI Geomagnetic Modeling Team and British Geological Survey 2019). The spatial data produced by the WMM can be used to correct for regional variations when estimating posture from magnetometer data.

Bio-logging often generates large amounts of data, requiring the development of novel analytical techniques (Moll et al. 2007; Rutz and Hays 2009) to allow rapid, automated processing of data that would take many hours to analyse manually (Moll et al. 2007). When using video data, estimating roll angles from the horizon is commonly used with unmanned aerial vehicles (UAVs) such as fixed-wing aeroplanes (Ettinger et al. 2002; Dusha et al. 2007) or for spatial orientation of ships at sea (Praczyk 2018). Most algorithms use some form of edge detection (Praczyk 2018), with the Canny edge detection filter (Canny 1986) being one of the most commonly used to extract strong edges from images. Tri-axial magnetometers have been successfully used in animal behaviour studies including derivation of heading for dead-reckoning applications (Mitani et al. 2003; Bidder et al. 2015) and more recently to infer average bank angle in thermal soaring *Gyps* vultures (Williams et al. 2018). However, when deriving heading (yaw angle – $\varphi$) from magnetometer data, pitch ($\theta$) and roll angles ($\phi$) of the sensor has to be taken into account (Wilson et al. 2007; Bidder et al. 2015). These pitch and roll angles are often derived from accelerometer data (Walker et al. 2015), but as stated above, this is problematic for dynamic soaring seabirds.

Here, I present two new methods to estimate body angles from video and magnetometer data, respectively. First, I explain how to extract bank angles from video footage obtained from free-ranging albatrosses. Second, I propose a new method to estimate $\varphi$ and $\phi$ angle from magnetometer data without postural information derived from accelerometers. My approach is based on assumptions relevant to dynamic soaring flight and requires having at least some information on the location of the animal. The results are compared to posture estimated using accelerometer data on a control logger and field tested on Wandering, Sooty *Phoebetria fusca* and Grey-headed Albatrosses *Thalassarche chrysostoma* where control roll angles were obtained from video loggers that were deployed with the magnetometers. Few studies have been able to estimate the roll angle of dynamic soaring seabirds and the presented methods will allow further research into their dynamic soaring behaviour. The magnetometer method might also be applicable to other species where dynamic movement limits the use of accelerometers when estimating body angles.

## Methods

A combination of bio-logging devices was deployed on 31 Wandering, two Grey-headed, and three Sooty Albatrosses between 2016 and 2020 (Table 4.1). Deployments were done on Marion Island (37° E, 46° S) during the brood-guard period for Grey-headed and Sooty Albatrosses (December), and during late incubation (February – March) and brood-guard (March – April) periods for Wandering Albatrosses. The loggers were a combination of customised video loggers, Daily Dairy inertial measurement loggers (DD – Wildbyte Technologies) and GPS loggers (CatTraQ – Catnip Technologies, Ltd., i-gotU GT-120 – Mobile Action Technology, Inc.). The loggers were deployed on the backs of the birds in a straight line to minimize drag and the combined masses (including waterproofing and attachment tape) were ~130 g for Wandering Albatrosses and ~70 g for Grey-headed and Sooty Albatrosses (< 3% of body mass; Tickell, 2000) with sampling intervals as shown in Table 4.1 (see Chapter 2 for details of attachment methods).

**Table 4.2:** Sampling intervals of bio-logging devices deployed on several albatross species on Marion Island between 2016 and 2020

| Year | Species | *n* | Video | DD | GPS | Video duration | Video Interval | GPS interval |
|---|---|---|---|---|---|---|---|---|
| 2016 | Wandering Albatross | 4 | x | - | x | 10 min | 6 hr | 60 min |
| 2017 | Wandering Albatross | 9 | x | x | x | 5–10 min | 3–6 hr | 60 min |
| 2018 | Wandering Albatross | 15 | x | x | x | 5–10 min | 3–6 hr | 60 min |
| 2020 | Wandering Albatross | 3 | x | x | x | continuous | N/A | 1 s |
| 2020 | Sooty Albatross | 3 | x | x | x | continuous | N/A | 1 s |
| 2020 | Grey-headed Albatross | 1 | x | - | x | continuous | N/A | 1 s |
| 2020 | Grey-headed Albatross | 1 | x | x | - | continuous | N/A | N/A |

## Analysis

Data recorded by the video and DD loggers were used to estimate body angles of the birds during flight using two new methods described below. Roll angles were estimated from video data by extracting the angle of the horizon in each frame, while the DD loggers were used to estimate heading and roll angles from magnetometry data. All video footage was inspected and clips where the birds were flying were isolated for analysis. Subsequently, the corresponding magnetometry data from the DD loggers were also isolated. Video data were analysed using the open source software *OpenCV* (www.opencv.org) in the Python programming language with all functions mentioned below found in the software documentation (https://docs.opencv.org/2.4.0/). The rest of the analyses were done with the R programming language (R Development Core Team 2018), but initial calculations were performed in the Julia programming language (Bezanson et al. 2017).

## Video analysis – roll angle estimation

### Image preparation

To be able to detect the horizon in an image, there needs to a be clear contrast between the sky and the surface (land or sea). This is normally the case for seabirds flying over the ocean but can be confounded by the presence of clouds (particularly dark clouds on the horizon) or the sun in an image. To overcome these obstacles the images were prepared to minimize contrasting colours other than that of the horizon.

- First, the isolated image (Figure 4.2a) was cropped to exclude the timestamp at the bottom right of the frame. Then the image was down-sampled (reducing the resolution) using a Gaussian Image Pyramid through the *pyrDown* function (Figure 4.2b) at a predetermined level $n_{down}$. This reduces the processing time for the following steps but also reduces the quality of the image, thus a $n_{down}$ value of more than three is not advisable for 1280 x 720 images.

- Next, the image was smoothed/blurred (Figure 4.2c) using multiple iterations ($n_{bilat}$) of a bilateral filter (function *bilateralFilter*). Using multiple iterations flattens the colours present in the image, resulting in a much smaller colour map but still retaining the edges. The bilateral filter assigns a new value to each pixel from weighted pixels within a given diameter ($b_{diameter}$) surrounding the input pixel. Pixel weights are determined by two factors: 1) the difference in colour intensity ($b_{colour}$) of the input and neighbouring pixels and 2) the spatial distance ($b_{spatial}$) between the input and neighbouring pixels.
- Lastly, the image was up-sampled to its original resolution with the *pyrUp* function. The reason for the up- and down-sampling is that the bilateral filtering process is quite slow (compared to other filters such as Gaussian) and the process takes an appreciable time when many frames are present, so lowering the image resolution reduces processing time.

### Horizon detection

Various algorithms have been used to identify the horizon in maritime images (Gershikov et al. 2013; Lipschutz et al. 2013) with the basic workings outlined by Praczyk (2017). To find the horizon in the smoothed image, it was converted to greyscale and detail was removed from the image until only the horizon remained.

- First, the greyscale image was smoothed using a Gaussian filter (*GaussianBlur* function) to remove any noise remaining following the bilateral filtering above (Figure 4.2d). The Gaussian filter is similar to the bilateral filter but does not consider colour intensities when weighting neighbouring pixels. The amount of smoothing performed by the Gaussian filter was determined by the size of the square window surrounding the input pixel (called the kernel) and was defined here as $g_x$ and $g_y$. It is important to remove as much noise as possible from the images for the next step.
- A Canny edge detection algorithm was used (*Canny* function) to identify the edges present in the smoothed image. The *Canny* function evaluates the gradient intensity and direction of a given pixel within a given range (usually 3 x 3 pixels) using a Sobel operator to retain pixels with the highest gradient within the specified range. To ensure that only the desired edges are identified, the *Canny* function uses a double threshold method (Canny 1986) where specified values ($th_1$ and $th_2$) are used to determine if the edges are strong enough to retain. Gradients above the upper threshold (larger of the *th* values) are retained as strong edges and gradients below the lower threshold are discarded, while gradients between the thresholds are retained only when they are

connected to strong edges. Canny edge detection results in a binary image where pixels identified as edges have a value of 1 and other pixels have a value of 0 (Figure 4.2e).

- The Canny edge detection results in many edges of various lengths being identified. To find the horizon, these edges were combined by first dilating (*dilate* function) the edges, then eroding (*erode* function) and dilating them again. Dilation is a method used in image processing where the bright areas of the image are expanded, and erosion has the opposite effect. The amount of expansion (for both bright and dark areas) is dependent on predetermined search window size ($n$ x $n$ matrix) and the number of iterations chosen. The process of dilation compares each pixel to neighbouring pixels falling within the search window and assigns the input pixel the same value as the maximum in the window. Erosion works in the same manner except that the minimum value within the search window is used. The resulting image is similar to Figure 4.2e, but the lines are much thicker and neighbouring edges are now fused together (Figure 4.2f).
- Canny edge detection is then performed for a second time on the thickened lines to generate several contours representing the lines with the highest contrast in the image. The contours were identified using the *findContours* function and a bounding box was computed for each contour with the *boundingRect* function. The bounding box provides the height and width of the contours and allowed me to exclude contours that did not represent a straight line (i.e. the horizon) where contour height/width < 0.05-0.2. It was assumed that the longest of the remaining contours would represent the horizon.
- Finally, a line was fitted to the points of the identified contour using a weighted least-squares algorithm with the *fitLine* function (Figure 4.2g). The angle of this line in relation to the horizontal axis of the image was then calculated and retained as the bank angle of the bird in degrees ranging from -180 to 180°. A video example of the process can be found at the following link: https://vimeo.com/475447736.

### Post-processing

The resulting bank angles were processed using R software to correct for missing or erroneous angles. Each angle was compared to the previous two angles and if they varied by more than 4° on average, the point was marked as incorrect. Thus, the first two data points after a gap in the data were always discarded. The threshold of 4° was identified through visual inspection of several video clips where successive angles never varied by more than 4°. Lastly, the gaps were filled in through interpolation using a Hermite cubic spline algorithm (see Results Figure 4.5a; Fritsch and Carlson 1980). To determine the extent to which interpolation would be biologically meaningful, data loss was simulated by removing chunks of data (ranging from one to 1000 data points = 0.04 to 41.67 s) every 50 s from existing data sets. Interpolation was performed on the simulated data sets and the error calculated for the interpolated values.

### Validation

To validate the automated process described above, horizon angles from 100 randomly selected images (10 images from 10 birds) were measured manually. Measurements were done with a protractor on a computer screen to an accuracy of approximately 1° by three observers. The same images were then run through the horizon detection code and the resulting bank angles were compared to the three sets of direct measurements. The test set of measured angles was not normally distributed and transformation (log, square- and cube root) did not improve normality of the data. Thus, a non-parametric Kruskal-Wallis rank sum test was used to determine if there was a significant difference between the direct measurements and the computer-generated angles.

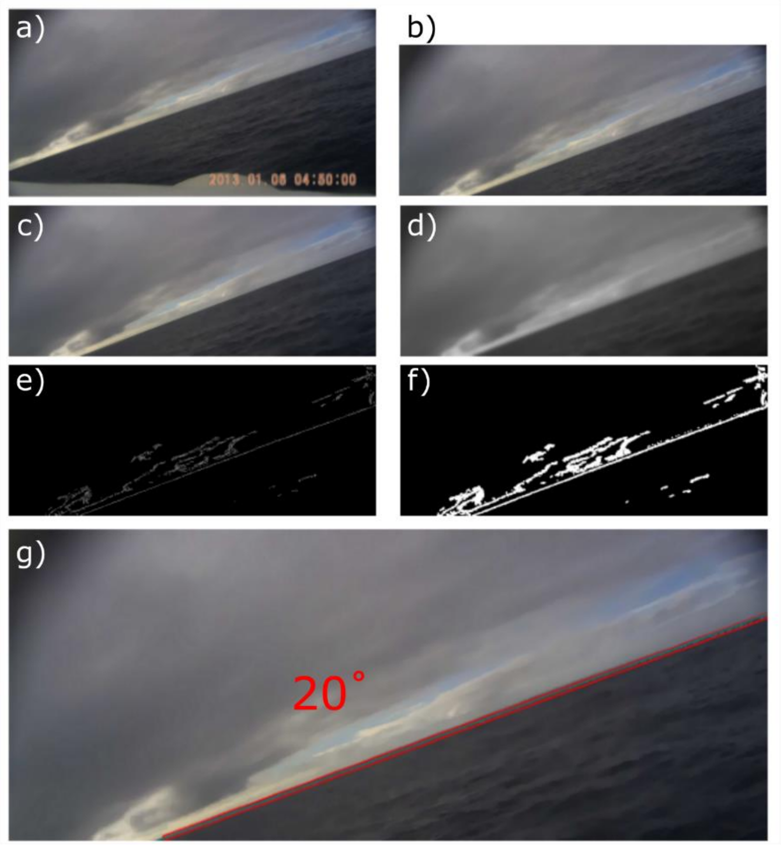

**Figure 4.2:** Illustrations of the method used to extract horizon angles from images isolated from albatross flight footage using algorithms from open-source software, OpenCV. The **a)** original image is **b)** down-sampled and cropped followed by smoothing through applying both **c)** bilateral and **d)** Gaussian filters to allow **e)** Canny edge detection. The edges are **f)** inflated to produce thicker contours which are used to identify the contour most likely representing the horizon and is **g)** used to estimate the angle of the horizon.

## Magnetometer analysis – yaw and roll angle estimation

The DD loggers contain a tri-axial magnetometer which produced data used to estimate yaw $\varphi$ and roll $\phi$ angles using a new method described below. These analyses were done using data collected from three albatross species in 2020 (Table 4.1) where priority was given to recording longer periods of flight with enough overlap between video and DD logger data for validation of the results. The roll angles estimated from video data (above) was compared with roll angles estimated from the magnetometry data to validate the efficacy of the method.

### Body angle calculation

Tri-axial magnetometers measure the earth's magnetic field along three axes. When the measured values are compared to the known magnetic field intensity at a given location, they reveal something about the rotation of the measurement device. Such a rotation can be presented as:

$$H_{xyz} = D_{NED}^{xyz} H_{NED} \tag{1}$$

Where $H_{xyz}$ are the values measured by the tri-axial magnetometer, $H_{NED}$ is the magnetic vector as given by the World Magnetic Model (WMM2020; https://www.ngdc.noaa.gov/geomag/WMM/DoDWMM.shtml) and $D_{NED}^{xyz}$ is the directional cosine matrix (DCM) from the north east down (NED) axis system to the xyz axis system (Figure 4.3). Equation (1) can be shortened by calling the xyz system $b$ (body axes) and the NED system $i$ (inertial axes).

$$H_b = D_i^b H_i \tag{2}$$

**Figure 4.3: a)** Body (xyz) coordinate system applied to an albatross, showing the three axes measured by the magnetometers (pitch $\theta$, roll $\phi$, and yaw $\varphi$) and resultant angles around each axis when compared to **b)** the north east down (NED) inertial axis system of the reference magnetic field.

There are several ways to represent such a rotation and it is important to note that the following steps are done using a passive intrinsic rotation (Figure 4.4), where $H_i$ is rotated around a fixed point on the $H_b$ axis system, in a yaw-pitch-roll order.

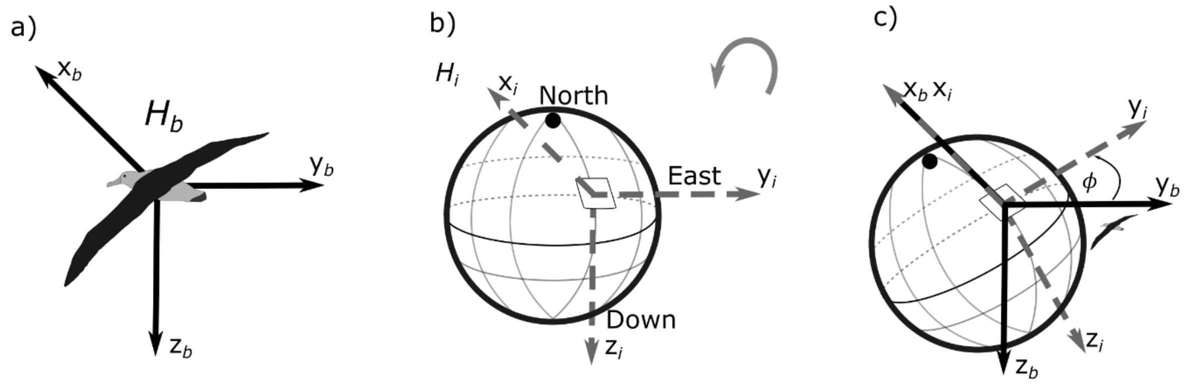

**Figure 4.4**: Example of a passive intrinsic rotation around the x-axis. **a)** The body axis system (*$H_b$*) stays fixed while **b)** the inertial axis system (*$H_i$*) is rotated in **c)** where $\phi$ is the roll angle and both pitch and yaw are zero.

Equation 2 can be expanded to a standard matrix form, but at least one of the angles (yaw, pitch, or roll) is needed to allow the calculation of the remaining two. Albatrosses do not regularly pitch at high angles for extended periods of time, which is evident from the video data, where the horizon is seen in the frame most of the time. If pitch angle $\theta$ is reduced to zero, equation 2 can be expanded to:

$$\begin{bmatrix} H_x \\ H_y \\ H_z \end{bmatrix} \doteq \begin{bmatrix} cos\varphi H_N & +sin\varphi H_E & 0 \\ -cos\phi sin\varphi H_N & +cos\phi cos\varphi H_E & +sin\phi H_D \\ sin\phi sin\varphi H_N & -sin\phi cos\varphi H_E & +cos\phi H_D \end{bmatrix} \tag{3}$$

allowing the calculation of the yaw angle $\varphi$:

$$\varphi = \pm\, cos^{-1}(h_x) + \beta \tag{4}$$

where $h_x$ is the raw magnetometer data from the surge axis ($H_x$) normalized to the NE plane of the $H_i$ reference data and $\beta$ is the magnetic declination angle at the given location. Once $\varphi$ is obtained, the roll angle $\phi$ can be calculated *via*:

$$\phi = \tan^{-1}\left(\frac{H_y}{H_z}\right) + \alpha \tag{5}$$

where $\alpha$ is a function of $\varphi$ and the reference magnetic field data $H_i$. A detailed explanation of the above equations is given in the Supplementary material. It has to be noted that the loss of sign in the $cos^{-1}$ operator (equation 4) results in two solutions of yaw (and consequently roll) and a *post hoc* decision has to be made to determine which of the solutions is correct.

### Validation

To determine how well $\phi$ estimation from magnetometer data worked, the estimated values were compared to $\phi$ derived from tri-axial accelerometer data on a control DD logger (*DDo*):

$$Accelerometer\ \phi = tan^{-1}\left(\frac{Acceleromter_y}{Acceleromter_z}\right) \tag{6}$$

The *DDo* logger was calibrated in the same manner as the loggers deployed on albatrosses. Next, a compass swing was performed, rotating *DDo* at 10° yaw angles (starting at magnetic north) and then rotating the logger around the x-axis to get roll at each yaw increment. Rotations on the *DDo* logger was undertaken slowly to ensure that the centripetal acceleration was minimal and thus roll angles derived from the accelerometer values could be used as a control.

Analyses of albatross data were restricted to individuals where enough high-quality data were present from both tri-axial magnetometers and video loggers. For equipped birds, reference roll angles were obtained from video where the horizon angle was used as a proxy for roll angle (see *Video analysis* above). The magnetometer data were down-scaled to fit the lower sampling frequency of the video data (24 Hz) and were matched temporally to the video data. The video data were recorded in 5-min video files (bins) and time synchronisation between video and magnetometry data was visually inspected for each of the bins to ensure correction of time lag that occurred in the video loggers. This resulted in a single dataset with comparable roll angles at 24 Hz where the error for each roll angle was calculated by subtracting the magnetometry estimate from the video estimate and mean error was calculated for data corresponding to each video bin. This was done for each section of flight across all individuals. In addition, the number of dynamic soaring cycles (identified by consecutive roll angle peaks) was counted manually from both the video and magnetometer data. To determine the importance of location accuracy when extracting reference magnetic field data from the WMM, roll estimates supplemented with tracking data were compared to roll estimates using a single coordinate (deployment site on Marion Island).

## Results

The 36 cameras, 32 DDs and 35 GPS loggers deployed on 36 birds (Table 4.1) were all recovered. Two cameras were water-logged and four malfunctioned, not recording any footage. From the 30 cameras producing useful footage, I isolated 17.5 hours of flight from 17 birds. However, cameras from two individuals (2018 deployments) only recorded three flights of 10 s each and were excluded from the analyses. The mean ± SD duration of flight recordings for the remaining birds was 7.1 ± 6.8 min ($n$ = 10; 2016-2018) and 43.9 ± 38.6 min ($n$ = 5; 2019-2020).

## Video analysis

The values used for different steps in the horizon extraction algorithm were determined for each 5-min video bin by examining the results of the first ~10 s of each video. This was necessary as the light levels and presence of clouds/sun varied between individual flights. Ideal conditions for horizon detection were flights over calmer waters on overcast days (i.e. in the absence of direct sunlight). High wind speeds caused white water while sunlight reflected off wave crests resulting in high contrasts that were detected as edges by the Canny algorithm. Changing the values of the Canny edge detection thresholds were sufficient to account for the changes in scenery and the rest of the values were kept constant (Table 4.2). Higher $th_1$ values were used when there was white water or reflected sunlight (or the sun itself) in video clips. Some video clips had to be cropped to remove the bird's head and body from the images. Using the values in Table 4.2 worked well on all video clips that were analysed and it took approximately one hour of processing time for a 10-min video clip (~14 000 frames) on a standard laptop computer (i5, 2.4 GHz CPU with 12 Gb memory and NVIDEA GeForce 840M graphics card). Using down sampling ($n_{down}$ = 2) was almost four times faster (0.3 s per frame) than without down sampling (1.1 s per frame). The simulation of data loss showed that interpolation was appropriate when data gaps were smaller than 45 data points (~2 s) as larger gaps resulted in mean errors that were larger than 10° (Figure 4.5b) and not meaningful within the current application. As a result, I excluded all data gaps > 45 frames from the analysis.

**Table 4.2:** Parameters and their associated values used in the horizon extraction algorithm

| Parameter | Value | Description |
|---|---|---|
| $n_{down}$ | 2 | Gaussian Image Pyramid down sampling |
| $n_{bilat}$ | 7 | Iterations of bilateral filter |
| $b_{diameter}$ | 9 | Bilateral filter: diameter for pixel weighting |
| $b_{colour}$ | 9 | Bilateral filter: colour intensity weighting |
| $b_{spatial}$ | 7 | Bilateral filter: spatial distance weighting |
| $q_x$ | 13 | Gaussian filter kernel parameters |
| $q_y$ | 13 | |
| $th_1$ | 8 to 20 | Thresholds for *Canny* function |
| $th_2$ | $th_1$ | |

| | | |
|---|---|---|
| *erosion* | 4 x 4 | erosion kernel size n x n |
| *dilation* | 4 x 4 | dilation kernel size n x n |

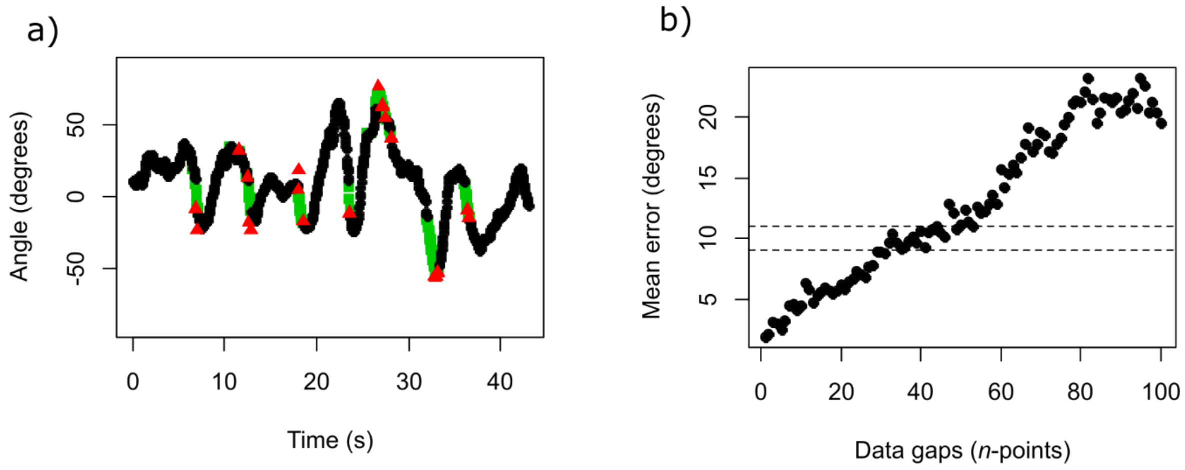

**Figure 4.5: a)** Subset of computer-generated bank angles from Wandering Albatross video footage during flight. This illustrates the post-processing of measured angles (black dots) where erroneous points (red triangles) are discarded and gaps filled in through cubic spline interpolation (green squares). **b)** Simulation of data-loss where gaps of varying lengths were removed from the data at regular intervals, missing values interpolated, and then compared to actual values to determine the mean error. The error band (above which data gaps resulted in errors larger than was deemed acceptable for this study) is indicated by dashed lines.

## Video validation

The mean standard deviation of measured angles by the three observers was 2°. There was no significant difference between the measured angles and the angles produced by computer analysis (Kruskal-Wallis rank sum test, $\chi^2 = 1.28$, df = 3, p = 0.73). The computer analysis was able to find angles for 93% of the images with 7% unobtainable due to low light conditions or bad image quality. The mean ± SD difference between the direct and computer estimated measurements was 3 ± 4°. Seven estimates (7%) had an error > 10° (maximum 18°). These large errors were caused by the presence of the bird's head in the image ($n = 6$) and a dark cloud bank on the horizon ($n = 1$). Manual scoring of images was confounded by the presence of large waves obscuring the horizon and curvature of the horizon caused by the wide-angle lens of the camera. The latter was resolved by measuring the angle from the centre of the image, but the former could not be corrected for and possibly resulted in some error in bank angle estimates.

## Magnetometer analysis

### Control logger (*DD₀*)

Roll and yaw angles could be estimated for most headings (magnetic), with some gaps around magnetic north and south (Figure 4.6). Yaw angles around magnetic north and south could not be estimated as the absolute $h_x$ values were often > 1, which is not a valid input for the $cos^{-1}$ operator. Missing roll angles (where $\varphi$ was not available to calculate $\alpha$), were estimated by using the nearest valid $\alpha$ value (Figure 4.6). When compared to the roll angles estimated from accelerometer data (regarded as the “true” rotation) a mean error of 4.5 ± 5.5° was found. Roll angles were successfully estimated from the magnetometer data recorded on the $DD_0$ logger for all headings (10° increments from 0° to 360°).

### Magnetometer validation

From the retrieved devices, good quality data were present from two Wandering Albatrosses (five flights, seven hours), one Grey-headed Albatross (six flights, 2.8 hours), and two Sooty Albatrosses (nine flights, 4.8 hours) that allowed comparison of video- and magnetometer-derived roll angles. Magnetometer-derived angles compared well to those derived from video loggers for all three albatross species, with a mean ± SD roll angle error of 12 ± 12° (Table 4.3 and Figure 4.7). Location accuracy did not have a large effect on the reference magnetic field within the range of the four individuals tracked with GPS loggers (maximum distance from Marion Island 300 - 500 km). The mean ± SD error for flights at the maximum distance was 1 ± 1° for both roll and yaw angles estimated from magnetometry data (Figure 4.8). The Grey-headed Albatross data did not include GPS tracking, and a single coordinate (Marion Island; 37° E, 46° S) was used for all magnetometer estimates, which still produced acceptable results (Figure 4.7c).

The newly described method produced the best results when the birds were not heading directly into magnetic north or south and when consecutive dynamic soaring cycles were present. This allowed for easy discernment between the two possible solutions from the yaw angle estimates (equation 4). The solution with the lowest mean value over 2-5 seconds (half of a dynamic soaring cycle) were assumed to be correct as roll angle regularly crosses the zero mark during dynamic soaring (Figure 4.9). Larger errors occurred when the birds were flying with a heading that was close to magnetic north or south for large portions of the flight. As shown above for the control logger, this resulted in $h_x$ values > 1 where yaw angles (and subsequently roll angles) could not be calculated. Interpolating the missing values by using the nearest valid yaw value to calculate the roll worked well in most cases, maintaining the shape of the soaring cycle (Figure 4.9). The direction of the roll (positive vs negative banking) was also mostly preserved, even when several seconds of flight path were interpolated (Figure 4.9). Another problem that arose from a heading that corresponded with magnetic north or south was that the choice between the two solutions for yaw angles (Equation 4) became less apparent (see Figure 4.9a). Even so, the overall shape of the dynamic soaring cycles as calculated through magnetometer data corresponded well with the video-derived data (Figure 4.7). When estimating the number of dynamic soaring cycles in a flight, the magnetometer data were just as effective as the video data, with 98.6% of the video cycles identified by magnetometer data (Table 4.3).

**Table 4.3:** Error estimates of roll angles derived from magnetometry (Mag) compared to roll angles from video loggers deployed on three albatross species. All values are degrees (-180° to 180°) unless otherwise stated.

| | | | | | | **Roll angle range** | | **Dyn. soaring cycles** | |
|---|---|---|---|---|---|---|---|---|---|
| **Bird ID** | **Flight number** | **Duration (min)** | **Mean error ± SD** | **Bearing** | **Heading** | **Video** | **Mag** | **Video (n)** | **Mag (n)** |
| | | | | **Wandering Albatrosses** | | | | | |
| WA1 | 1 | 109 | 13 ± 12 | -83 | -39 | -84 – 57 | -82 – 68 | 602 | 591 |
| WA1 | 2 | 50 | 15 ± 13 | -103 | -52 | -100 – 60 | -88 – 59 | 366 | 362 |
| WA1 | 3 | 45 | 16 ± 13 | -85 | -54 | -99 – 58 | -89 – 53 | 363 | 353 |
| WA2 | 1 | 120 | 9 ± 9 | 126 | -35 | -93 – 46 | -88 – 55 | 715 | 722 |
| WA2 | 2 | 94 | 10 ± 11 | 150 | -50 | -93 – 46 | -88 – 52 | 627 | 637 |
| **Total average error ± SD** | | | **13 ± 11** | | | | | | |
| | | | | **Sooty Albatrosses** | | | | | |
| SA1 | 1 | 106 | 12 ± 12 | -142 | -31 | -96 – 63 | -104 – 86 | 876 | 893 |
| SA1 | 2 | 50 | 13 ± 13 | -127 | -41 | -78 – 60 | -84 – 84 | 415 | 410 |
| SA2 | 1 | 8 | 19 ± 15 | 170 | -16 | -100 – 64 | -94 – 95 | 66 | 63 |
| SA2 | 2 | 2 | 26 ± 19 | -115 | -16 | -88 – 84 | -66 – 87 | 15 | 15 |
| SA2 | 3 | 5 | 24 ± 14 | -100 | -23 | -96 – 68 | -100 – 83 | 36 | 33 |
| SA2 | 4 | 49 | 19 ± 14 | -48 | -16 | -93 – 71 | -92 – 94 | 261 | 245 |
| SA2 | 5 | 46 | 21 ± 15 | -58 | -17 | -85 – 75 | -100 – 94 | 213 | 200 |
| SA2 | 6 | 5 | 19 ± 15 | -66 | -14 | -90 – 79 | -121 – 114 | 30 | 30 |
| SA2 | 7 | 19 | 13 ± 12 | 63 | -3 | -79 – 107 | -79 – 112 | 163 | 162 |
| **Total average error ± SD** | | | **18 ± 14** | | | | | | |
| | | | | **Grey-headed Albatrosses** | | | | | |
| GA1 | 1 | 75 | 11 ± 9 | - | -51 | -85 – 78 | -93 – 86 | 601 | 597 |
| GA1 | 2 | 38 | 12 ± 10 | - | -52 | -88 – 78 | -102 – 82 | 325 | 327 |
| GA1 | 3 | 13 | 13 ± 13 | - | -53 | -88 – 89 | -103 – 76 | 98 | 100 |
| GA1 | 4 | 5 | 13 ± 13 | - | -49 | -90 – 86 | -120 – 91 | 38 | 38 |
| GA1 | 5 | 35 | 13 ± 11 | - | -53 | -92 – 80 | -110 – 90 | 271 | 270 |
| GA1 | 6 | 4 | 15 ± 14 | - | -51 | -90 – 88 | -93 – 76 | 35 | 35 |
| **Total average error ± SD** | | | **13 ± 12** | | | | | | |

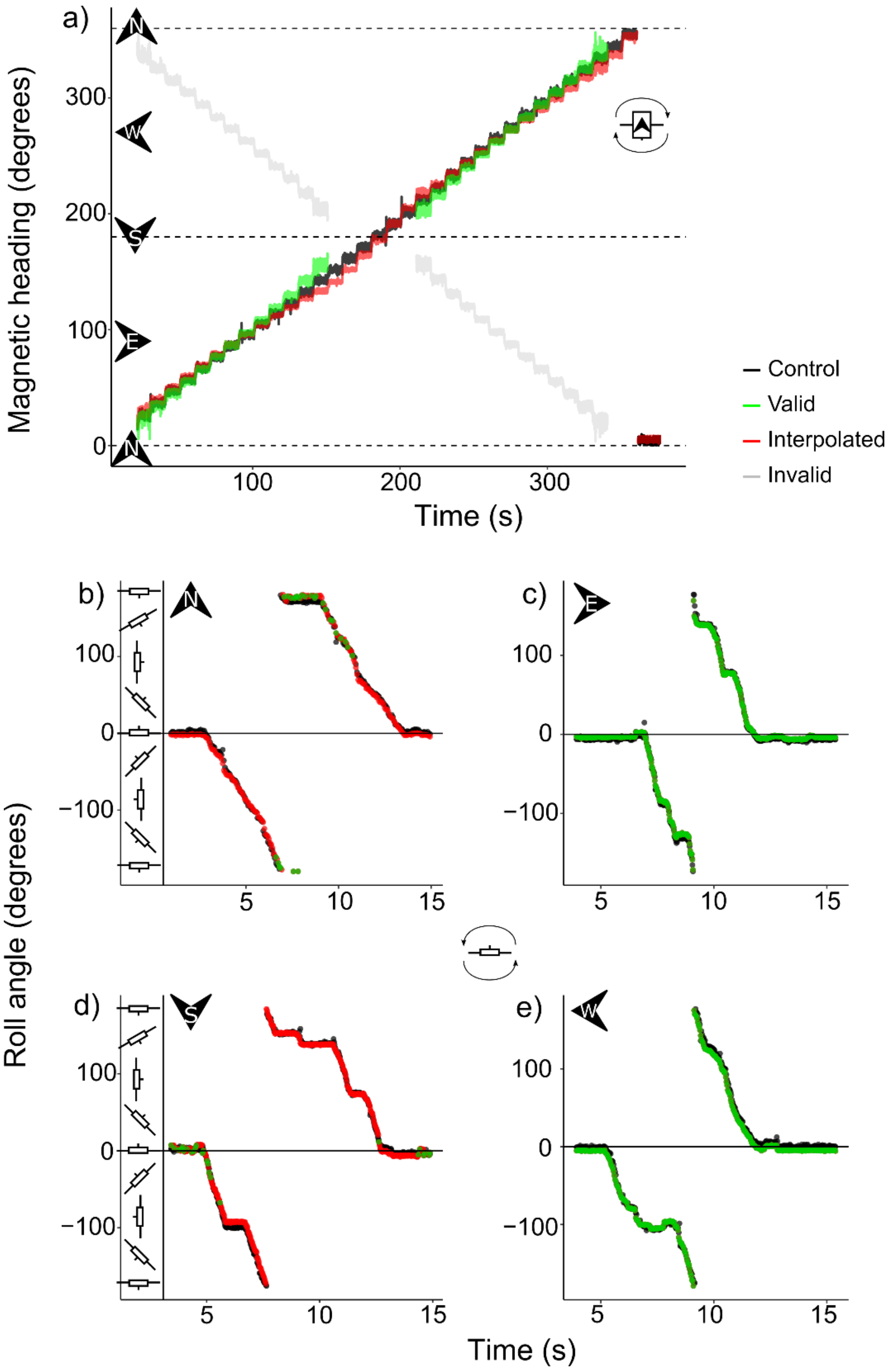

**Figure 4.6**: Control logger *DD₀* results showing performance of the newly described method for estimating yaw and roll from tri-axial magnetometer data. **a)** The two solutions of yaw (see equation 4) showing valid (green) and invalid (grey) angles when performing a compass swing of magnetic heading at 10° increments for constant roll angle (0°). Magnetic north and south are indicated by dashed lines. **b-e)** Roll angle estimated from *DD₀* data at varying magnetic headings (north, east, south, and west) while performing a full rotation of roll angles. Black lines are control angles from accelerometer data compared to valid (green) and interpolated (red; using the closest $\alpha$ value) magnetometer angles.

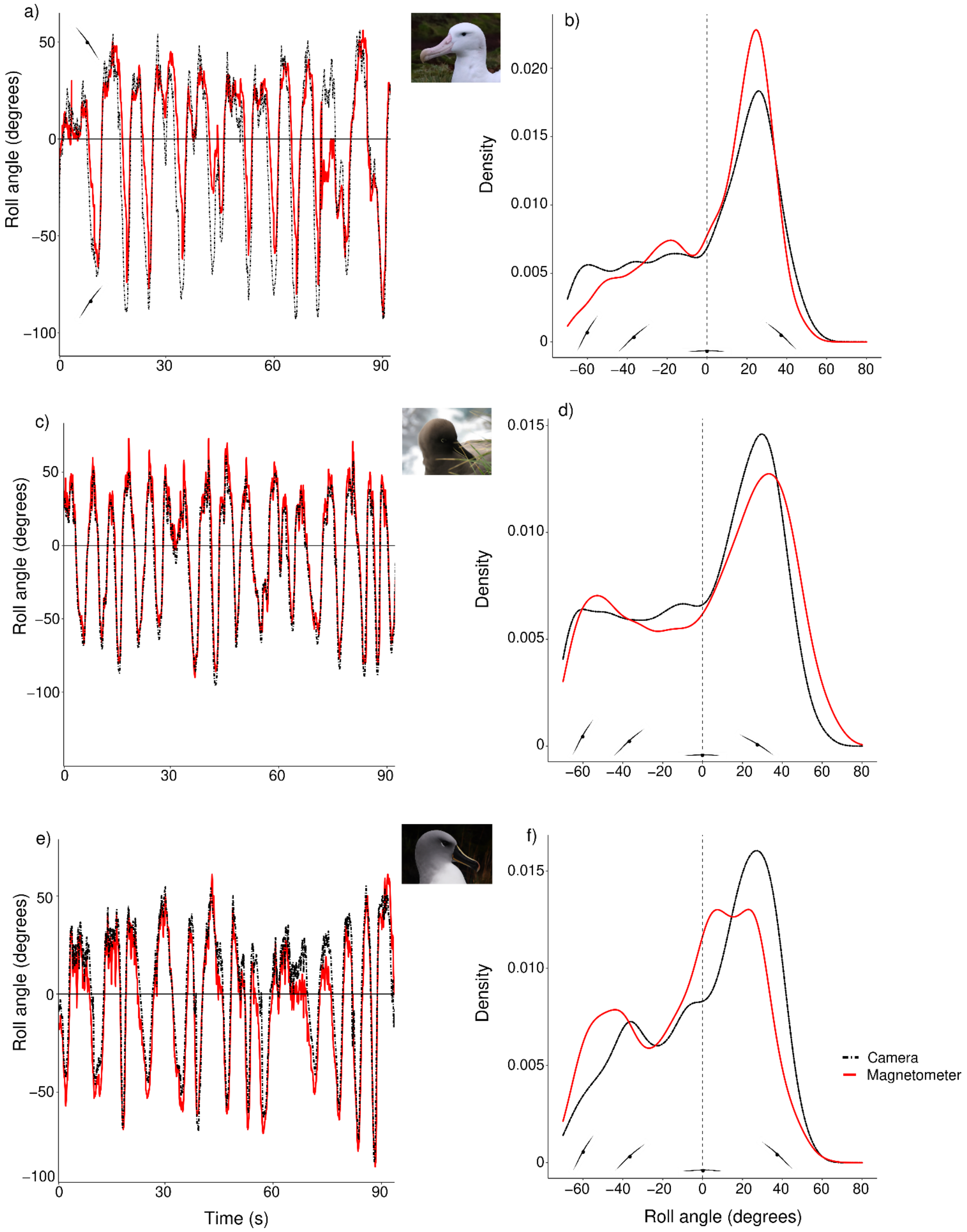

**Figure 4.7:** Examples of roll angle estimates from magnetometer data (red lines) for three albatross species (Wandering, Sooty and Grey-headed Albatross). **a, c, e)** show roll angles from a 90 s flight section while **b, d, f)** are density plots of roll angles for respective species. Control angles were estimated from video loggers (black dashed line) deployed with the magnetometers.

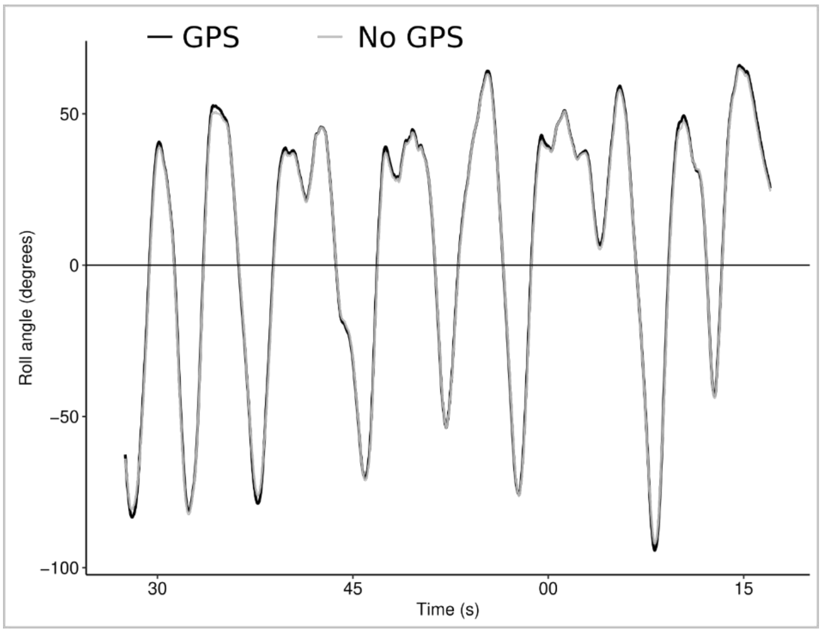

**Figure 4.8:** Roll angles extracted from a 90 s Sooty Albatross flight ~330 km from Marion Island. Roll angles were estimated using reference magnetometer data at GPS locations (5-min interval; black line) and using reference data from a single coordinate (Marion Island; grey line).

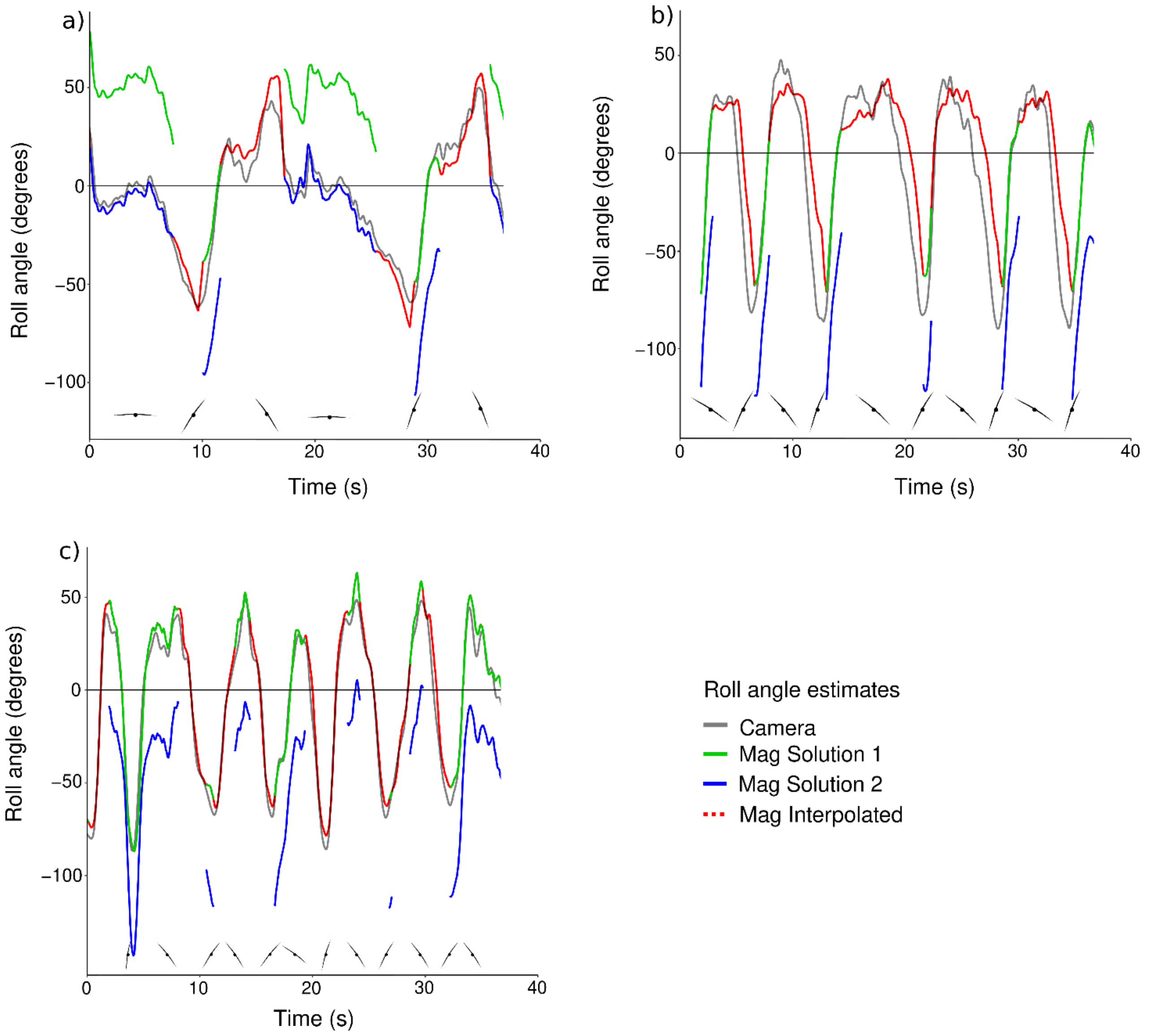

**Figure 4.9:** Examples of roll angle estimates from magnetometer data under varying circumstances. The two possible solutions from equation 4 are shown (green and blue lines) with interpolated values (red lines) where no valid solution was available. **a)** Irregular dynamic soaring cycles where both solutions produce correct values. **b-c)** Regular dynamic soaring cycles with valid roll angles mainly in the turning phases (**b**) or during the ascent/descent phases of the cycles (**c**) with only one correct solution.

## Discussion

Using bird-borne cameras and tri-axial magnetometers proved to be a viable method for fine-scale analysis of seabird flight behaviour. Roll angles were successfully extracted from the video data and were used to validate roll angles estimated from magnetometer data. A substantial amount of flying footage was obtained with the filming intervals used in the present study, but the magnetometers still produced significantly more data over a longer period. Both methods (video and magnetometry) have their own limitations that should be taken into consideration when interpreting results from these technologies. To my knowledge, this is the first study to directly measure the fine-scale bank angle of dynamic soaring seabirds using either video or magnetometry data.

## Video

The horizon extraction algorithm described here worked well for all three albatross species studied and should work equally well for other procellariiforms large enough to carry a camera. However, camera placement can influence the accuracy of the results. If the camera is too far back, the head and body is in the frame. This can be overcome by cropping the images, but this can result in a lot of images where the horizon is absent. However, even if very small cameras were available, they cannot be mounted on the head, because it is clear from the back-mounted footage that albatrosses keep their heads more or less level during flight, and thus head-mounted footage would not record bank angles.

The automated extraction of bank angle performed well compared to manual measurements from the images, with larger observed errors attributed to bad image quality or the presence of objects on the horizon's plane. Here I used manual measurements as a baseline for comparison, but is has to be noted that manual measurements may not always be possible as curvature of the horizon (due to lens effects) and large waves (when the bird is very close to the ocean surface) makes it difficult to measure the horizon angle. Automated extraction overcame these problems in many instances by removing potentially erroneous angles and replacing them with interpolated values. Computer vision techniques have been used to track the posture of a range of animals in a controlled environment (Gomez-Marin et al. 2012), but here it is shown how it is possible for free-ranging animals as well. Detecting the horizon from images is often confounded by irregularities in the images, such as complex environments and particularly when the sun (and its reflections) is present in images (Wang et al. 2009). The horizon detection algorithm performed best in the absence of direct sunlight, but with enough light to differentiate ocean from sky. At twilight, light levels were often too low to accurately detect the horizon. Direct sunlight was only a problem when the sun was directly on the horizon (i.e. sunrise or sunset). White clouds did not hinder the detection of the horizon, but dark cloud banks on the horizon caused problems when they were similar to the ocean colour.

The method used is only one of several options for detecting the horizon in marine environments. Most horizon detection algorithms use Canny edge detection followed by Hough transformation (Duda and Hart 1972) to detect straight lines. However, Hough transformation did not work in my study as the horizon was often distorted as a result of large waves or bad image quality, and using contours proved more effective. A faster method that might allow for real-time analysis of bank-angles utilizes a range of interest (ROI) approach, where the approximate location of the horizon is found, and images are cropped to only use pixels within this ROI (Praczyk 2018). OpenCV proved to be a useful tool for analysing video footage from bird-borne cameras. This open-source software is extremely powerful, well documented and although I used the Python programming language, OpenCV is available for a variety of computer languages.

In the past, footage obtained from animal-borne cameras was mainly considered to be useful in the public domain or for educational purposes with low scientific potential (Moll et al. 2007). However, more recently, video cameras have been used to study the effect of wind on juvenile Brown Booby *Sula leucogaster* flight, by manually measuring bank angle from the horizon as seen in the video frames (Yamamoto et al. 2017). Back-mounted cameras have also been used on captive *Gyps* vultures to study the effect of bank-angle on soaring-flight (Williams et al. 2018) or used in conjunction with accelerometers and ground-based video to estimate the body and tail movement of a Steppe Eagle *Aquila nipalensis* in flight (Gillies et al. 2011).

## Magnetometry

By assuming that dynamic soaring albatrosses do not routinely pitch at large angles during flight, magnetometer data were used effectively to extract yaw and roll angles from three albatross species breeding on Marion Island. Albatrosses observed flying around their breeding colonies or out on the ocean seldom pitch significantly (personal observation). This is also evident from the video data, where the horizon is visible in most of the frames, allowing the extraction of roll angle from the horizon. The yaw angle could then be used to estimate heading by adjusting the value according to the magnetic declination at the given location.

Fine-scale location data were available for all but one (Grey-headed Albatross) of the individuals that were used in the magnetometer validation study. Where tracking data were not available, the deployment location was used, and the roll angle estimates done in this manner still produced acceptable results. The amount of location data that are necessary to extract body angles of dynamic soaring seabirds using magnetometers will depend on the species, location and the questions that are being asked. For example, birds that stay close to their breeding colony for an entire foraging trip will not require additional location data, but birds that traverse ocean basins will need at least some location estimates. The frequency of location data needed will also depend on the range of the bird as the magnetic declination becomes increasingly variable closer to the dip poles (where magnetic inclination is 90°)

which is located at approximately 65° S, 140° W in the Southern Hemisphere. Where accurate heading is necessary, more frequent location estimates (e.g. hourly GPS fixes) are appropriate, but coarse location data (e.g. daily estimates from geolocators) should provide sufficient accuracy to estimate roll angles within a dynamic soaring cycle.

Accelerometers are effective tools to study animal movement but cannot be used to infer the direction of these movements. Using magnetometers to determine the direction of movement of an animal (Noda et al. 2014) and the ability to measure instantaneous heading at high resolution is thus a valuable tool for studying fine-scale animal behaviour. When accurate heading estimates are known, fine-scale movement patterns can be studied by means of dead-reckoning (Wilson et al. 2007, 2008; Bidder et al. 2015). Dead-reckoning has been used to study long distance routes of flying birds (Bramanti et al. 1988; Dall'Antonia et al. 1995). These days, satellite tracking can provide accurate tracks of seabirds' movement spanning days to months, depending on sampling intervals and battery size or even the addition of solar panels (Weimerskirch et al. 2020). Satellite tracking has been used extensively to study the flight behaviour of dynamic soaring seabirds (Weimerskirch et al. 2000; Wakefield et al. 2009; Sachs et al. 2013; Richardson 2015; Gibb et al. 2017), but these studies are limited to inferences from displacement of the birds. Dead-reckoning from magnetometer heading estimates can produce tracks at much finer scales (> 100 Hz) when speed of movement can be inferred (see Chapter 7 for challenges relating to movement speed). Reducing the time between heading estimates increases the accuracy of dead-reckoned tracks and can shed light on the decisions an animal makes prior to certain behaviours (Wilson 2001). Although satellite trackers can now be used on even smaller seabird species, the use of magnetometers to estimate tracks might be a better alternative due to their low power consumption. GPS tracks can give information regarding the course over ground, which is not the same as heading when a bird is flying in variable wind conditions. The heading of a dynamic soaring bird in relation to the wind is important when studying its flying behaviour, but this information is rarely available.

The estimation of roll angles from magnetometer data is equally valuable in providing a new means of studying dynamic soaring flight. Magnetometers have been used to estimate the average bank angle of *Gyps* vultures while soaring in thermals (Williams et al. 2018), or to identify different behavioural states in terrestrial and marine environments, but instantaneous measurements of body angles are usually limited to heading for dead-reckoning studies (Gómez Laich et al. 2008; Williams et al. 2017; Chakravarty et al. 2019). Studies of avian flight that utilises IMU technology are mostly limited to the identification of flapping flight (Williams et al. 2015). Accurate estimates of roll angles are crucial to understand dynamic soaring flight, as it is an integral part of this flight mode (Richardson 2011, 2012; Sachs et al. 2012).

### Limitations and possible solutions

There are several limitations to the above calculations that must be considered before it is applied to any study. Firstly, this method is only applicable to species where it can be assumed that the pitch angle is very small for most of its movement. Secondly, the $\cos^{-1}$ operation in equation 4 will only give an answer when $h_x$ is between -1 and 1. Outlying values can be the result of electronic noise or bad calibration and will result in the inability to calculate yaw and consequently roll angles. Fortunately, data gaps that result from such outliers may be estimated by assuming that $\alpha$ will not change significantly within a short period of time. Then, roll angles can be calculated by substituting $\alpha$ from previous reliable estimates into equation 5. Thirdly, if both $H_y$ and $H_z$ are zero (yaw coincides with magnetic north) the outcome of equation 5 is undefined, which will also be the case on the magnetic equator where this method will not work. In general, whenever a bird is flying in the same direction as the magnetic field, the entire magnetic field is only measured on the x-axis and it becomes impossible to infer roll angle. Finally, the $\cos^{-1}$ operation in equation 4 will result in two valid solutions (and consequently two solutions for $\phi$), but only one of them will represent the rotation of the magnetometer axes. There are two ways to determine which of the solutions is correct. First, if positional data are available (e.g. GPS positions), the average yaw angle can be compared to the average heading for a specific section of flight to determine which is correct (but bearing in mind the effects of wind drift). Second, if the flight behaviour of a study species results in frequent changes in roll angle (such as the case for dynamic soaring seabirds), the solution with the lowest average roll angle will be the correct one. It must be noted that the accuracy of the above calculations relies on the quality of the calibration and how well the hard- and soft-iron offsets are accounted for. Additionally, the calibration values might have to be adjusted for deployments spanning several days where individuals are subjected to varying magnetic field intensities. Future studies could use IMUs that include accelerometers, magnetometers and gyroscopes to estimate accurate body angles for several seabird species. These data could then be used to determine the efficacy of the methods described in the present study for seabirds ranging in body size and flight modes.

## Conclusions

The fine-scale study of dynamic soaring flight in seabirds has mainly been done by looking at trajectories of flight from location estimates. IMUs provide new methods to study animal movement, but they currently rely heavily on the use of accelerometers, which have limited use for the study of dynamic soaring flight due to the increased centripetal acceleration produced by this flight mode. This chapter presents two new methods of body angle extraction from bird-borne video cameras and tri-axial magnetometers that are not affected by the large changes in acceleration experienced by dynamic soaring seabirds. The video data were automatically processed using computer vision algorithms, drastically reducing the time needed to analyse the video data (that is often done manually). The magnetometer data could be used to estimate the yaw and roll angles of three albatross species while dynamic soaring in the southern Indian Ocean surrounding Marion Island, validated by roll angles extracted from the video loggers. The high energy demand of video cameras currently limits their use in seabird behavioural studies, but the present study shows how bird-borne cameras can be used as an effective tool to validate estimates from other bio-logging devices. These methods provide new tools for the analysis of bio-logging data that will provide new insights into the dynamic soaring flight mode of seabirds. This is particularly relevant for seabirds in the Southern Ocean, where changing wind patterns could have significant effects on their behaviour (Clay et al. 2020).

# Supplementary material

This supplementary section provides a detailed explanation of the calculations performed to estimate yaw and roll angles from a tri-axial magnetometer in Chapter 4.

The values recorded by a tri-axial magnetometer can be presented as a rotation in terms of the known magnetic field at its location:

$$H_{xyz} = D_{NED}^{xyz} H_{NED} \tag{1}$$

where $H_{xyz}$ are the values measured by the tri-axial magnetometer, $D_{NED}^{xyz}$ is the directional cosine matrix (DCM) from the north east down (NED) axis system to the xyz axis system, and $H_{NED}$ is the magnetic vector as given by the World Magnetic Model (WMM2020; https://www.ngdc.noaa.gov/geomag/WMM/DoDWMM.shtml). Equation (1) can be shortened by calling the xyz system $b$ (body axes) and the NED system $i$ (inertial axes):

$$H_b = D_i^b H_i \tag{2}$$

$D_i^b$ is the resultant 3 x 3 matrix when the rotation matrices around each separate axis ($R_{xyz}$) are multiplied with each other (yaw-pitch-roll order), where the yaw pitch and roll angles are $\varphi$, $\theta$ and $\phi$, respectively.

$$R_z(\varphi) = \begin{bmatrix} cos\varphi & sin\varphi & 0 \\ -sin\varphi & cos\varphi & 0 \\ 0 & 0 & 1 \end{bmatrix} \tag{3}$$

$$R_y(\theta) = \begin{bmatrix} cos\theta & 0 & -sin\theta \\ 0 & 1 & 0 \\ sin\theta & 0 & cos\theta \end{bmatrix} \tag{4}$$

$$R_x(\phi) = \begin{bmatrix} 1 & 0 & 0 \\ 0 & cos\phi & sin\phi \\ 0 & -sin\phi & cos\phi \end{bmatrix} \tag{5}$$

When $R_z$ is left-multiplied by $R_y$ and the result is multiplied by $R_x$, we get:

$$D_i^b = \begin{bmatrix} cos\theta cos\varphi & cos\theta sin\varphi & -sin\theta \\ sin\phi sin\theta cos\varphi - cos\phi sin\varphi & sin\phi sin\theta sin\varphi + cos\phi cos\varphi & sin\phi cos\theta \\ cos\phi sin\theta cos\varphi + sin\phi sin\varphi & cos\phi sin\theta sin\varphi - sin\phi cos\varphi & cos\phi cos\theta \end{bmatrix} \tag{6}$$

In equation (2), $H_b$ and $H_i$ are both vectors and can thus also be written as:

$$\begin{bmatrix} H_x \\ H_y \\ H_z \end{bmatrix} = D_i^b \begin{bmatrix} H_N \\ H_E \\ H_D \end{bmatrix} \tag{7}$$

Using equation (6), equation (7) can be expanded to:

$$\begin{bmatrix} H_x \\ H_y \\ H_z \end{bmatrix} = \begin{bmatrix} cos\theta cos\varphi H_N & +cos\theta sin\varphi H_E & -sin\theta H_D \\ (sin\phi sin\theta cos\varphi - cos\phi sin\varphi)H_N & +(sin\phi sin\theta sin\varphi + cos\phi cos\varphi)H_E & +sin\phi cos\theta H_D \\ (cos\phi s\theta cos\varphi + sin\phi sin\varphi)H_N & +(cos\phi sin\theta sin\varphi - sin\phi cos\varphi)H_E & +cos\phi cos\theta H_D \end{bmatrix} \tag{8}$$

From equation (8) it is apparent that at least two known angles are required per axis in order to calculate the third angle. Thus yaw, pitch and roll can't be calculated with only $H_b$ and $H_i$ as known values. Without additional information, the only way forward is to make certain assumptions. For the purpose of this study, I assume that soaring birds do not pitch significantly, which is a reasonable assumption given personal observation of several albatross species in flight. If the pitch angle $(\theta) = 0$, $sin\theta = 0$ and $cos\theta = 1$, and equation (8) can be simplified to:

$$\begin{bmatrix} H_x \\ H_y \\ H_z \end{bmatrix} \doteq \begin{bmatrix} cos\varphi H_N & +sin\varphi H_E & 0 \\ -cos\phi sin\varphi H_N & +cos\phi cos\varphi H_E & +sin\phi H_D \\ sin\phi sin\varphi H_N & -sin\phi cos\varphi H_E & +cos\phi H_D \end{bmatrix} \tag{9}$$

## Yaw angle calculation

We can get $\varphi$ from the first row in equation (9) and, by substituting $\varphi$ into the second and third rows, we can calculate $\phi$ by solving these equations simultaneously. These equations are solved by first mapping the $H_N$ and $H_E$ values to a unit circle, so that they can be normalized according to the radius of the circle ($\sqrt{(H_N^2 + H_E^2)}$ denoted as $\|H_{NE}\|_2$) and expressed as sine and cosine terms of a single angle ($\beta$), which is the magnetic declination angle (Figure S4.1).

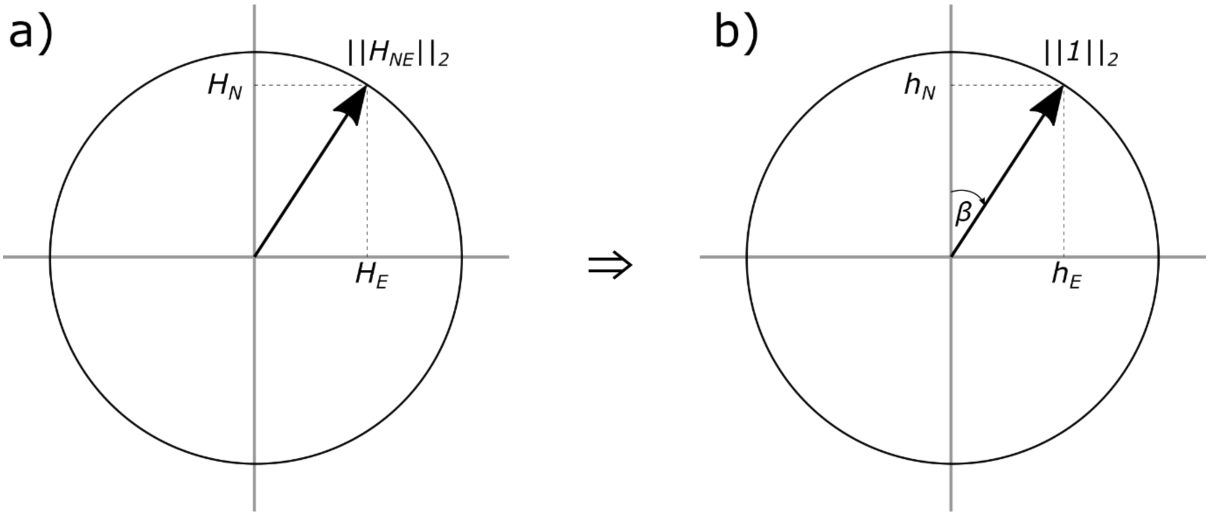

**Figure S4.1: a)** The N and E axes of the reference magnetic field is mapped to a unit circle with radius $\|H_{NE}\|_2$ and **b)** normalized by dividing by this radius, where $\beta$ will represent the magnetic declination angle.

This angle is chosen to be an angle from the North axis as this is the conventional definition of the magnetic declination angle. Thus,

$h_N = H_N / \|H_{NE}\|_2$ and

$h_E = H_E / \|H_{NE}\|_2$ so that

$\beta = \tan^{-1}(h_E/h_N)$, ultimately allowing the first row of equation (9) to be rewritten as:

$$\frac{H_x}{\|H_{NE}\|_2} = h_x = cos\varphi cos\beta + sin\varphi sin\beta \tag{10}$$

Which simplifies to:

$$\varphi = \pm\, cos^{-1}(h_x) + \beta \tag{11}$$

The loss of sign implied in the $cos^{-1}$ operation is unavoidable, thus resulting in two possible solutions, which are discussed in the main text of Chapter 4.

## Roll angle calculation

To calculate the roll angle $\phi$, the same procedure is followed as above with the resultant values from the above calculations substituted into the second and third rows of equation (9). Note that $\phi$ is solvable for both the second and third lines of equation (9) on their own, but this again results in ambiguous answers. However, if both these equations are solved simultaneously, a single value is returned. Substituting the resultant values into the second and third rows of equation (9) simplifies to:

$$H_y = -cos\phi \|H_{NE}\|_2 sin(\varphi - \beta) + \; sin\phi H_D \tag{12}$$

$$H_z = \; sin\phi \|H_{NE}\|_2 sin(\varphi - \beta) + \; cos\phi H_D \tag{13}$$

For both equations (12) and (13) $\|H_{NE}\|_2 sin(\varphi - \beta)$ and $H_D$ can be mapped to a unit circle and the radius used for normalization ($\sqrt{(H_N^2 + H_E^2) sin^2(\varphi - \beta) + \; H_D^2}$) here will be referred to as $\|H_{NED'}\|_2$ (Figure S4.2).

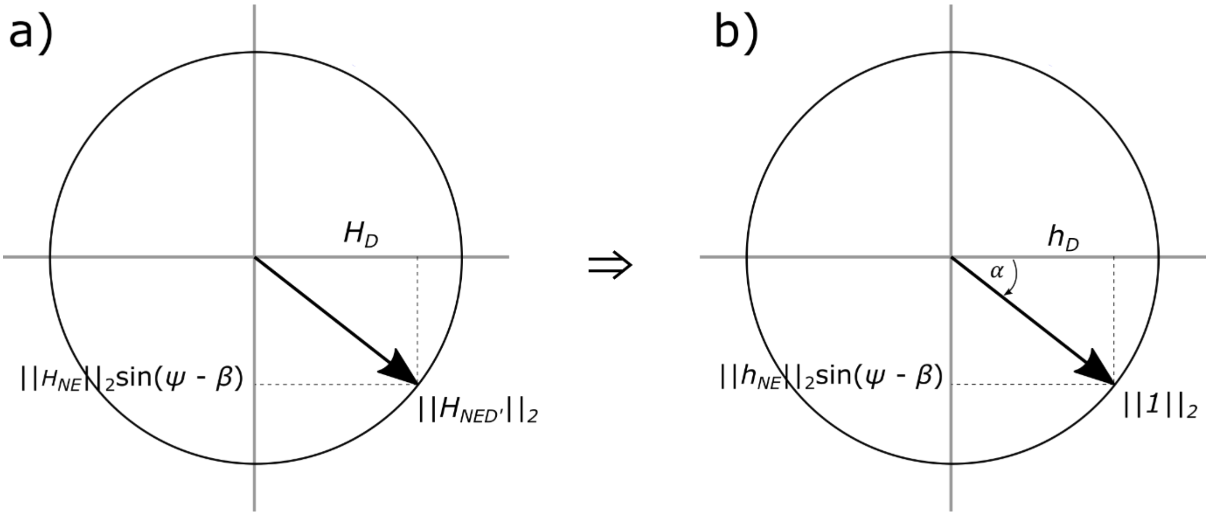

**Figure S4.2: a)** Representation of the unit circle where the axes $H_D$ and $\|H_{NE}\|_2 sin(\varphi - \beta)$ has a radius $\|H_{NED'}\|_2$ and **b)** normalized by dividing by $\|H_{NED'}\|_2$, where $\alpha$ is measured from $H_D$. Note that the bottom hemisphere is positive due to the NED axis convention.

This time the angle ($\alpha$) is calculated from the z-axis (positive down axis) so that:

$$\alpha = \; \tan^{-1}\left( \left( \|H_{NE}\|_2 sin(\varphi - \beta) \right) / H_D \right) \tag{14}$$

Now, when $H_y$ and $H_z$ are normalized by $\|H_{NED'}\|_2$. the resultant equations are:

$$h_y = sin(\phi - \alpha) \tag{15}$$

$$h_z = cos(\phi - \alpha) \tag{16}$$

And finally, by dividing $h_y$ by $h_z$, the roll angle can be calculated by applying a four-quadrant tan$^{-1}$ operation while preserving the sign:

$$\phi = \tan^{-1}\left(\frac{H_y}{H_z}\right) + \alpha \tag{17}$$

Note that, because the same normalization factor is used in both $h_y$ and $h_z$ calculations, the original $H_y$ and $H_z$ values can be used in the final equation (17).

# Chapter 5: Wandering around the Southern Ocean: fine-scale description of Wandering Albatross flight using a multisensor approach

## Abstract

Wandering Albatrosses are among the largest flying birds. Their highly energy-efficient dynamic soaring flight allows them to travel large distances by exploiting the gradient in wind strength above the sea surface. The topic of dynamic soaring flight has received increased attention in recent years, with the advancement of bio-logging technology providing new insights into this flight mode. Dynamic soaring can be defined as a cycle consisting of 1) a windward climb, 2) a turn with the wind, 3) a leeward descent, and 4) a turn into the wind to restart the climb. However, the exact means of energy gain from this cycle is still contentious. I use bio-logging devices to study the dynamic soaring flight behaviour of Wandering Albatrosses. Roll (bank) angles are derived from video and tri-axial magnetometers, and flapping events from tri-axial accelerometers. The birds flew mostly in westerly winds coming from their left during outbound flights from their breeding colonies and from their right when returning. They compensated for wind speed by varying their roll angles and predominantly turning into the wind, resulting in a net displacement that was perpendicular to the wind. Flapping flight was influenced by wind speed, with birds spending more time flapping in light winds and in head winds. Combining roll angles and flapping data, I show that flapping occurred at the upper turn of the dynamic soaring cycle, a stage previously considered devoid of flapping. Although the results were only marginally significant, there were some evidence of sexual differences in flight behaviour of Wandering Albatrosses, with females flapping less than males. However, males possibly differ from females during take-off, with males almost exclusively taking off into head winds, while females utilized cross winds as well. These results add new perspectives to our knowledge of dynamic soaring and show how the birds react to their dynamic environment at a fine scale.

## Introduction

Wandering Albatrosses are among the largest flying birds and have the largest wingspan of extant birds (Tickell 2000). They can cover thousands of kilometres in a single foraging trip, making them one of the widest ranging pelagic seabirds (Jouventin and Weimerskirch 1990; Weimerskirch and Wilson 2000; Mackley et al. 2010; Weimerskirch et al. 2012, 2014). This is achieved by spending extended periods in flight, with bouts lasting up to 17 hours (Weimerskirch et al. 1997; Mackley et al. 2010). In general, Wandering Albatrosses land less frequently than smaller albatrosses (Phalan et al. 2007) and breeding birds either forage throughout long looping trips or direct flights to specific foraging areas (Weimerskirch et al. 1997). Female Wandering Albatrosses take off in lighter winds than males (Clay et al. 2020), suggesting that males avoid landing in light winds where they might have increased energetic costs when taking off again.

The heart rates of flying Wandering Albatrosses are often only slightly elevated above resting rates, with lowest rates when ground speed is high (Weimerskirch et al. 2000). To achieve such energy efficient flight, Wandering Albatrosses minimize flapping and favour gliding flight (Pennycuick 1982). Flapping flight is an expensive flight mode for large soaring birds (Alerstam et al. 1993; Weimerskirch et al. 2000; Williams et al. 2020a) and Wandering Albatrosses follow flight strategies that limit energy expensive take-offs, especially in light winds (Mackley et al. 2010). They are more prone to take-off when favourable wind conditions arise and adjust their flight patterns in changing wind conditions (Clay et al. 2020). Like most procellariiform species, Wandering Albatross flight is centred around the wind, where the birds utilize dynamic soaring as a means of low-energy flight (Pennycuick 1982; Weimerskirch et al. 2000, 2012; Sachs 2005; Richardson 2011; Sachs et al. 2012).

In the past two decades, our knowledge of dynamic soaring flight has increased substantially, largely due to advances in bio-logging technology providing accurate, fine-scale (1–10 Hz) location estimates for extended periods of albatross flight (Weimerskirch et al. 2002; Sachs et al. 2012, 2013). Such data have shown that dynamic soaring consists of sequential cycles, each lasting 10–15 s (Sachs 2005; Richardson 2011; see Figure 4.1). The leeward turn is pivotal for dynamic soaring (Sachs et al. 2013), and upwind flight is possible through variations of tacking flight modes (Sachs 2016; Richardson et al. 2018). There is much debate regarding the exact means of energy gain from dynamic soaring (Richardson 2011; Sachs et al. 2012, 2013), but flapping flight is usually excluded as a means of energy gain (Sachs et al. 2013).

Direct observations of flying albatrosses confirm that they seldom flap, but occasionally flap-glide in light winds (Pennycuick 1982; Spear and Ainley 1997; Richardson 2011). Initial studies using bird-borne heart rate monitors suggested that flapping flight in Wandering Albatrosses is mainly limited to take-off and landing events (Weimerskirch et al. 2000; Shaffer et al. 2001a). More recently, accelerometers have shown that albatrosses have two flapping modes, with higher flapping frequencies during take-off as opposed to cruising flight (Sato et al. 2009). These studies highlight the complexity of seabird flight and how new technologies can improve our understanding of these processes. In recent years, the use of IMUs (including accelerometers and magnetometers) have been extended from the study of marine mammals and penguins, to include flying birds (Wilmers et al. 2015). These have mainly been limited to identify flapping flight (oscillations of the vertical accelerometers axis around 1 *g*; Gómez Laich et al. 2008; Shepard et al. 2008), but more recently magnetometers have been used to study body/wing angles of thermal soaring birds (Williams et al. 2018, 2020a).

Although body angle (roll/bank angle) is often mentioned in dynamic soaring studies (Sachs 2005; Richardson 2011; Sachs et al. 2013) there have been no direct measurements of such angles. A change in roll angle is an important aspect of the dynamic soaring process as it determines the rate at which the birds turn and consequently the direction in which they fly. Likewise, although it has been inferred that flapping is not part of dynamic soaring flight (Sachs et al. 2013), flapping has not been explicitly quantified in conjunction with the dynamic soaring cycle. Here I show how magnetometer-derived roll angles can be used to add to our knowledge of albatross dynamic soaring flight. I use video loggers and IMUs to estimate roll angles of Wandering Albatrosses (Chapter 4), which can then be used to identify individual dynamic soaring cycles. The IMUs are also used to identify individual flaps, which can be matched to different elements of the dynamic soaring cycle to provide new insights into the flight mechanics of albatrosses and how they manage to fly in a dynamic environment.

## Methods

To study the fine-scale flight behaviour of Wandering Albatrosses, I used data collected from 33 individuals breeding on Marion Island between 2016 and 2020. The devices and methods used during deployment are detailed in Chapter 2. In short, a combination of GPS, video camera, and daily diary (DD) loggers were deployed on the backs of the birds in a straight line, except for eight individuals where the DD was attached to 4–5 tail feathers (see Results Table 5.1). DD loggers deployed in 2017 had a small magnet in a silicone paddle attached to the casing of the logger to estimate airspeed, but these data were not used in the current study. GPS loggers provided location estimates at varying intervals ranging from 1 s to 60 min but were re-discretized at 60-min intervals to conform to the lowest sampling rate. Hourly GPS locations were deemed acceptable it was the same resolution as the wind data (see below) and Chapter 4 showed that coarse location estimates were appropriate for magnetometer-derived metrics. The GPS locations were linked to hourly wind data at 10 m a.s.l. from the European Centre for Medium Range Weather Forecasts (ECMWF) ERA5 reanalysis dataset (Hersbach et al. 2018). The ERA5 dataset comprises zonal and meridional wind speed components at a spatial resolution of 0.25° (which equates to 27 km latitudinally and 16–23 km longitudinally within the range of the tracked birds). The wind speed components were used to calculate wind speed and direction using the *uv2ds* function from the R-package *rWind*. The relative flight course for each GPS location was calculated as the difference between GPS course and wind direction and was classified into three wind types so that the absolute relative course was: 1) ≤ 45° for tail winds, 2) between 45° and 135° for cross winds, and 3) ≥ 135° for head winds. GPS-derived data were temporally matched with the DD data, using the closest location where exact matches were not possible. Metrics derived from the DD loggers were averaged for each GPS-hour (i.e. individual track points) when comparisons were made with environmental variables. The camera data were also temporally matched to the DD data, and visual inspection of roll angles (from both DD and video loggers) allowed for exact matching of the data at infrasecond resolution.

## Flight isolation

For the purpose of this study, I limited the data collected to in-flight data. This was initially done by visual inspection of the data using custom software for the DD loggers (DDMT, Wildbytes, http://wildbytetechnologies.com/research.html). The dynamic soaring nature of albatross flight produces a repeated pattern in tri-axial magnetometer data during flight, which can be easily identified through visual inspection (Figure 5.1a). Additionally, the increased centripetal forces experienced by the birds during dynamic soaring results in a distinct tri-axial accelerometer pattern, where the mean vertical axis ($A_Z$ – the heave axis) follow the cyclical pattern of the magnetometer data, while the remaining two axes (longitudinal axis – $A_X$, latitudinal axis – $A_Y$) stay relatively constant (Figure 5.1b).

Visual inspection allows the simultaneous interpretation of multiple data streams and can be an effective means of filtering data, but it is time-consuming and not practical for very large data sets. I tested how well automated extraction of flight periods would work by following the approach of Collins et al. (2015) to identify periods of flight by examining frequency histograms of accelerometer data. Density histograms of standard deviation (SD) $A_Z$ (over 10 s) were produced for each individual bird. The histograms were examined and where a bimodal distribution was present a threshold value (minimum frequency between peaks) was chosen for standard deviation($th_{SD}$) values. Where > 2 modes were present in the distributions, the minimum between the largest two modes were chosen. Flying periods were then identified where SD $A_Z$ over 10 s > $th_{SD}$. The 10-s smoothing interval was chosen because the mean dynamic soaring cycle duration for Wandering Albatrosses is ~10 s (Richardson 2011; Sachs et al. 2012). Time gaps < 60 s in flight periods were removed and flights < 60 s also were disregarded. This resulted in the exclusion of short periods on the water and very short flights, but this was deemed acceptable for the scope of the study as the emphasis is on flying behaviour in general and Wandering Albatrosses do not land frequently (Weimerskirch et al. 1997). The above was done to evaluate the efficacy of using an automated approach to separate flying from non-flying data in future studies and the analyses and averages reported in this chapter (Chapter 5) were from periods separated by visual inspection and included flights < 60 s.

To analyse the effect of wind on take-off events, the first 10 s of every flight was isolated. The total number of flaps (see below) and mean instantaneous heading (derived from magnetometer data, see Chapter 4) during take-off was compared to the wind speed and direction at the nearest GPS location.

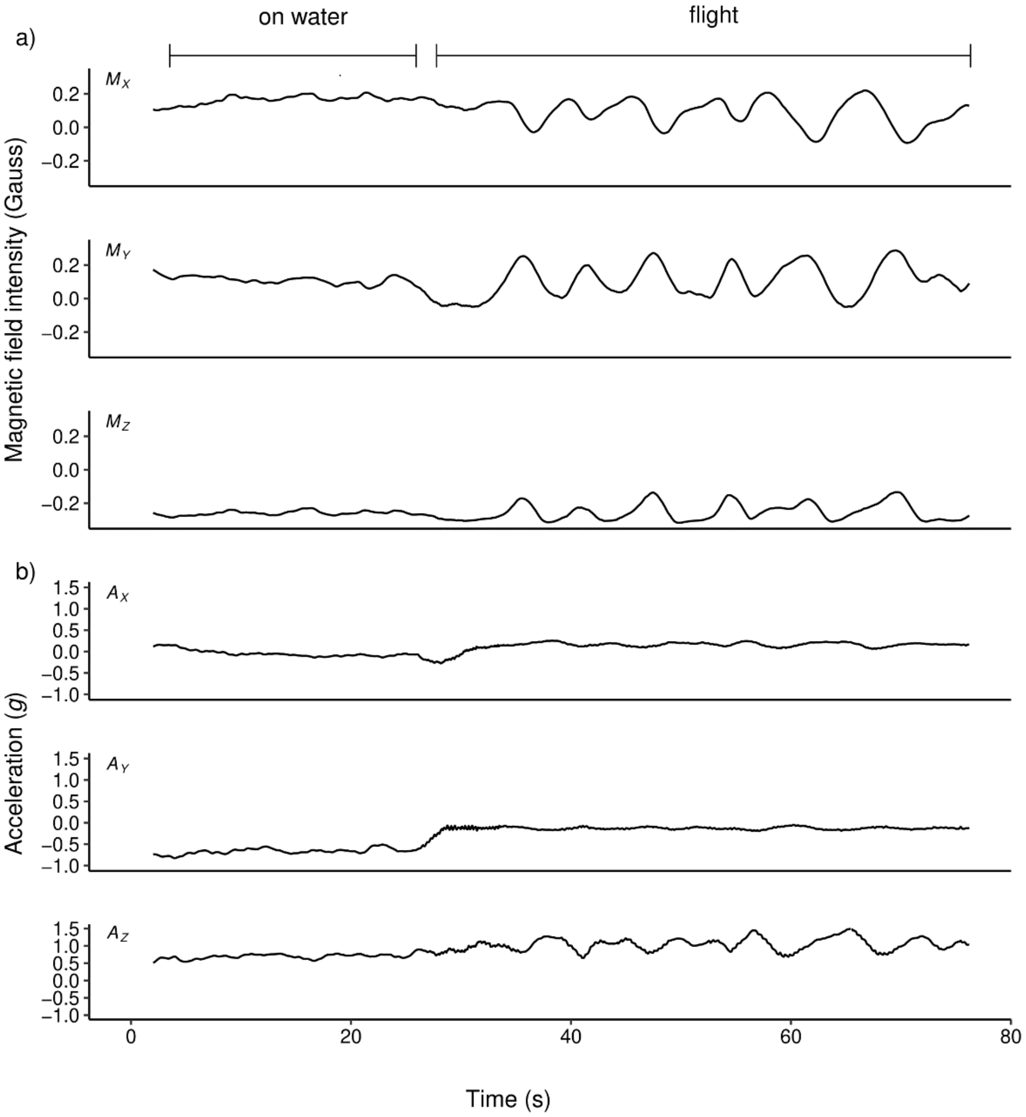

**Figure 5.1:** Data traces (smoothed over 60 s) showing tri-axial **a)** magnetometer ($M_{XYZ}$) and **b)** accelerometer ($A_{XYZ}$) data from a sequence showing the take-off from the water by a Wandering Albatross.

## Dynamic soaring cycles

Roll angles (rotation around the longitudinal axis) were estimated for Wandering Albatross flight from DD and video logger data, as described in Chapter 4. Accurate roll angles could not be estimated from the 2017 deployments because the windspeed paddle magnet interfered with the calibration of the magnetometer axes. However, the relative roll angles could still be used to estimate the shape of the dynamic soaring cycle. This was done by normalizing the roll angles and then identifying the turns in the dynamic soaring cycle (see below). Tail-mounted DD loggers were not effective at estimating soaring cycles because tail movement is independent of body roll when birds turn with steep bank angles (Gillies et al. 2011). The roll angles were smoothed with a 1-s running mean to remove outliers. Peaks in roll angles were identified as points where the slope changed from positive to negative (right turn) or *vice versa* (left turn), where a right turn peak had to be followed by a left turn peak to be valid (Figure 5.2). Peaks within 2 s of each other were disregarded as a typical dynamic soaring cycle generally lasts ~10 s (Richardson 2011; Sachs et al. 2012). The number of cycles per 1 min of flight was summed for each flight. Additionally, the accelerometer data from the DD loggers were used to estimate the centripetal force experienced by the birds during flight. This was done by first calculating the vector sum of static body acceleration (VeSBA), where the static component of each of the three axes was calculated by applying a rolling mean of 2 s on each axis respectively and subtracting 1 $g$ (Williams et al. 2015). The vector sum of the static components of an accelerometer should be 1 $g$ as a result of gravity and where VeSBA > 1 $g$ it indicates increased centripetal forces experienced by the birds.

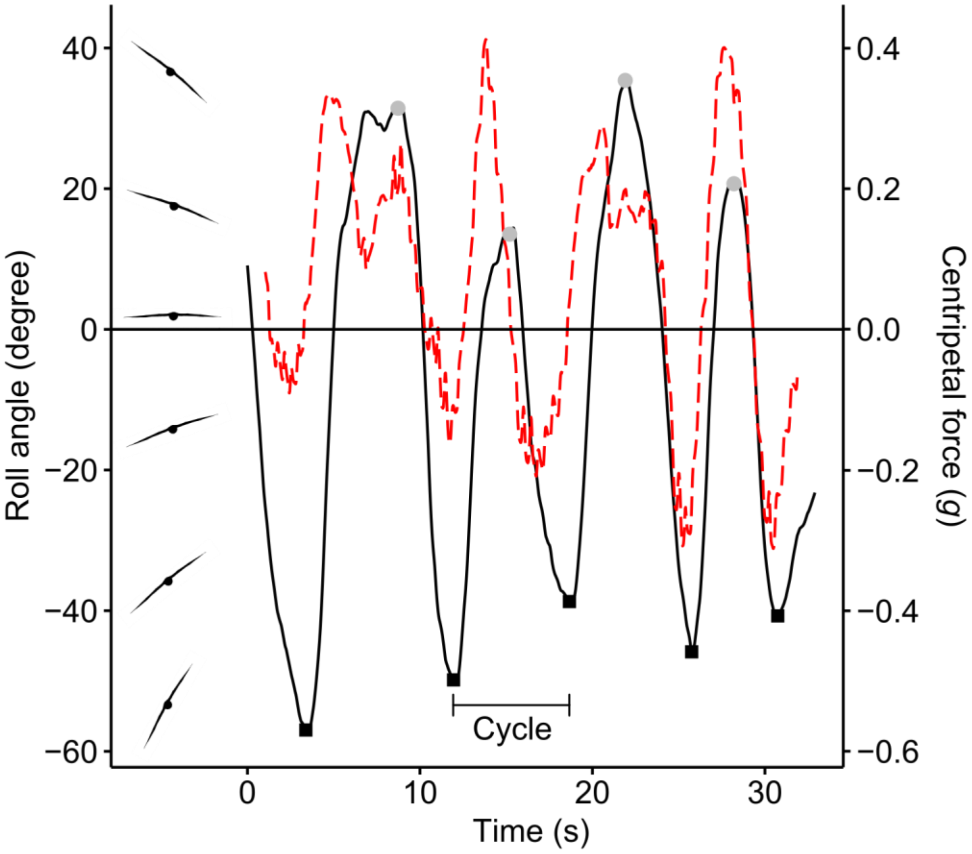

**Figure 5.2:** Identification of dynamic soaring cycles from roll angles extracted from a video logger on a Wandering Albatross. Data between positive (grey circle – right turn) or negative (black square – left turn) pulses are counted as individual dynamic soaring cycles. Red dashed line shows the centripetal acceleration (*g*) calculated from the accelerometer data.

## Flap identification

Data from the tail-mounted loggers ($n$ = 7) were excluded from the analysis of flapping flight as these loggers were not aligned with the birds' centre of gravity. Flaps were identified as pulses in the $A_Z$ data. These peaks were isolated following Lotz & Clilverd (2019) using a type of band-pass filter (based on LULU operators) to isolate downward pulses within a range of bandwidths ($k$ – lower limit, $m$ – upper limit). This method identifies peaks purely based on the duration of the pulse, regardless of intensity. Pulses below a chosen threshold ($th_{flap}$) were subsequently labelled as flaps (Figure 5.3), while ignoring pulses that were < $m/2$ apart. The $th_{flap}$ value was chosen by plotting the total number of flaps isolated while incrementing $th_{flap}$ by 0.1 $g$ (range -2 $g$ to 0 $g$), while keeping $k$ and $m$ constant at 40 Hz (sampling frequency of DD) and 3 Hz (Wandering Albatross flapping frequency; Sato et al. 2009), respectively. Where the slope of the plots started levelling out (Figure 5.4a), the corresponding $th_{flap}$ was chosen for each individual bird. Next, the optimal $m$ value was chosen for each individual as above, by incrementing $m$ by 1 sample unit (range 1–20 sample units, i.e. 2–40 Hz) while keeping $k$ at 1 sample unit (40 Hz) and $th_{flap}$ at the value chosen in the previous step. Again, the $m$ value that corresponded to the point where the slope started levelling out was chosen (Figure 5.4b). Random sections of flight were visually inspected for each individual to see if the identified flaps seemed plausible. To estimate the time spent flapping, the flight data were rounded to 1-s intervals and each 1-s interval with at least one flap was labelled as *single flaps* while intervals with > 2 flaps were labelled as *sequential flaps*. These intervals were presented as percentages of the total flight duration. The vector sum of dynamic body acceleration (VeDBA) was used to estimate flapping intensity. The dynamic component of the accelerometer axes was calculated by subtracting the static component (see above) for each respective axis, before performing the vector sum (Qasem et al. 2012).

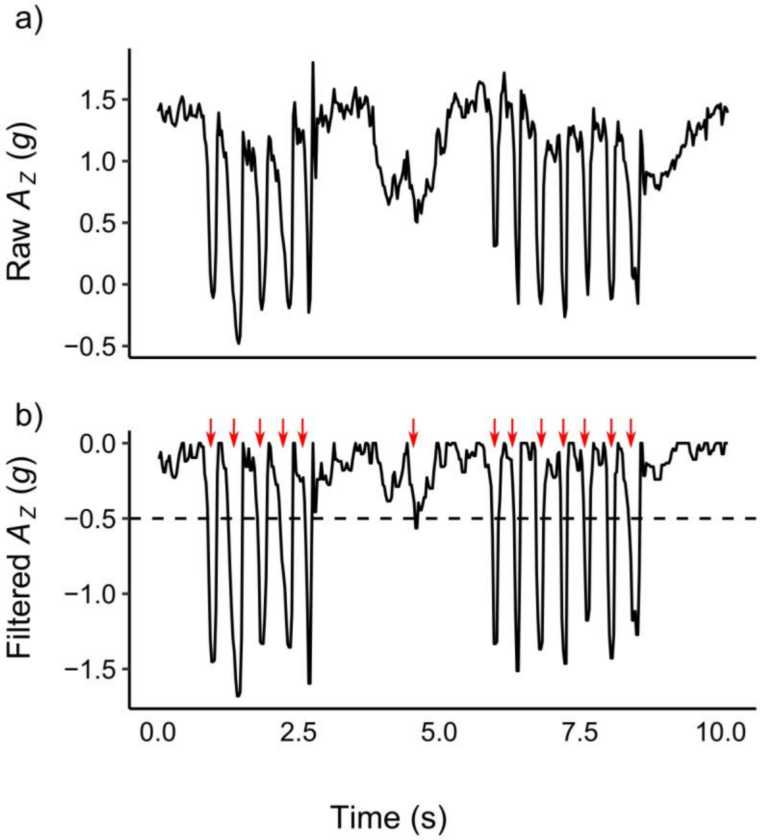

**Figure 5.3:** Isolation of flaps (red arrows) from the vertical accelerometer axis ($A_Z$) showing how a) the raw data were b) filtered and minimum values below a threshold (dashed line) were used to identify individual flaps.

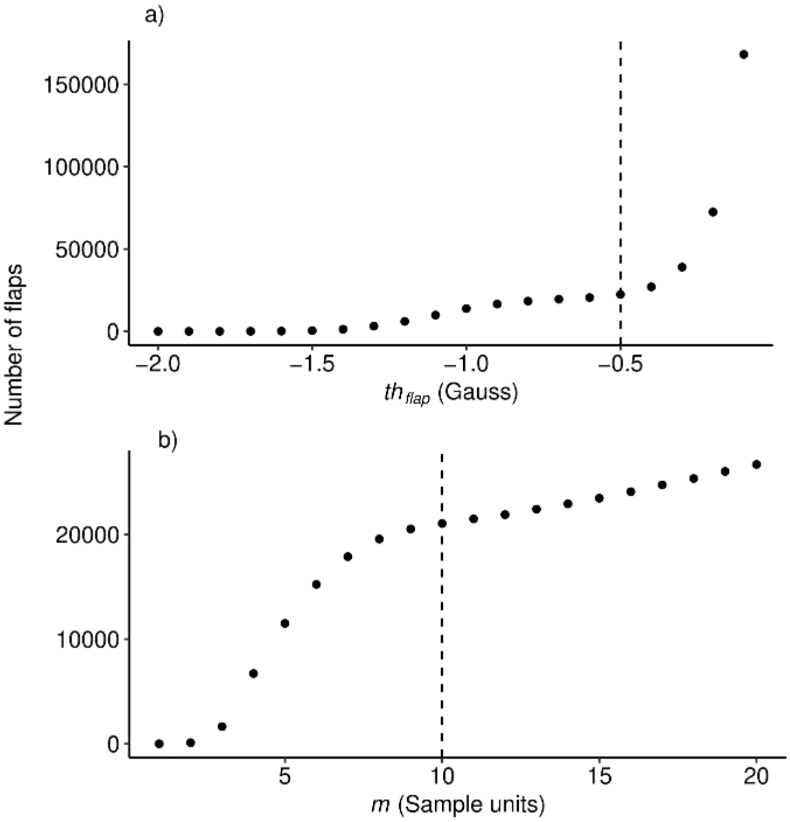

**Figure 5.4:** Example of how parameters **a)** $th_{flap}$ and **b)** *m* values were chosen for flap identification from a Wandering Albatross individual. The dashed lines represent the chosen value for each parameter.

To test for significant differences in means (reported as mean ± SD unless otherwise stated) between groups, two-sample *t*-tests were used, or Wilcoxon rank-sum tests were used when normality of the data could not be attained. A non-parametric generalised additive model (GAM) was used to show the relationship between flapping intensity and centripetal forces (*g*) as well as the relationship between flapping flight and wind speed. This was done using a penalised cubic regression spline with the smoother function *s* in the R package *mgcv* (Wood 2011). All statistical analyses were performed in the R software environment (R Development Core Team 2018).

## Results

All but one of the 33 loggers were retrieved with useful DD data from 19 individuals (Table 5.1); the remaining 14 birds had devices that did not record any data or ran out of battery charge before the birds left their nests. All the valid DD deployments had accompanying location data from GPS loggers and eight individuals had overlapping video data during flight (Table 5.1).

**Table 5.1:** Summary of Daily Diary (DD) data recorded from 19 breeding Wandering Albatrosses on Marion Island between 2016 and 2020. Values are averages across flights per individual unless total values are stated.

| | | | | | **Flights** | | | | **Dynamic soaring** | | **Flapping** | | | |
|---|---|---|---|---|---|---|---|---|---|---|---|---|---|---|
| **ID** | **Date** | **Sex** | **Video total dur. (min)** | **Total dur. (hr)** | **Auto flight accuracy (%)** | **Total manual flights (automated)** | **Flights per day** | **Flight dur. (s)** | **Cycles per minute** | **Cycle dur. (s)** | **Flaps per minute** | **Flapping intensity (*g*)** | **Single flap (% of flight)** | **Sequential flaps (% of flight)** |
| A1 | 2016-04-14 | f | 0 | 32 | 99 | 22 (14) | 16 | 4485 | 7 | 8 | 15 | 0.88 | 16 | 2 |
| A2* | 2016-04-14 | m | 0 | 119 | 83 | 50 (87) | 10 | 5367 | - | - | - | - | - | - |
| A3* | 2016-04-14 | m | 0 | 65 | 88 | 17 (30) | 6 | 7609 | - | - | - | - | - | - |
| A4 | 2016-04-15 | m | 0 | 93 | 95 | 24 (49) | 6 | 8383 | 5 | 11 | 25 | 1.15 | 27 | 3 |
| B1 | 2017-02-16 | f | 0 | 40 | 98 | 24 (36) | 14 | 4457 | 6 | 8 | 21 | 0.75 | 22 | 3 |
| B2 | 2017-03-16 | f | 17 | 46 | 91 | 25 (58) | 13 | 3698 | 6 | 11 | 14 | 0.76 | 13 | 3 |
| B3 | 2017-03-24 | f | 45 | 42 | 97 | 14 (20) | 8 | 4233 | 5 | 13 | 8 | 0.81 | 8 | 1 |
| B4 | 2017-03-23 | m | 0 | 6 | 80 | 7 (10) | - | 576 | 8 | 7 | 65 | 0.88 | 57 | 13 |
| B5 | 2017-04-08 | m | 12 | 44 | 97 | 35 (32) | 19 | 2265 | 6 | 9 | 15 | 0.8 | 15 | 2 |
| B6 | 2017-04-08 | m | 1 | 34 | 92 | 25 (32) | 18 | 3891 | 7 | 8 | 15 | 0.89 | 15 | 2 |
| C1* | 2018-04-13 | f | 2 | 168 | 94 | 83 (121) | 12 | 4128 | - | - | - | - | - | - |
| C2* | 2018-04-14 | f | 2 | 89 | 95 | 45 (54) | 12 | 3393 | - | - | - | - | - | - |
| C3 | 2018-04-15 | f | 0 | 36 | 99 | 26 (23) | 17 | 4096 | 6 | 9 | 6 | 0.82 | 6 | 2 |
| C4* | 2018-04-15 | f | 0 | 146 | 79 | 48 (209) | 8 | 6508 | - | - | - | - | - | - |
| C5* | 2018-04-13 | m | 0 | 71 | 98 | 50 (34) | 17 | 3755 | - | - | - | - | - | - |
| C6* | 2018-04-13 | m | 0 | 46 | 88 | 37 (44) | 19 | 2409 | - | - | - | - | - | - |
| C7 | 2018-04-15 | m | 0 | 59 | 92 | 54 (73) | 22 | 2926 | 6 | 9 | 29 | 0.85 | 26 | 5 |
| D1 | 2020-03-13 | f | 202 | 35 | 99 | 14 (13) | 10 | 4376 | 7 | 9 | 22 | 1.09 | 23 | 2 |
| D2 | 2020-03-15 | m | 212 | 69 | 99 | 24 (23) | 8 | 7545 | 6 | 10 | 14 | 0.93 | 15 | 2 |
| | **Mean ± SD** | | | | **93 ± 6** | **33 (51) ± 18 (47)** | **14 ± 6** | **4426 ± 1959** | **6 ± 1** | **9 ± 2** | **21 ± 15** | **0.88 ± 0.12** | **20 ± 13** | **3 ± 3** |

***Tail-mounted devices***

## Flights

A total of 624 flights were isolated from 1238 hours DD data, of which 694 hours was flight data. Most of the DD (76%) and all the video data were recorded during outbound sections of foraging trips. However, GPS tracks covered the total duration of the foraging trip for all but one individual (bird D2). The video loggers recorded 8.1 hours of flight from 13 flights (eight individual birds) and all flying footage recorded on the video loggers was correctly identified as flying periods from the matched DD data (visual inspection). Automated isolation of flying periods from $A_Z$ histograms was effective in most cases, with 93 ± 6% of points corresponding to points identified through visual inspection (Table 5.1). Flight identification from tail-mounted loggers were less successful with 89 ± 7% success rate compared to 95 ± 6% for back-mounted loggers but was not successful at identifying exact take-off and landing events. Figure 5.5 shows a comparison between two individuals, bird A1 and C7, where the automated method under- and overestimated the exact number of flights respectively, but the total flight time was still accurately represented (99% and 92%). The automated approach was not successful at identifying take-off and landing events with large variation between individuals (Table 5.1). Standard deviation of $A_Z$ over 10 s yielded good results when isolating periods of flight with the values being 0.19 ± 0.04 *g* on average. Birds performed 14 ± 6 flights per day (range 6–40) with an average duration of 1.2 ± 0.5 hr (range 8 s – 12 hr) per flight.

Westerly winds dominated the winds experienced by Wandering Albatrosses during the study (Supplemental Figure S5.1). However, more northerly winds were experienced during the inbound period of foraging trips, when the birds were returning to their colony (Figure 5.6a). Wandering Albatrosses flew mostly with cross winds (76%) from their left (outbound flights) and right (inbound flights), as well as tail winds (22%) during inbound flights (Figure 5.6b). The birds flew with an average wind speed of 12 ± 5 $m \cdot s^{-1}$ (range 1–25 $m \cdot s^{-1}$).

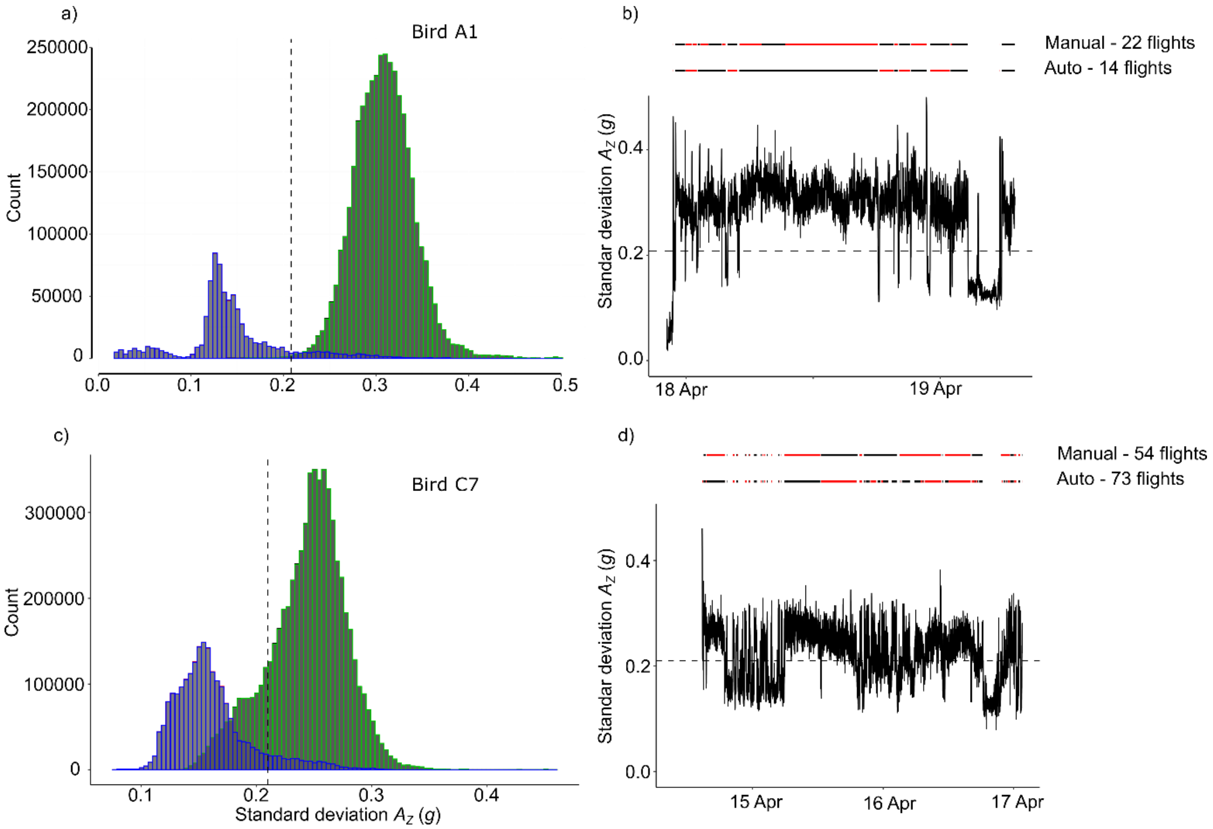

**Figure 5.5:** Automated identification of flying periods from two Wandering Albatrosses, bird A1 and C7. **a & c)** Show histogram plots of standard deviation $A_Z$ separated into flying (green bars) and non-flying (blue bars) periods through visual observation and dashed lines show the threshold used in for the automated method. **c & d)** Shows the raw data of SD $A_Z$ and the threshold (dashed line) used to identify flying periods. Lines at the top of the graphs show periods of flight identified through the automated and manual methods where alternating colours indicate where individual flights are separated.

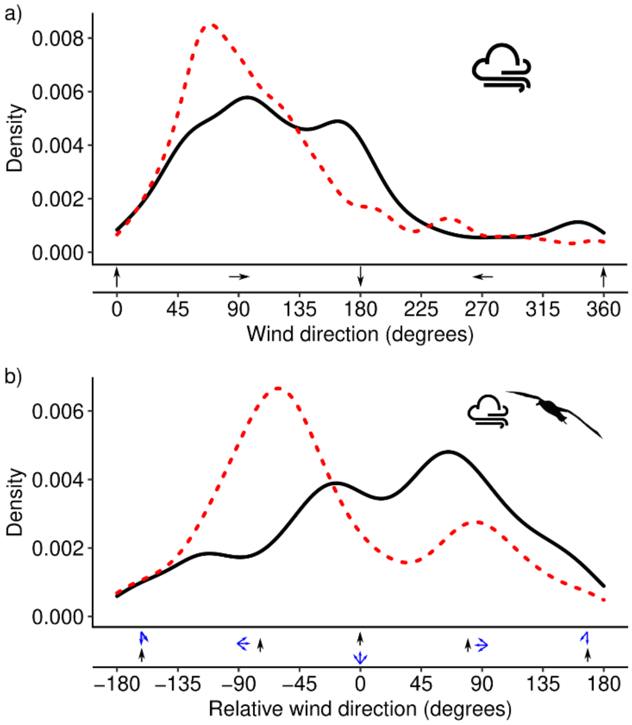

**Figure 5.6:** Winds experienced by 32 Wandering Albatrosses tracked during the study period (Feb – Apr, 2016-2020). **a)** The absolute wind direction where values are the direction the wind is blowing in (i.e. 0° is wind blowing to the north). **b)** Difference between the bird's course over ground and the wind direction, so that negative values are wind coming from the left and positive values for winds from the right. Data for both outbound (red dashed lines) and inbound (solid black lines) sections of foraging trips are shown.

## Dynamic soaring cycles

Roll angle analyses were only performed for six individuals with back mounted loggers without magnetic paddles (birds A1, A4, C3, C7, D1, and D2) or where video data were available. Dynamic soaring cycles estimated from the video-derived roll angles were compared to cycles from DD derived angles. Dynamic soaring cycles estimated from video data had a mean duration of 8.4 ± 1.6 s and frequency of 7 ± 2 cycles per minute (Table 5.2), and this was not significantly different from DD-derived cycles ($t$-test, $t_{26} = 1.84$, $p = 0.08$ and Wilcoxon rank sum test, $Z = 0.57$, $p = 0.57$). The estimated centripetal forces ($g$) experienced by the birds were compared to the estimated roll angles. This proved to be an effective way to estimate the different periods of the dynamic soaring cycles (see Figure 5.2). Centripetal forces ($g$) are expected to be highest during the descent phase (lowest altitude in the cycle) and lowest when the bird is at the upper turn (highest altitude). Wandering Albatrosses had a mean roll angle of 25 ± 9° (range -109° to 89°) during flight and had higher roll angles (29 ± 8°) when turning with the wind (low *g* turns) as opposed to turning into the wind (25 ± 9°; Wilcoxon rank sum test $Z = 5.39$, $p < 0.01$). When flying in cross winds (the majority of flights), the roll angle distribution was skewed, with birds spending more time at angles turning into the wind (i.e. with the wind blowing onto the back of the birds; Figure 5.7). Birds flying with tail winds had a more uniform distribution of roll angles, while one individual filmed flying into a head wind showed a bimodal distribution of roll angles (Figure 5.7). As expected, the distribution of roll angles was influenced by wind speed, with more extreme angles at higher wind speeds (Figure 5.7).

**Table 5.2:** Comparison of Wandering Albatross dynamic soaring cycles estimated from video and DD loggers.

| | | | **Total cycles** | | **Cycles per minute** | | **Cycle duration (s)** | |
|---|---|---|---|---|---|---|---|---|
| **Bird ID** | **Flight section** | **Duration (min)** | **Video** | **DD** | **Video** | **DD** | **Video** | **DD** |
| B2 | 1 | 17 | 115 | 118 | 7 | 7 | 9 | 9 |
| sB3 | 2 | 10 | 68 | 79 | 6 | 8 | 9 | 8 |
| B3 | 3 | 19 | 133 | 142 | 7 | 8 | 8 | 8 |
| B3 | 4 | 9 | 69 | 78 | 7 | 8 | 8 | 7 |
| B5 | 1 | 2 | 19 | 14 | 8 | 6 | 7 | 9 |
| B5 | 2 | 4 | 23 | 34 | 5 | 8 | 10 | 8 |
| B5 | 3 | 5 | 26 | 41 | 6 | 9 | 10 | 7 |
| B6 | 1 | 0.5 | 2 | 3 | 5 | 7 | 12 | 7 |
| C1* | 1 | 2 | 20 | 12 | 10 | 6 | 6 | 5 |
| C1* | 2 | 2 | 20 | 10 | 10 | 5 | 6 | 6 |
| D1 | 1 | 158 | 1036 | 1002 | 7 | 6 | 9 | 9 |
| D1 | 2 | 44 | 352 | 369 | 8 | 8 | 8 | 7 |
| D2 | 1 | 212 | 1375 | 1454 | 6 | 7 | 9 | 9 |

***Tail-mounted devices***

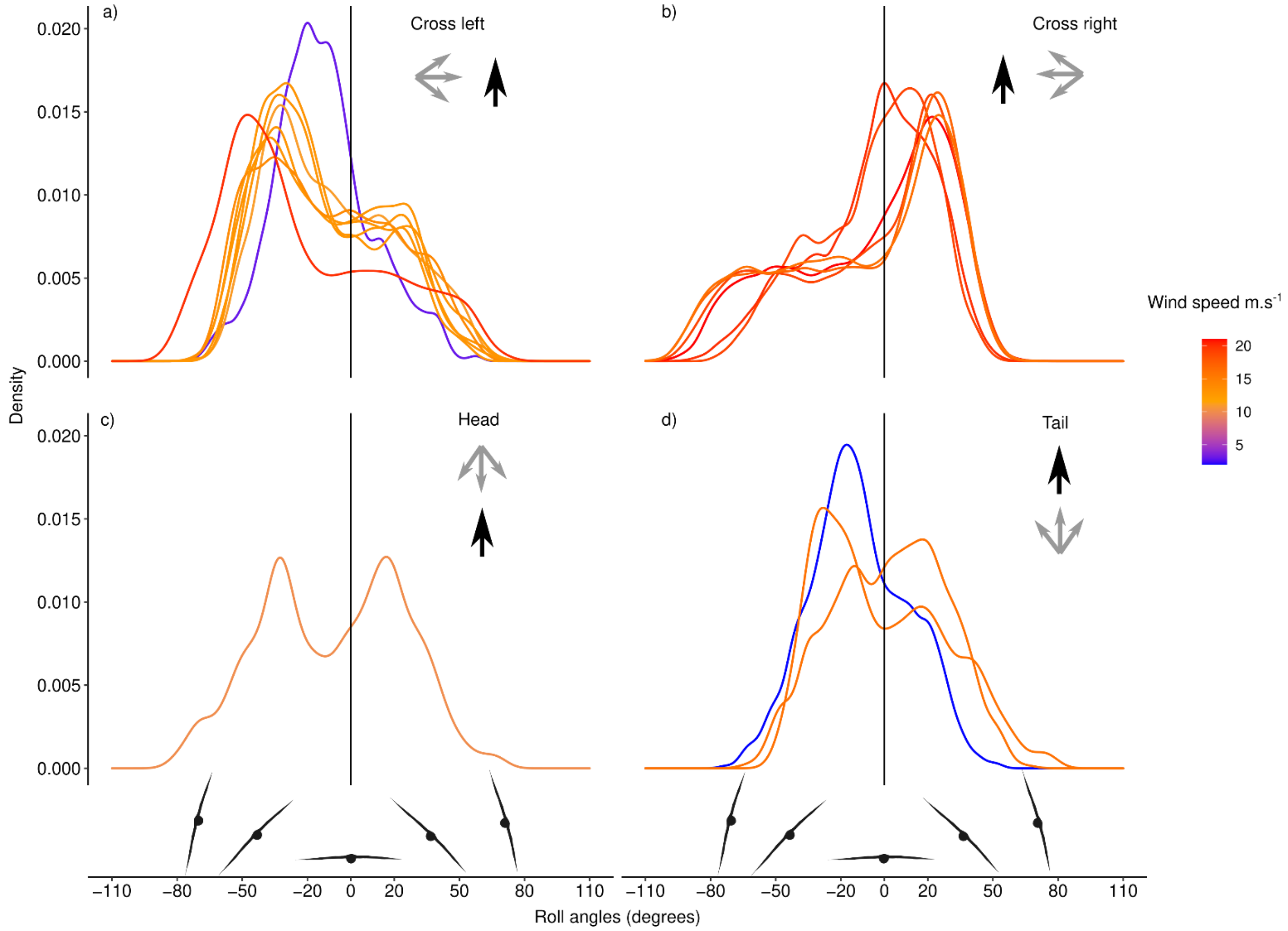

**Figure 5.7:** Frequency distribution of roll angles extracted from video loggers on Wandering Albatrosses in relation to wind speed and relative direction. The relative wind direction was grouped into four categories: **a)** cross wind coming from the left, **b)** cross wind coming from the right, **c)** head wind, and **d)** tail wind.

## Flapping behaviour

Individual flaps were isolated from back-mounted DD loggers ($n$ = 13). On average, Wandering Albatrosses performed 21 ± 15 flaps per minute of flight with the largest number occurring at the start and ends of flights (Figure 5.8). These *single flaps* represented 21 ± 13% of flight time, but *sequential flapping* (> 2 flaps·s$^{-1}$) only represented 3 ± 4%. However, it must be noted that the number of flaps per minute of flight is likely overestimated due to the potential inclusion of erroneous "low intensity" flaps (see below). Likewise, averaging over individual flights could skew the data towards shorter flights where flapping is likely more pronounced, and the flapping rate was lower when averaged over hourly periods of flight as opposed to complete flights (see Chapter 6). Most flaps occurred in periods with lower centripetal acceleration ($g$), which corresponded to the upper turn and the leeward descent of the dynamic soaring cycle (see Figure 5.2 and Supplementary Video S5.1 and S5.2 for examples of Wandering Albatross flapping behaviour). The mean VeDBA (representing intensity) of flaps was 0.68 ± 0.28 *g* with a decreasing trend in VeDBA as centripetal acceleration increased (Figure 5.9). Flapping intensity was not significantly different between sexes (male - 0.68 ± 0.09 *g*, female - 0.74 ± 0.13 *g*; $t_9 = 0.92$, $p = 0.38$) and was the same when restricted to take-off periods (0.86 ± 0.13 *g*; $t_{10} = 10.0$, $p = 0.95$). However, males had significantly higher flapping intensities during take-off (0.86 ± 0.14 *g*) than during the rest of the flight (0.68 ± 0.09 *g*; $t_8 = 2.58$, $p = 0.03$).

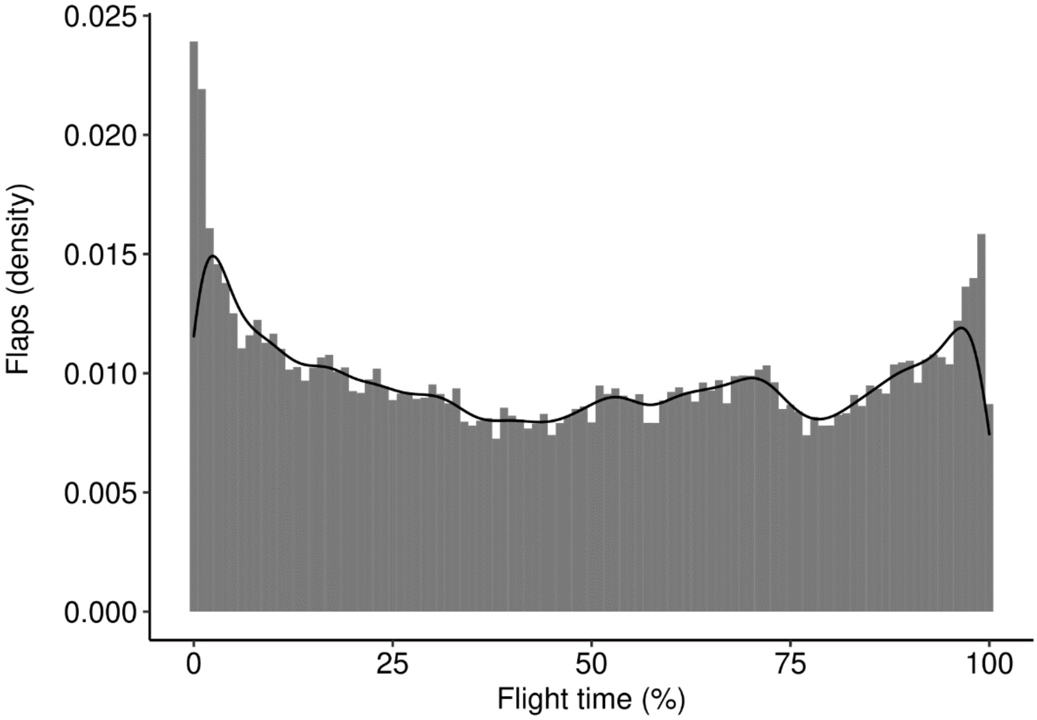

**Figure 5.8:** Distribution of the number of flaps through the course of individual flights of Wandering Albatrosses.

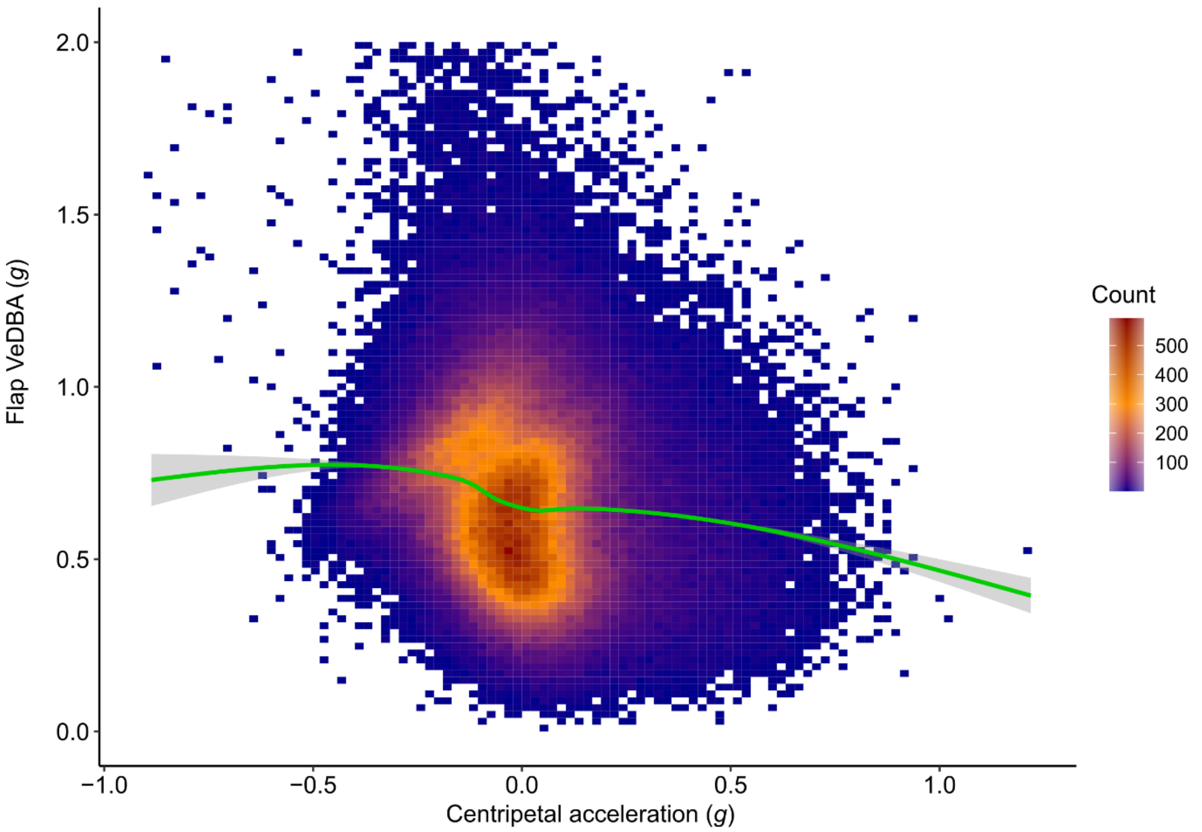

**Figure 5.9:** 2D Density plot showing the relationship between centripetal acceleration and flapping intensity (VeDBA) for Wandering Albatross flapping flight. A generalised additive model (GAM) curve is shown as a green line.

Wandering Albatrosses were more likely to flap when flying in low wind speeds, with the highest frequency of flapping occurring during head winds (Figure 5.10). Interestingly, the amount of flapping seemingly increased again at the highest wind speeds for cross and head winds, but this was only the case for "low intensity flaps" (Figure 5.10). The birds were able to fly in lower wind speeds without flapping when flying with tail winds, which had less flapping in general (Figure 5.10). Males flapped more often (27 ± 18 flaps·min$^{-1}$) than females (14 ± 7 flaps·min$^{-1}$), but this was only marginally significant (Welch two sample *t*-test, $t_{11}$ = 2.134, p = 0.056), likely due to the modest sample size. Males had a strong affinity for taking-off into headwinds, while females took off into both head and cross winds (Figure 5.11a). Lower wind speeds resulted in more flapping during take-off, with males also flapping marginally more than females (Figure 5.11b). One male Wandering Albatross flew into the wind for ~1 hr flapping almost every second of the flight (54 flaps·min$^{-1}$). This was just before the bird reached its maximum distance from Marion Island, where it spent ~12 hours presumably foraging, before returning to the island.

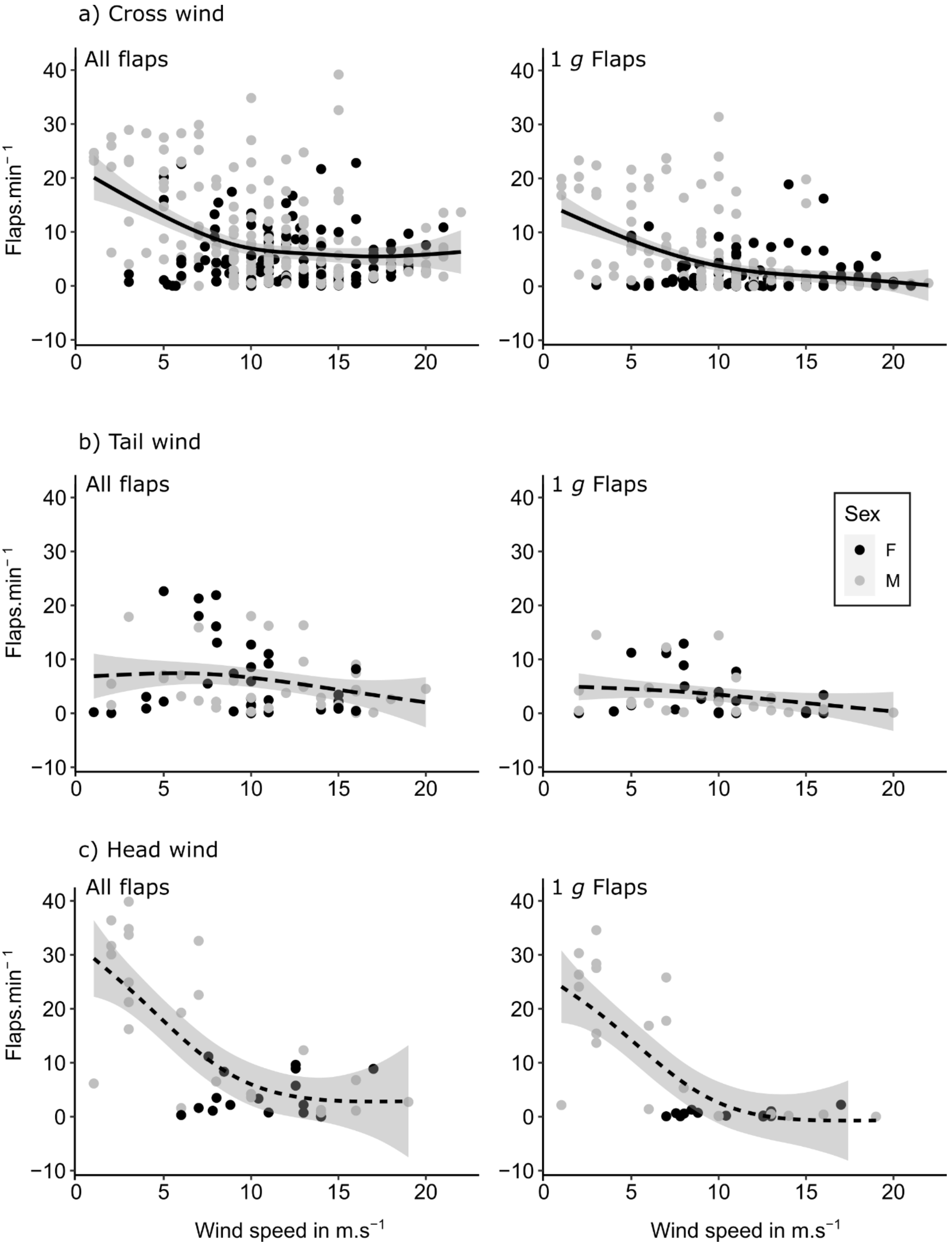

**Figure 5.10:** Relationship of flapping flight and wind speed for Wandering Albatrosses flying with **a)** cross winds, **b)** tail winds, and c) head winds. The first panel shows results for all flaps as identified by the chosen $th_{flap}$ value (see Methods), while the second panel shows results for “high intensity flaps” where the flap intensity was > 1 *g*. Generalised additive model (GAM) curves show trends for both sexes, while sexes are differentiated by point colours (male – grey, females – black).

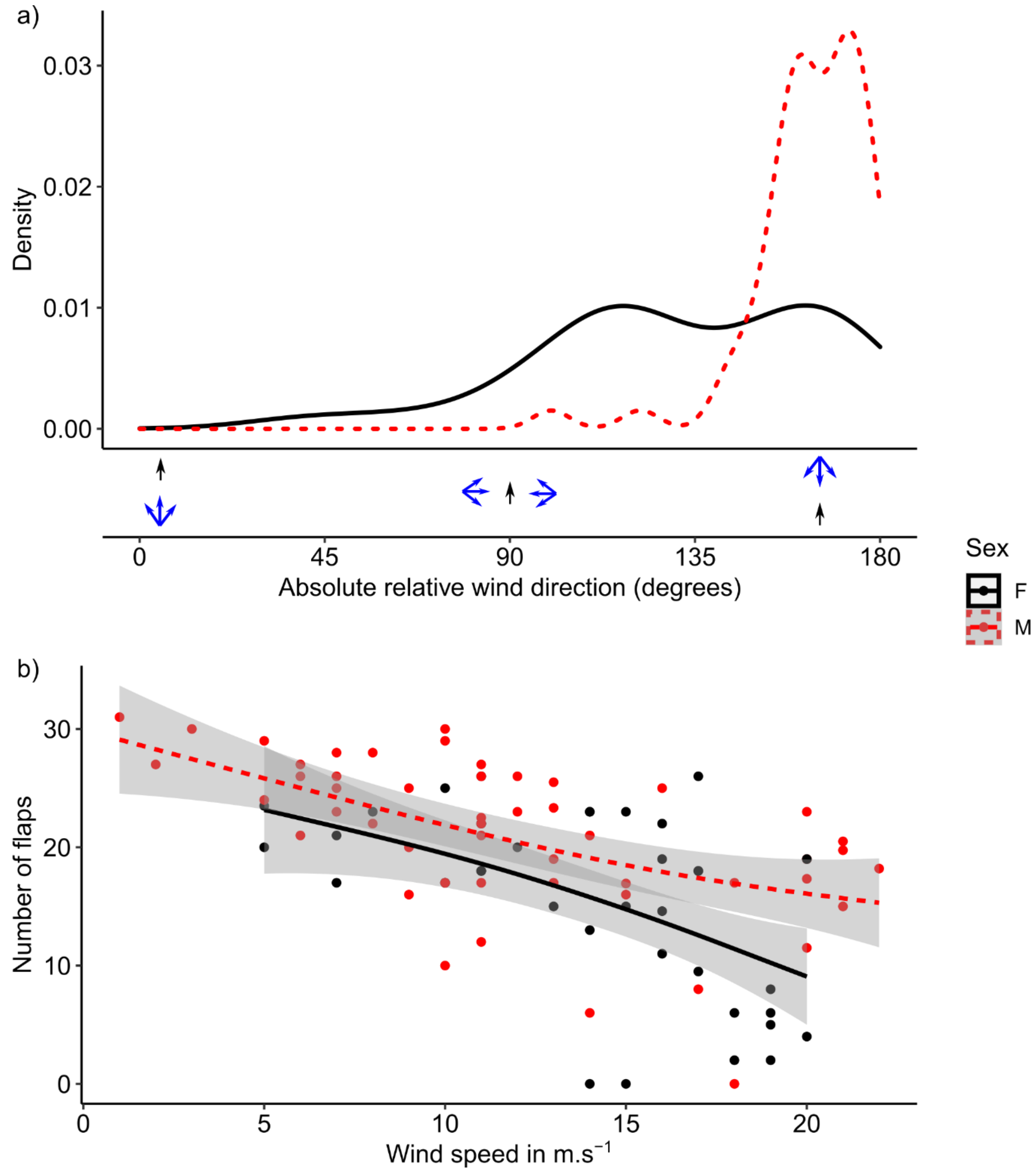

**Figure 5.11:** Effect of wind direction and speed on the take-off behaviour of female (black solid lines) and male (red dashed line) Wandering Albatrosses. **a)** Shows the wind direction relative to the take-off heading of the birds and **b)** the number of flaps occurring at varying wind speeds. Take-off periods were regarded as the first 10 s of individual flights.

A detailed illustration of the above results is shown in Figure 5.12 and Supplementary Video S5.2, where the outbound section of a female Wandering Albatross (bird D1) foraging trip is shown. The bird flew into the wind heading north-west, while frequently flapping at a high intensity (flight 7 Figure 5.12). As the northwesterly wind speed increased, the bird flapped less (flaps with very low intensity) and had more extreme roll angles when turning with the wind, resulting in the bird heading west. When the wind speed decreased (flight 11 Figure 5.12), the amount of flapping and flapping intensity increased, while the roll angles were less extreme. The wind then turned, coming from the south-west, resulting in the bird rolling towards the left (into the wind) more often and heading north-northwest while flapping infrequently. Supplementary Video S5.3 shows the flight behaviour of all the tracked individuals in relation to wind.

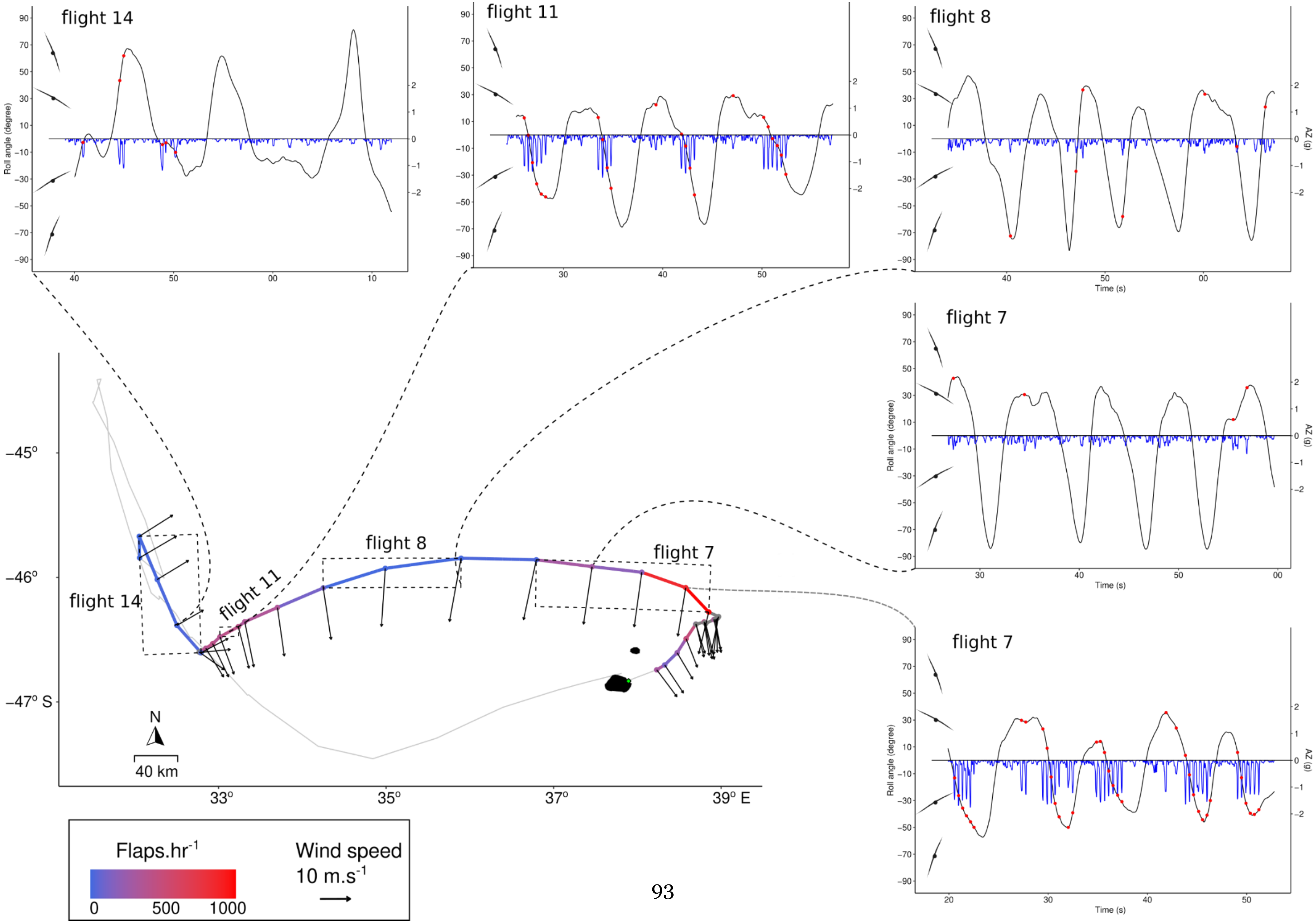
flight 14
flight 11
flight 8
flight 7
flight 7
Roll angle (degree)
AZ (g)
Time (s)
−45°
−46°
−47° S
33°
35°
37°
39° E
N
40 km
Flaps.hr$^{-1}$
0
500
1000
Wind speed
10 m.s$^{-1}$

**Figure 5.12 (previous page):** Example of the flight behaviour of a female Wandering Albatross (bird D1) flying in varying wind conditions. Points are hourly GPS locations with colour representing the number of flaps for every location where DD data were available. Wind vectors are also shown for locations with DD data while the total track is shown as a shaded grey line. Inserts are 30 s extracts of 40 Hz DD data showing roll angles (black) and the vertical accelerometer axis ($A_Z$) with individual flaps indicated by red dots in relation to the roll angles. Accompanying video is shown in Supplementary Video S5.2.

## Discussion

With the rapid advancement of bio-logging technology and the introduction of new analytical tools, the multisensor approach has revolutionised the way in which we conduct ecological research (Rutz and Hays 2009; Williams et al. 2020b). In this study, using a range of bio-loggers, I show how Wandering Albatrosses use dynamic soaring as an energy efficient flight mode in the harsh Southern Ocean environment. My results show how male and female albatrosses differ in their flight behaviour, possibly influencing their spatial distribution. To my knowledge, this is the first study to directly measure the fine-scale body angles of a dynamic soaring seabird.

While dynamic soaring, albatrosses subject themselves to rapidly changing centripetal forces (Figure 5.2; Sachs et al. 2012). These changes in acceleration could be used to identify periods of flight from acceleration measured on the vertical (heave) axis of an accelerometer, using an automated approach (Collins et al. 2015). These automated flight periods matched well with manually identified periods, but the exact number of flights could not be identified. This was due to short gaps, incorrectly subdividing longer flights into several shorter flights (overestimating flights) or when short flights were merged into a single longer flight (underestimate). This happened more often where the loggers were deployed on the tail feathers and stresses the importance of logger placement (Williams et al. 2020b). The average number of flights per day (14 ± 6) was similar to values from a previous study of Wandering Albatross activity (~14 flights per day; Weimerskirch et al. 2000). The distribution of flight duration was similar for both sexes, with both males and females flying for up to 12 hours at a time. A considerable proportion of flights (6%, $n = 41$) lasted < 30 s. Video footage showed that some of these flights were during foraging events, but visual inspection of DD data suggests that some might be failed take-off events (when a bird had been sitting for some time, then attempted to take-off a minute or two before the start of a long flight). Weimerskirch et al. (2000) measured an increased heart rate prior to take-off and hypothesised that this could be an anticipatory response. However, my data show that this increase in heart rate might also be due to failed take-off events.

Dynamic soaring cycles were identified from the roll angle estimates, even when the absolute roll angles had a large error (due to magnetic interference caused by a magnetic paddle in deployments in 2017). Such magnetic interferences caused a shift in the roll angle estimates, but the general shape of the cycle was maintained. By normalizing the roll angles to a range of -1 to 1, the cycles could still be identified, and durations estimated. Unsurprisingly, data from tail-mounted loggers could not be used to estimate roll angles or dynamic soaring cycles because these loggers were not in line with the birds' centre of gravity and because the tail may be angled independent of the body when turning. Roll angles from tail-mounted loggers could provide information on how tail movement responded to sudden changes in the wind, but this would need further validation (e.g. back facing cameras) and is beyond the scope of this study. The dynamic soaring cycles of Wandering Albatrosses lasted ~9 s, which is similar to estimates from fine-scale tracking data (~10 s; Sachs et al. 2013). By coupling the centripetal force (estimated from accelerometer data) to the estimates of roll angles, the wind- and leeward turns of the dynamic soaring cycle could be identified, assuming that these forces peak during the descent phase of the cycle while the birds are turning into the wind.

Roll angle distribution during Wandering Albatross flight changed with wind conditions, and individuals often maintained a heading perpendicular to the wind by predominantly banking in the direction from which the wind was coming. Albatrosses and petrels tend to favour cross winds in the Southern Ocean (Sachs 2005; Nevitt et al. 2008; Weimerskirch et al. 2014; Tarroux et al. 2016) because these winds are seemingly predictable to the birds (Weimerskirch et al. 2000) and allow flight with minimal energy expenditure (Sachs et al. 2012). Flying with a cross wind can result in windward drift and birds must either compensate or tolerate such drift when trying to maintain a specific heading. Antarctic Petrels *Thalassoica antarctica* might be able to compensate for drift, but are apparently not always able to detect how much they are drifting (Tarroux et al. 2016). My results suggest that Wandering Albatrosses may compensate for wind drift by altering their roll angle in response to changing wind conditions. The ability to compensate in this manner is probably influenced by body size. Male Wandering Albatrosses average 20% heavier than females with ~7% more wing area, and thus have 12% greater wing loading (Shaffer et al. 2001b), allowing them to fly with faster airspeeds in stronger winds, where the aerodynamic forces on the birds are higher (Richardson 2011). Most of the IMU and video data were recorded during the outbound period of respective foraging trips and were dominated by westerly winds. During these flights, Wandering Albatrosses were flying with the wind coming from their left and spent more time turning into the wind (left turn) and less time with the wind (right turn). By turning into the wind for longer periods, their net displacement was more or less perpendicular to the wind and resulted in a northerly bearing. The shape of the upper turn of the dynamic soaring cycle is likely to be relatively constant (Sachs 2016), thus the birds are probably banking towards the left during the leeward decent, causing a net displacement perpendicular to the wind. Inbound sections of flight were dominated by northerly as well as westerly winds and the birds mostly flew with the wind coming from the right or from behind.

As expected, the amount of flapping (deduced using the accelerometer data) was highest during take-off and landing (Weimerskirch et al. 2000). However, there was appreciable flapping during cruising flight, with ~3% of flights consisting of continuous flapping (> 2 flaps·$s^{-1}$). Wandering Albatrosses spend between 1.2–14.5% of their time flapping according to accelerometer-based evidence (Sato et al. 2009), but the sample size on which these results are based is not clear. Smaller Black-browed Albatrosses *Thalassarche melanophris* spend ~4% of their time flapping, amounting to 14% of their total energy expenditure during flight (Sakamoto et al. 2013). Flapping is not regarded as being part of the dynamic soaring cycle and the exact means of energy gain from the cycle remains contentious (Richardson 2011, 2015; Sachs et al. 2012, 2013; Sachs 2016). This debate is of particular relevance to the design of unmanned aerial vehicles (UAVs) to travel across the ocean in the absence of powered flight, where upwind flight is of particular concern (Richardson 2015; Sachs 2016). My results show how one male Wandering Albatross flew for an extensive period (~1 hr) against the wind while flapping at a high rate (54 flaps·$min^{-1}$). Flapping behaviour occurred during periods of low centripetal acceleration, which was often associated with the upper turn of the dynamic soaring cycle, as identified by roll angles at lower $g$ values (see Figures 5.2, 5.9 and 5.12). The upper turn of the dynamic soaring cycles is hypothesised to be where energy gain takes place, independent of flapping flight (Sachs et al. 2013; Sachs 2016). My results suggest that this is not always the case and that Wandering Albatrosses might supplement dynamic soaring with flapping flight.

Albatrosses and petrels seem to have two modes of flapping, a high frequency flap during take-off and a low frequency flap during cruising flight (Sato et al. 2009). There appeared to be a difference in flapping intensity depending on the timing in the dynamic soaring cycle of Wandering Albatrosses, possibly adding a third flapping mode. High intensity flapping occurred at low centripetal acceleration values (upper turn of the dynamic soaring cycle) while intensity decreased with increasing centripetal acceleration (lower turn). The latter were normally sporadic flaps during flights with low flapping percentages (see Figure 5.12) and their lower intensity was expected as presumably the airspeed was higher, reducing gains of flaps and increasing the effort required to flap. Wing morphing (the flexing of wings) is important for stabilisation of seabirds in flight, especially when experiencing high wind speeds or gusts (Harvey et al. 2019). The low intensity flaps observed in Wandering

Albatrosses might be wing morphing events for stability rather than power generating flaps, but this requires further investigation. Another explanation for these low intensity movements could be minor attitude corrections that the birds undergo to avoid lumps in the sea surface when flying very close to the water.

As expected, the time spent flapping increased at lower wind speeds when the birds were flying with cross winds, but minimal flapping was required for flight at low wind speeds in a tail wind. In the absence of wind, albatrosses may utilize updrafts caused by large waves to perform a type of wave-slope soaring (Pennycuick 1982; Richardson 2011). With a tail wind, the birds could travel perpendicular to the waves and possibly supplement dynamic soaring flight with wave-slope soaring where wind speeds do not allow continuous dynamic soaring without flapping (Richardson 2011). Wandering Albatrosses seldom fly into head winds, and sample sizes were too small to obtain clear results. However, males almost exclusively flew into the wind during take-off, while females took off into cross winds as well as head winds. Flapping intensity (VeDBA) was significantly higher during take-off than during routine flight for male Wandering Albatrosses. Although not explicitly tested for albatrosses, dynamic acceleration metrics have shown promise as indicators of energy expenditure during flapping flight (Van Walsum et al. 2020). Take-off events in large soaring birds are seemingly the most energy expensive part of the flight (Weimerskirch et al. 2000; Williams et al. 2020a), so male Wandering Albatrosses might limit their take-offs to favourable wind conditions (Clay et al. 2020) and once airborne may increase flapping rather than landing when wind conditions become temporarily unfavourable. Taking off in favourable wind conditions may not be restricted to albatrosses, as this behaviour has been observed for smaller seabird species as well (Kogure et al. 2016).

Although the small sample size rendered the result only marginally significant, female Wandering Albatrosses also tended to flap less than males. Female Wandering Albatrosses are predicted to fly in lower winds (Shaffer et al. 2001) as they are smaller (~20%) and have lower wing loading resulting in lower stall speeds (Warham 1977). Female Wandering Albatrosses from the Crozet archipelago and South Georgia are more likely to take-off in lower wind speeds and males fly in higher wind speeds than females (Clay et al. 2020). Birds from Marion Island (present study) flew in similar wind conditions regardless of sex during the breeding period, similar to a previous study of Wandering Albatrosses from South Georgia (Wakefield et al. 2009). Female Wandering Albatrosses from the Crozet archipelago (neighbouring Marion Island) are spatially segregated from males during the breeding period, but to a lesser extent during the non-breeding period (Weimerskirch et al. 2014). Although the data I collected were mostly during the brood-guard period (when foraging trips are short), and during outbound sections of flight, I did see some evidence of sexual differences. Females flapped less and were seemingly more tolerant of low wind speeds. This could explain the affinity of males for higher wind speeds (Clay et al. 2020), as birds that are unable to take-off in low wind conditions likely have reduced foraging efficiency (Jouventin and Weimerskirch 1990). Flying in higher wind speeds could result in a larger degree of wind drift, and coupled with increased flight speeds could result in the wider distribution of males during the breeding period (Weimerskirch et al. 2014).

## Conclusions

This chapter demonstrates how multiple sensor bio-logging can be used to infer fine-scale patterns in seabird flight behaviour. I show how wind drives the flight behaviour of Wandering Albatrosses and how they react to wind conditions by altering roll angles. I also show that flapping flight is present in most flights and how it might be a key part of the dynamic soaring cycle where wind conditions are not optimal. Future studies could add to these results using additional loggers, such as gyroscopes or side facing cameras, to further study albatross flapping behaviour. One drawback of fine-scale studies is the lack of matching fine-scale environmental data. How a dynamic soaring seabird's behaviour changes in response to fine-scale wind patterns is difficult to study with relatively coarse environmental data. Future studies, incorporating accurate measures of bird airspeed, might help to answer some of these questions (Williams et al. 2020b). Likewise, most of the positional data used in my study were relatively coarse and fine-scale positional data could benefit future studies looking at body angles and flapping behaviour. It is likely that Wandering Albatrosses are also physically limited with regards to their roll angles when flying in high wind speeds, and research into their mechanical limits could also be beneficial to understanding their behaviour. Lastly, I showed that Marion Island Wandering Albatrosses displayed sexual differences in flight behaviour and responses to changing wind patterns. However, my sample sizes were modest, and the study of more individuals could further highlight these patterns.

# Supplementary material

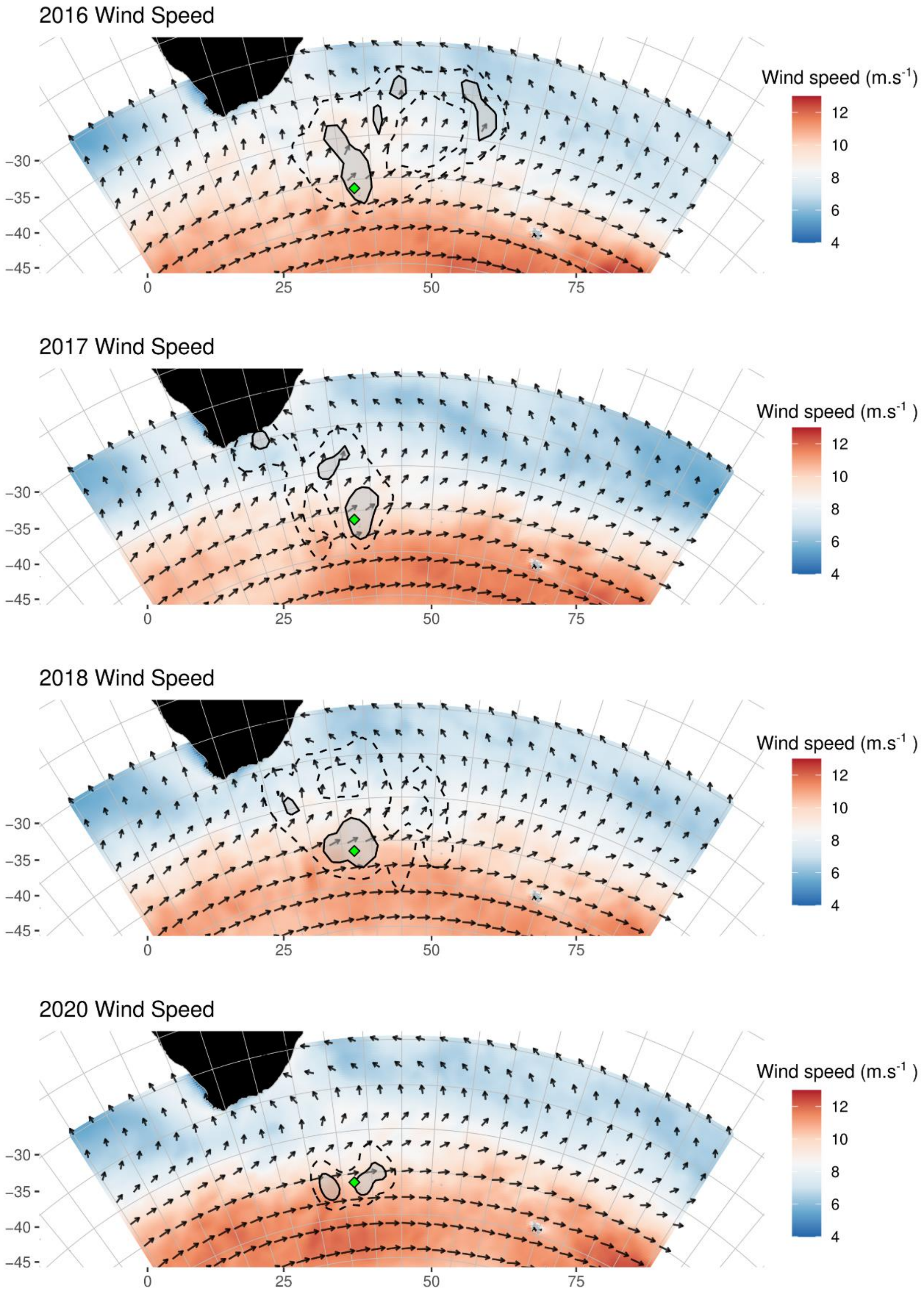

**Figure S5.1:** Average wind speed and direction across the study period with kernel density estimations (50% and 90%) of track points corresponding to DD data.

**Video S5.1:** Examples of Wandering Albatross flapping flight filmed from Marion Island where birds are: 1) sequentially flapping at the upper turn of the dynamic soaring cycles, 2) a single flap at the lower turn, 3) continuous flapping with intermittent gliding, and 4) a low intensity flap at the lower turn. Video at https://vimeo.com/507438059

**Video S5.2:** Bird-borne video footage showing the flying behaviour of a Wandering Albatross (bird D1), exhibiting: 1) sequential flapping at the upper turn of the dynamic soaring cycle, 2) reduced flapping at higher wind speeds. This footage corresponds to flights 7 and 8 from Figure 5.12 respectively. Video at https://vimeo.com/507436974

**Video S5.3:** Animation of Wandering Albatross GPS tracks in relation to hourly averages of wind speed and direction (arrows). The points are hourly GPS locations with the number of flaps within the hour represented by colour. Video at https://vimeo.com/507437755

# Chapter 6: The incredible flight of albatrosses and petrels: how do central place foragers of varying sizes cover the same extensive ranges?

## Abstract

Breeding albatrosses and petrels are extreme central place foragers, commuting between offshore foraging areas and their nests to incubate eggs or feed chicks. Each foraging trip covers hundreds to thousands of kilometres, largely irrespective of body size. They achieve these astonishing flights, often in harsh weather conditions, by employing an energy efficient dynamic soaring flight mode that allows them to travel large distances while extracting energy from fine-scale changes in wind speed. I assess how body size affects flight behaviour in relation to the wind. Larger dynamic soaring seabirds have higher wing loadings, with faster flight speeds to avoid stalling, especially in light winds. In contrast, smaller species also rely on flapping flight and often fly closer to the sea surface (where wind speed is lower) in high wind speeds. To investigate the behavioural responses of albatrosses and petrels to varying wind conditions, I equipped 101 birds from six species with bio-logging devices recording a multitude of data. The birds ranged in body size from Great Shearwaters (~800 g) to Wandering Albatrosses (~9 kg). Roll angles during dynamic soaring flight were estimated from video (albatrosses only) and tri-axial magnetometer data (all species), while periods of flight as well as flapping flight were identified from tri-axial accelerometer data. GPS loggers provided location estimates that allowed coupling of flight data to local estimates of wind speed and direction. Birds mostly flew in westerly winds with an average speed of 10 $m \cdot s^{-1}$, but wind speed averaged less for birds flying in the south Atlantic Ocean (8 $m \cdot s^{-1}$) than in the southwest Indian Ocean (11 $m \cdot s^{-1}$). All species flew with cross winds but had varying responses to wind direction. For example, Wandering and Atlantic Yellow-nosed Albatrosses alternated flying in cross winds from the left and right during outbound and inbound flights, respectively, whereas Grey-headed Albatrosses on occasion flew with tail winds during outbound flights to rapidly reach frontal systems. Variation in roll angles and flapping behaviour was related to wind speed and direction, with birds rolling at more extreme angles in high winds and flapping more in low winds. When turning into the wind, Wandering Albatrosses appeared to be more limited in roll angles they could achieve than smaller, more manoeuvrable species. This could explain why these large birds often perform long looping trips when foraging in the Southern Ocean. The Great Shearwater flapped most often but surprisingly, Grey-headed Albatrosses flapped least of all the studied birds. The flight behaviour of dynamic soaring seabirds is evidently complex and does not seem to follow a clear allometric relationship. The use of multisensory data loggers allows us to

improve our understanding of the complex behavioural patterns that allow seabirds to survive in a harsh environment such as the Southern Ocean.

## Introduction

The Southern Ocean is home to many procellariiform seabirds, where they spend most of their time (Weimerskirch et al. 2014), only returning to land when breeding or courting. Albatrosses and petrels are extremely efficient flyers, with albatrosses thought to have the lowest energy expenditure of all seabirds while flying (Weimerskirch et al. 2000; Shaffer et al. 2001a), only rivalled by the thermal soaring of frigate birds (Weimerskirch et al. 2016). This enables them to travel extreme distances while foraging (Phillips et al. 2008; Weimerskirch et al. 2014), relying on wind when travelling over the open ocean (Pennycuick 1982) where they mostly use dynamic soaring to travel with minimal energy expenditure (Weimerskirch et al. 2000; Shaffer et al. 2001b; Sachs 2005; Richardson 2011). The size of seabirds using dynamic soaring may be a limiting factor to their ability to take-off and sustain flight by flapping their wings in unfavourable wind conditions (Shaffer et al. 2001a; Sato et al. 2009). However, size does not seem to limit how far these birds can travel, as smaller shearwaters can travel to areas that are > 5000 km away from their nesting sites while breeding (Cleeland et al. 2014; Schoombie et al. 2018), at least as far as the largest albatrosses (Weimerskirch et al. 2014). Even the small Leach's Storm Petrel *Oceanodroma leucorhoa* (50 g) can reach distant foraging areas up to 1400 km from their nests while breeding (Hedd et al. 2018).

In order to explain how seabirds with such a wide range of body sizes can forage over equally large areas we need to understand their fine-scale behaviour at sea. Studying the characteristics of seabirds over a range of body sizes can help to indicate appropriate sampling strategies for different species (Hebblewhite and Haydon 2010). Most studies scaling behaviour with size of birds have been with regards to predator-prey interactions (Dial et al. 2008). More recently Sato et al. (2009) studied the fine-scale behaviour of a range of seabirds, showing that larger bodied birds flap less during flight, which is applicable to birds in general (Bale et al. 2014; Watanabe 2016). However, Sato et al. (2009) did not take local wind conditions into account. Behaviour is the response of an animal to its environment and when studying the behaviour of seabirds, it is important to consider environmental conditions. One of the reasons that behaviour is not often compared across species is that it might be difficult to accurately quantify animal behaviour (Dial et al. 2008). Recent advances in bio-logging technology (Wilmers et al. 2015) have made it easier to quantify discrete behaviours and this has been used on several seabirds (e.g. Ropert-Coudert et al. 2004, Sato et al. 2008, 2009, Sakamoto et al. 2013).

One of the fundamental aspects to consider in conservation is the energetic status and demands of animals (Cooke et al. 2004; Wilson et al. 2008). Traditionally, the energetic demands of free-ranging animals have been estimated using doubly labelled water or heart-rate monitors (Wilson et al. 2006). More recently, we can estimate the energy usage of free-ranging animals at a much higher resolution using metrics derived from accelerometer data (Halsey et al. 2009a). Experimental studies on a range of birds have shown that dynamic body acceleration serves as a valid proxy for energy expenditure (Wilson et al. 2006, 2012; Halsey et al. 2009b; Hicks et al. 2017). The overall energy efficiency of birds probably does not scale with size (Bale et al. 2014), but this might be different when looking at behaviour at a smaller scale (i.e. flapping flight and take-off) as well as in different wind conditions. Fritz et al. (2003) concluded that the small and medium scale (up to 10 km) movements of foraging Wandering Albatrosses seems to be independent of wind conditions, but wind patterns may show a significant effect if examined at smaller scales than was available in their study.

Birds in the order Procellariiformes span a wide range of body sizes, from 30 g Least Storm-petrels *Oceanodroma microsoma* to 9 kg Wandering Albatrosses. However, the distances they can cover over the ocean does not scale strongly with size, as is the case for soaring seabirds where migration ranges are mass-independent (Watanabe 2016). In this chapter I report differences in fine-scale flight behaviours between species and how these behaviours are influenced by varying wind conditions. This provides insights into the different strategies that species of varying body sizes use to travel large distances across the ocean. Seabirds with varying morphologies display similar behavioural patterns (i.e. far-ranging foraging trips) and through the exploration of individual behaviours we can identify the mechanisms behind these general behaviours (Cooke et al. 2004). Understanding the behaviour of individual species may help us predict how they respond to changing environmental conditions and could help shape future conservation measures.

## Methods

Daily Diary (DD) loggers were deployed on four procellariiform species breeding on Marion Island (46° S, 37° E, southwestern Indian Ocean) and three species on islands in the Tristan da Cunha archipelago (37° S, 12° W) and Gough Island (40° S, 9° W, central south Atlantic Ocean; Table 6.1). Deployments were done on breeding adults, incubating eggs or brood-guarding small chicks, from Feb–Apr (Wandering Albatrosses) and Nov–Dec for the remaining species (Table 6.1). In addition to the DD loggers, GPS loggers were deployed on all birds except one Sooty Albatross, one Grey-headed Albatross, and two Atlantic Yellow-nosed Albatrosses (from here on referred to as Yellow-nosed Albatrosses). The GPS loggers were programmed to record locations at intervals between 1 s and 1 hr. Video loggers were also deployed on some Wandering, Grey-headed and Sooty Albatrosses. The details of logger deployment, and logger attachment in general is detailed in Chapter 2. Only back-mounted devices deployed on Wandering Albatrosses were used (tail-mounted loggers were excluded), and the 2017 loggers used on Wandering Albatrosses were excluded from the magnetometer analysis because their magnetic paddle compromised the calibration of the magnetometers (see Chapter 5 for further details).

## Analysis

Periods of flight were isolated from the DD data by examining frequency histograms of the vertical accelerometer axis $A_Z$ (Collins et al. 2015; see Chapter 5) and subsequent analyses were only performed on the in-flight data. Roll angles were extracted from tri-axial magnetometer and video data (see Chapter 4). The length of individual dynamic soaring cycles was estimated from the time between peaks in roll angles (see Figure 5.2 in Chapter 5).

Individual flaps were extracted using a modified LULU filter (Lotz & Clilverd 2019; Chapter 5). Analyses from Chapter 5 suggest that erroneous low intensity flaps could be detected for Wandering Albatrosses at high wind speeds. Thus, analysis of flapping flight was also done using data where low intensity flaps were excluded based on the vector sum of dynamic body acceleration (VeDBA) of the flap (see Chapter 5). Based on visual observation of accelerometer data, most clear flaps (see Figure 5.3 in Chapter 5) had VeDBA values > 0.7 *g* so this was used as the threshold when excluding low intensity flaps. Results of flapping analyses are shown separately where low intensity flaps are included and excluded respectively, but statistical analyses are only reported from data where low intensity flaps were excluded. Flapping was summed for every second of DD data (40 Hz) so that every second with at least one flap was labelled as flapping flight and the percentage of seconds with flapping flight is reported. Flapping rates were calculated by counting the number of flaps for every minute of flight. To estimate the effect of wind on flapping rate, the flapping rates were averaged across a grid of the available wind speeds and direction for individual species. However, sample sizes were small and only Wandering Albatrosses had a good representation of wind speeds and relative directions.

Location estimates from GPS data were transformed to trajectories and rediscretized at hourly intervals using the R package adehabitatLT (Calenge 2006). GPS tracks were split into outbound and inbound sections of a foraging trip based on the maximum distance travelled during the trip (i.e. outbound ends at the maximum distance, where inbound starts). The DD (and video) data were matched temporally to the nearest GPS location (when available) and hourly wind data were extracted from the ERA5 reanalysis dataset (Hersbach et al. 2018; see Chapter 5) for each location. A linear mixed effects model with individual birds as random effect was used to determine if there were significant differences in wind variables between species and breeding location while generalised additive models (GAM) were used to show trends in roll angle with varying wind speeds. The distribution of wind direction was square root transformed to conform to a normal distribution.

**Table 6.1** List of species and breeding location of birds equipped with Daily Diary loggers in respective years.

| **Species** | **Breeding Island** | ***n*** | **Useful DD data (GPS data)** | **Year of Deployment** |
|---|---|---|---|---|
| Wandering Albatross | Marion Island | 33 | 19*(19) | 2016–18, 2020 |
| Grey-headed Albatross | Marion Island | 21 | 11(8) | 2018,2019 |
| Sooty Albatross | Marion Island | 7 | 2(2) | 2018,2019 |
| | Gough Island | 3 | 1(0) | 2017 |
| Atlantic Yellow-nosed Albatross | Gough Island | 10 | 9(8) | 2018 |
| | Nightingale Island | 14 | 0 | 2017 |
| White-chinned Petrel | Marion Island | 4 | 1(0) | 2019 |
| Great Shearwater | Nightingale Island | 9 | 1(1) | 2018 |

* Only 12 individuals with back-mounted DD loggers were used in this chapter

## Results

All but one of the 101 equipped individuals were recaptured upon returning to their respective breeding islands. Ten DD loggers were lost and from the remaining 91, useful data could only be obtained from 44, with the remaining 47 loggers running out of power before the birds departed or had corrupted data. Logger retrieval rate was lowest for the smaller burrowing birds, White-chinned Petrels *Procellaria aequinoctialis* and Great Shearwaters, but useful DD data were obtained for at least one individual of every species (Table 6.1). In addition to the DD data, accompanying GPS tracks were recorded for all but six individuals, representing five species (Table 6.1). Video data overlapping with DD data (flight periods) were recorded for Wandering (*n* = 8), Grey-headed (*n* = 1), and Sooty Albatrosses (*n* = 2), see Chapter 4 for details. The DD loggers recorded data for an average of 74 ± 23 hours across all species with 75% of data from the outbound section of the foraging trip. Where GPS tracks were available, the tracks covered the whole foraging trip, except for two Sooty Albatross and one Grey-headed Albatross tracks (2019), where GPS tracks were only recorded during the outbound section of the trip.

Wandering Albatrosses spent less time in flight than smaller species from Marion Island and the Sooty Albatross from Gough Island (Table 6.2), but Wandering Albatrosses were tracked towards the end of summer when day lengths were shorter. Yellow-nosed Albatrosses spent less time in flight than the other albatrosses, while Great Shearwaters spent the least amount of time in flight (Table 6.2). The birds flew in similar wind conditions, with an average wind direction of 112 ± 63° (i.e. WNW) and speed of 10 ± 4 $\mathrm{m{\cdot}s^{-1}}$. There was no significant difference ($p > 0.1$) in wind conditions between species, but the sample sizes were inconsistent. Marginally significant results were obtained for Wandering Albatrosses that flew in the stronger winds than the other species (11 ± 5 $\mathrm{m{\cdot}s^{-1}}$; $t_{33} = 1.85$, $p = 0.07$) and Sooty Albatrosses that flew in different wind direction (151 ± 29°; $t_{33} = 1.94$, p = 0.06) than other species. When grouping birds by breeding location, Marion Island birds experienced stronger winds in the southwest Indian Ocean (11 ± 4 $\mathrm{m{\cdot}s^{-1}}$) than birds from Tristan and Gough in the south Atlantic Ocean (8 ± 3 $\mathrm{m{\cdot}s^{-1}}$; $t_{32} = 4.95$, $p < 001$). The birds flew in different wind conditions during outbound and inbound flights, except for Grey-headed Albatrosses that consistently flew in westerly winds and Sooty Albatrosses where only outbound flights were tracked (Figure 6.1a). Wandering and Yellow-nosed Albatrosses mainly flew with cross winds from the left during outbound flights and switched to cross winds from the right when inbound, but Wandering Albatrosses also flew with some inbound tail winds (Figure 6.1b). Grey-headed Albatrosses flew with tail winds during outbound flights and alternated between cross winds from the left and right (majority) during inbound flights while tacking back into the wind (Figure 6.1b). The Great Shearwater started foraging within a day of leaving its nest and flew in various directions relative to the wind while outbound, but mainly flew with cross winds from the left when returning to its nest (Figure 6.1b). Sooty Albatrosses were only tracked for the first part of their foraging trips, when they mainly flew with cross winds from the right (Figure 6.1b).

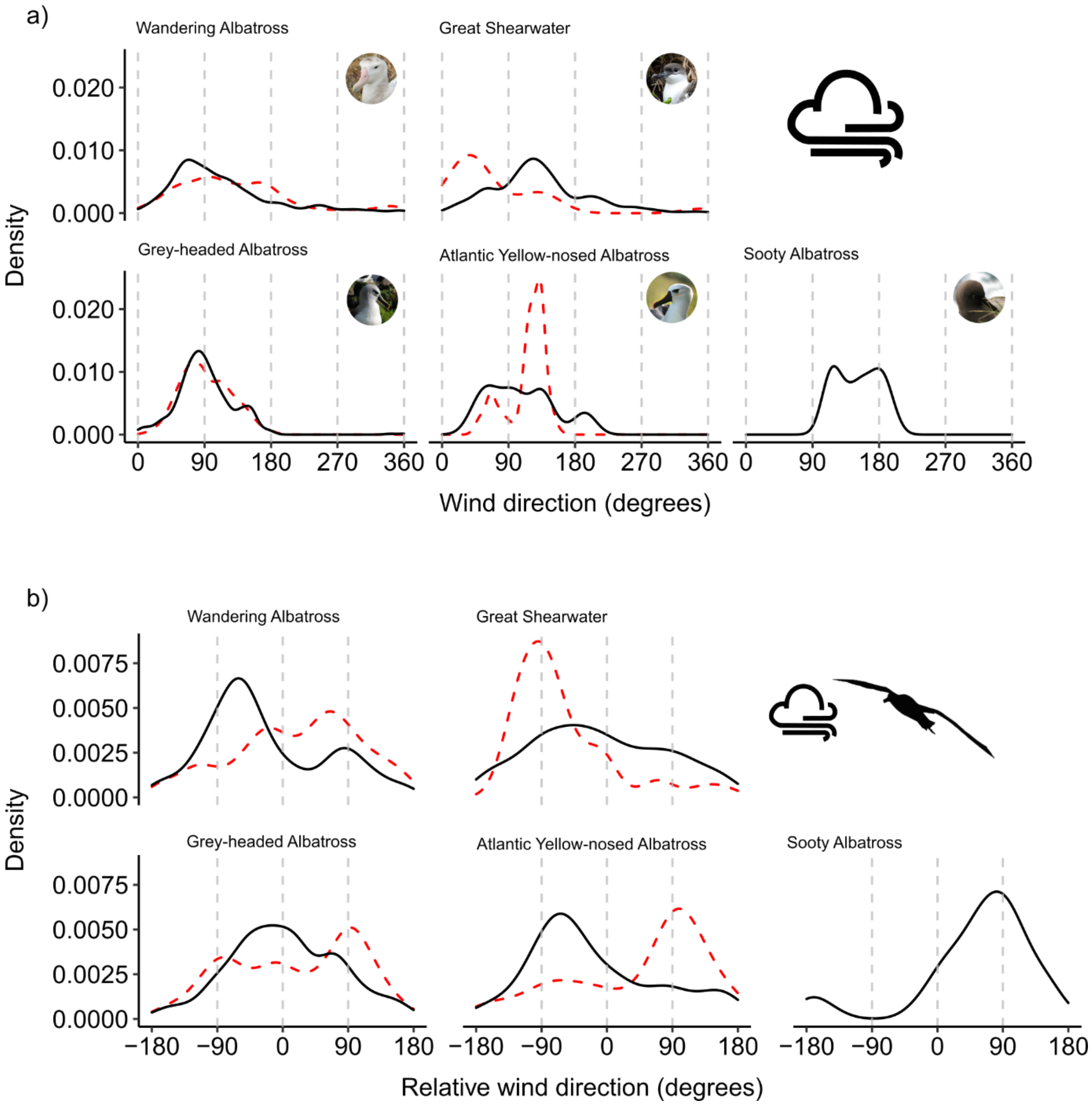

**Figure 6.1:** Distribution of wind direction experienced by five seabird species during outbound (black solid line) and inbound (dashed red line) sections of foraging trips. There were no inbound data for Sooty Albatrosses and thus no red dashed line. **a)** Shows the absolute wind direction where the angles represent the direction the wind is blowing in, i.e. 0° is a southerly wind blowing from south to north. **b)** Is the relative wind direction, i.e. the direction of the wind relative to the course of the bird, where smaller values represent tail winds and negative values are winds coming from the left of the birds.

Bird-borne video loggers recorded 18 hours of flight footage from three species: Wandering, Grey-headed and Sooty Albatrosses. However, most of the data were from five individuals (see Table 4.3 in Chapter 4). The maximum roll angle recorded was 114° from a Sooty Albatross, 108° from a Wandering Albatross and 103° for a Grey-headed Albatross.

Examples of extreme roll angles from bird-borne video can be seen for Wandering Albatross (https://vimeo.com/511513395), Grey-headed Albatross (https://vimeo.com/511513520) and Sooty Albatross (https://vimeo.com/511513742) at the respective links. However, angles > 80° accounted for only 1% (~10 min) of the recorded flight time across all three species. As shown for Wandering Albatrosses in Chapter 5, the roll angle distribution (from video data) of Sooty and Grey-headed Albatrosses were also skewed, presumably in response to wind conditions (Figure 6.2). However, the sample sizes were much smaller for Sooty (*n* = 2) and Grey-headed Albatrosses (*n* = 1) than Wandering Albatrosses, and no GPS data were available for the Grey-headed Albatross.

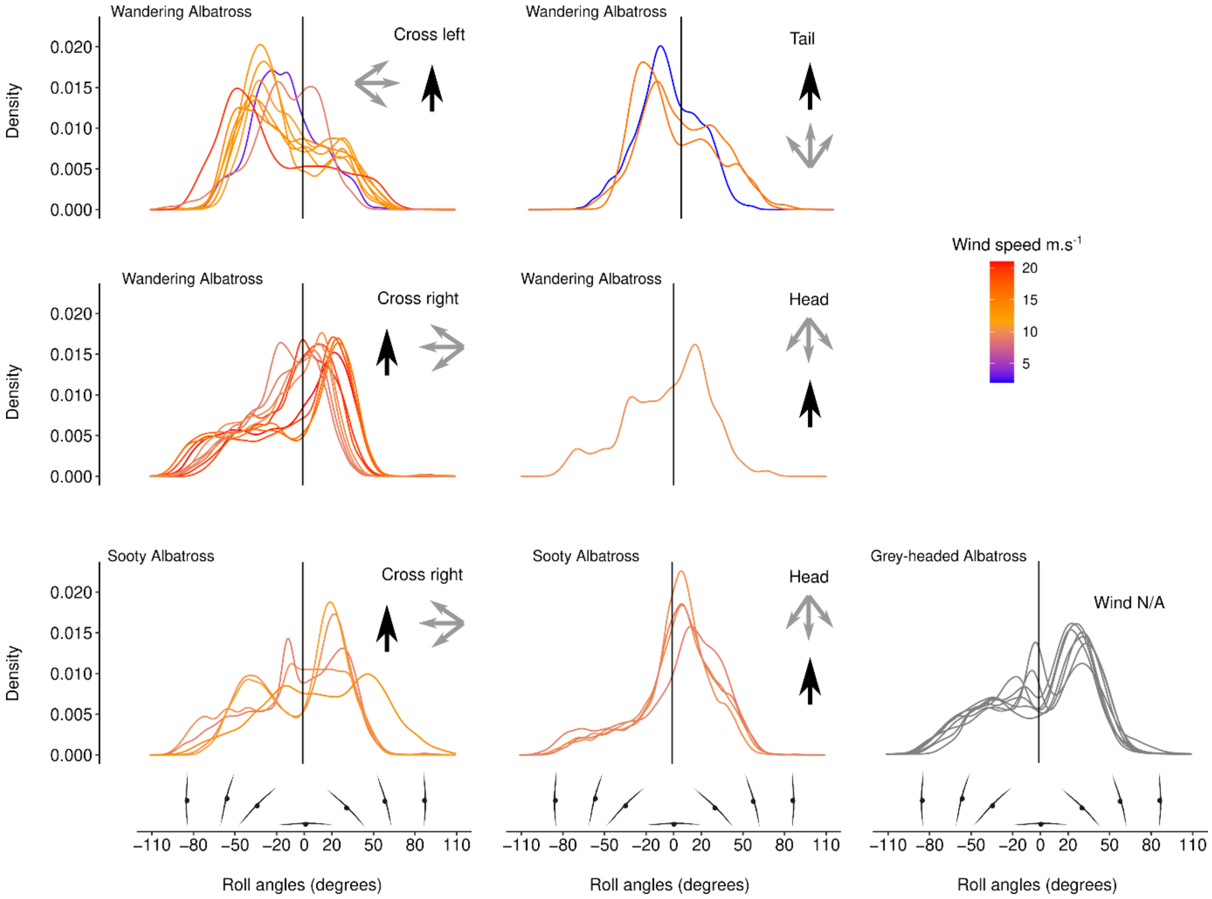

**Figure 6.2:** Frequency distribution of roll angles extracted from video loggers for Wandering, Sooty and Grey-headed Albatrosses in relation to wind speed and relative direction. The relative wind direction was grouped into four categories: **a)** cross wind coming from the left, **b)** cross wind coming from the right, **c)** head wind, and **d)** tail wind while colour represents wind speed (apart from Grey-headed Albatrosses where wind speed and relative direction was not available).

The average maximum roll angles (at the respective turns of dynamic soaring cycles) were similar for all albatrosses and the White-chinned Petrel (~39°) but was significantly lower for the Great Shearwater (20°; $t_{22} = 3.07$, $p = 0.006$). Indeed, the Great Shearwater's flight behaviour was consistently different from the other species (Table 6.2). The mean duration of dynamic soaring cycles was 10 ± 1 s for Wandering Albatrosses, 9 ± 1 s for Grey-headed Albatrosses and 8 ± 1 s for Sooty and Yellow-nosed Albatrosses (Table 6.2). The duration of dynamic soaring cycles could not be reliably estimated for the White-chinned Petrel or Great Shearwater as neither showed consistent repetition of roll angle patterns associated with dynamic soaring. Visual observation of DD data where repetitive cycles did occur suggests that dynamic soaring cycles for White-chinned Petrels and Great Shearwaters most likely last 6–7 s. All species constantly experienced centripetal forces > 0 *g* and all species apart from Wandering Albatrosses and the Great Shearwater experienced centripetal forces > 1 *g* at least every hour of flight. The maximum recorded centripetal force was 1.98 *g* from a Grey-headed Albatross flying in a 11 $m \cdot s^{-1}$ cross wind, while Wandering Albatrosses had the lowest maximum value (1.26 *g*). The absolute difference between maximum roll angles of individual dynamic soaring cycles (i.e. difference between peaks at the respective turns of the cycle) was greatest for the smaller albatrosses and the White-chinned Petrel (total roll, Table 6.2).

Birds breeding at Tristan and Gough flapped considerably more (20% of the time) than birds breeding on Marion Island (10%; $t_{32} = 3.38$, $p = 0.002$). Among Marion albatrosses, Wandering Albatrosses spent more time flapping than smaller Grey-headed Albatrosses (Table 6.2) and had the lowest flapping intensity, but only the latter was significantly different ($t_{21} = 2.95$, $p = 0.008$). The Great Shearwater and White-chinned Petrel spent the most time flapping among birds tracked from their respective breeding sites (Tristan and Marion Island) and the Great Shearwater had the highest flapping intensity of all species (Table 6.2). Overall, wind speed influenced flapping behaviour where low winds resulted in increased flapping as well as increased flapping in head winds in general (Figure 6.3). However, most species were only tracked in a single breeding year and experienced little variation in wind conditions. Only Wandering and Grey-headed Albatrosses were tracked flying in strong winds (>15 $m \cdot s^{-1}$); Sooty and Yellow-nosed Albatrosses were only tracked in moderate winds (5–15 $m \cdot s^{-1}$). Albatrosses had the highest flapping rate in head winds and tail winds where wind speeds were lower. Wandering Albatrosses had increased flapping rates in moderate cross winds as well as very strong winds (Figure 6.4; but see Chapter 5 for discussion on the flapping of Wandering Albatrosses). Yellow-nosed albatrosses had moderate flapping rates regardless of wind direction with highest rates in stronger head winds, but again, the birds were only tracked flying in moderate wind speeds (Figure 6.4). Wind speed also affected roll angles, with stronger winds resulting in more extreme roll angles (Figure 6.5). The effect of wind speed on roll angle was less pronounced for the Great Shearwater and two Sooty Albatrosses, but the sample sizes were too low for meaningful comparisons. Wandering Albatrosses seemed to increase their roll angles up to a point, but the angles were again lower at very high wind speeds (Figure 6.5).

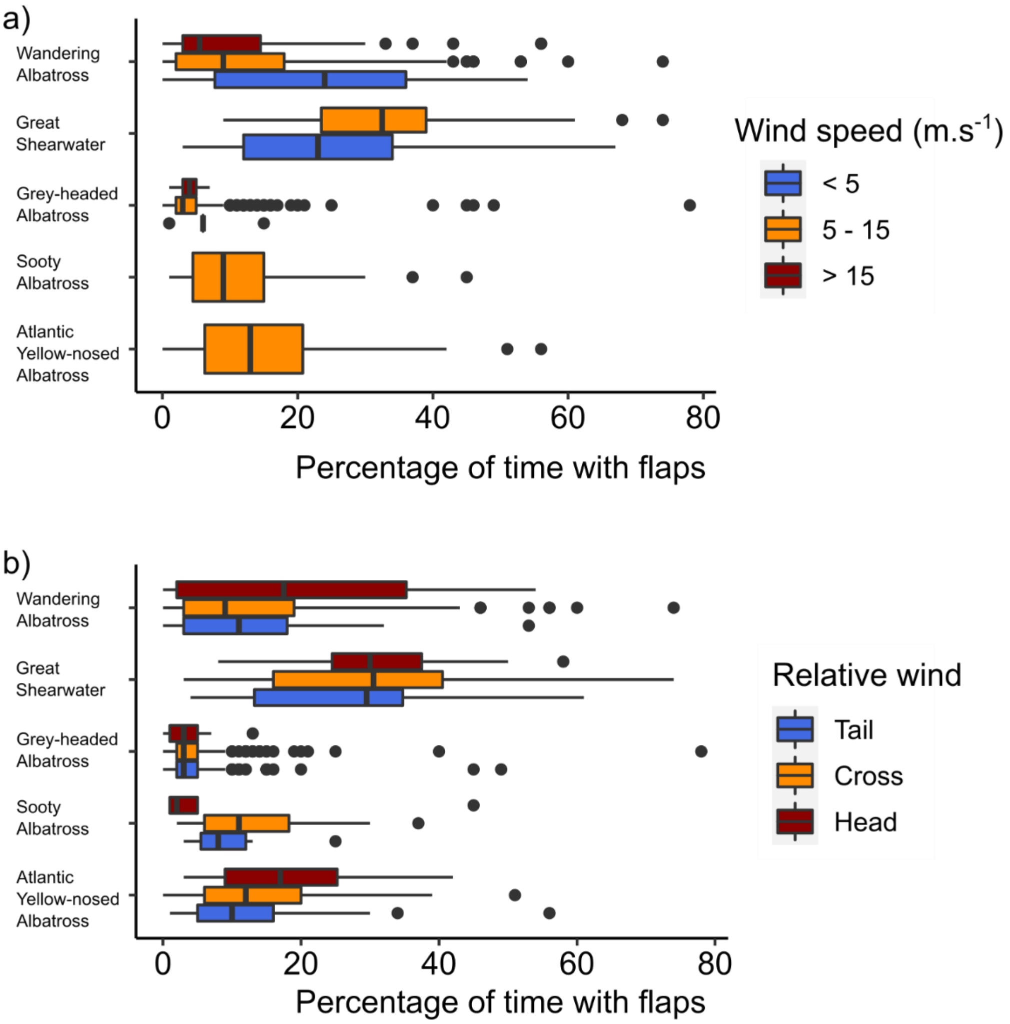

**Figure 6.3:** Presence of flaps in flight in relation to **a)** wind speed and **b)** direction for several seabird species. The percentage of seconds with at least one flap is shown where wind speed and direction are grouped into three broad categories.

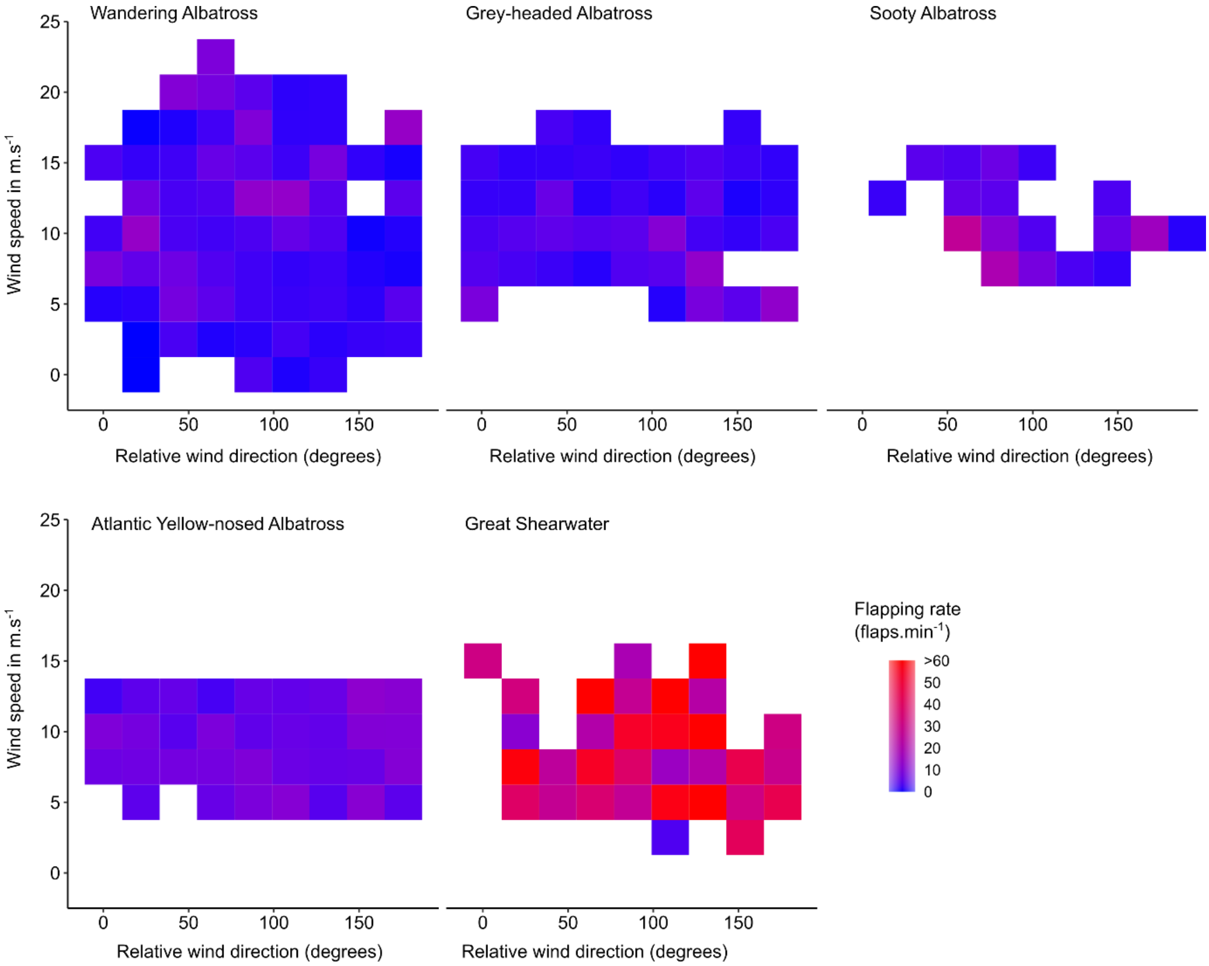

**Figure 6.4:** Flapping rate of several seabird species at varying wind speeds and relative wind directions.

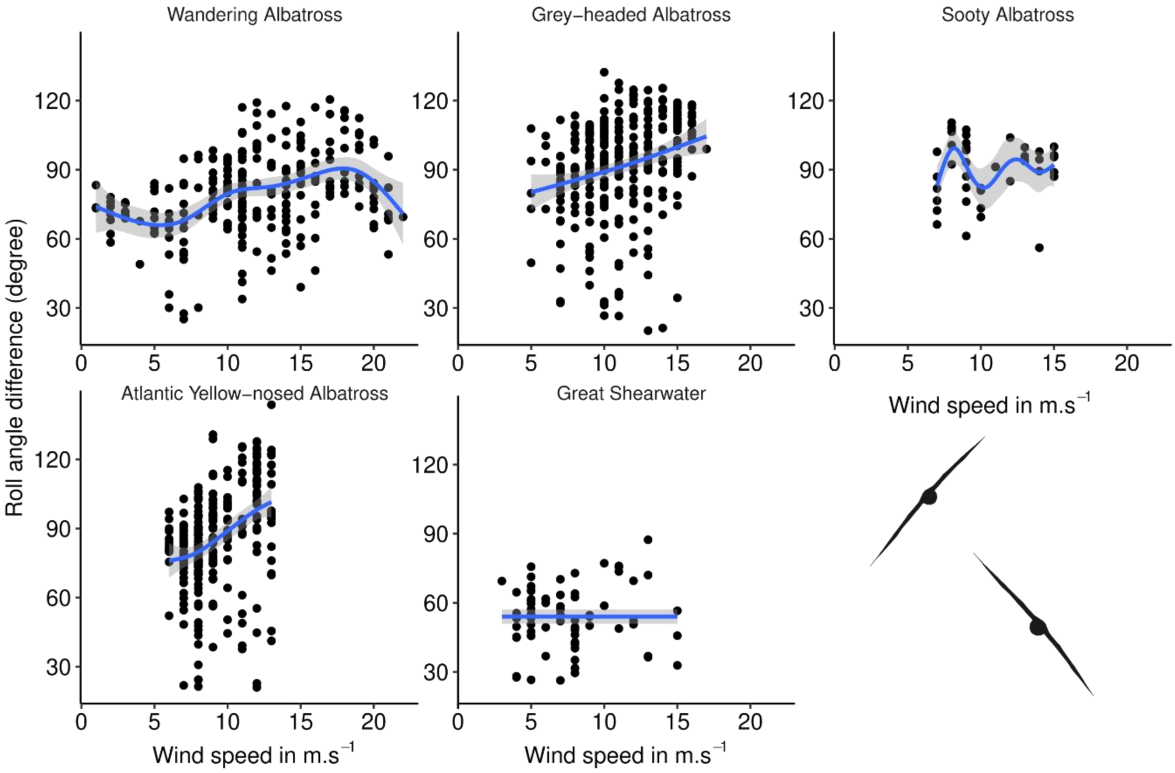

**Figure 6.5:** The effect of wind speed on the range of roll angles (absolute difference of roll angles at both upper and lower turns of dynamic soaring cycle) of several seabird species with fitted curves (GAM).

**Table 6.2**: Summary of estimated metric pertaining to the flight of several Procellariiformes species breeding in the southern Indian and Atlantic Ocean. Values are means ± SD across all sampled individuals where valid data were available.

| | | **Time flapping (%)** | | **Flap rate (flaps·min$^{-1}$)** | | **Flap intensity (VeDBA *g*)** | | | | |
|---|---|---|---|---|---|---|---|---|---|---|
| **Species** | **Flight %** | **All flaps** | **VeDBA > 0.7 flaps** | **All flaps** | **VeDBA > 0.7 flaps** | **All flaps** | **VeDBA > 0.7 flaps** | **Cycle duration (s)** | **Total roll (°)** | **Max *g*** |
| **Indian Ocean - Marion Island** | | | | | | | | | | |
| Wandering Albatross | 56 ± 19 | 12.4 ± 6.3 | 6.9 ± 4.6 | 12 ± 6 | 5 ± 4 | 0.73 ± 0.1 | 0.86 ± 0.05 | 10 ± 1.2 | 56 ± 5 | 1.26 |
| Grey-headed Albatross | 67 ± 15 | 5.1 ± 2 | 3.7 ± 1.7 | 5 ± 2 | 3 ± 1 | 0.91 ± 0.11 | 0.96 ± 0.04 | 9 ± 0.8 | 63 ± 7 | 1.98 |
| Sooty Albatross | 73 ± 4 | 8.6 ± 1.5 | 6.3 ± 0.2 | 8 ± 1 | 5 ± 2 | 0.83 ± 0.02 | 0.96 ± 0.02 | 8.2 ± 0.9 | 61 ± 4 | 1.69 |
| White-chinned Petrel | 77 | 12.8 | 10.5 | 17 | 11 | 0.85 | 0.92 | - | 67 | 1.67 |
| **Mean ± SD** | **68 ± 9** | **9.7 ± 3.6** | **6.9 ± 3.0** | **11 ± 5** | **6 ± 3** | **0.83 ± 0.07** | **0.93 ± 0.05** | **9 ± 1** | **62 ± 5** | **1.65 ± 0.30** |
| **Atlantic Ocean - Tristan da Cunha archipelago** | | | | | | | | | | |
| Sooty Albatross | 76 | 17.2 | 15.1 | 19 | 14 | 0.89 | 0.93 | 7.5 | | 1.43 |
| Atlantic Yellow-nosed Albatross | 53 ± 20 | 14.5 ± 4 | 12 ± 3.7 | 15 ± 4 | 7 ± 2 | 0.82 ± 0.02 | 0.89 ± 0.01 | 7.9 ± 0.29 | 60 ± 5 | 1.79 |
| Great Shearwater | 45 | 30.1 | 28.4 | 43 | 40 | 1.06 | 1.05 | - | 38 | 1.67 |
| **Mean ± SD** | **58 ± 16** | **20.6 ± 8.3** | **18.5 ± 8.7** | **26 ± 15** | **20 ± 17** | **0.92 ± 0.12** | **0.96 ± 0.08** | **7.7 ± 0.0** | **49 ± 16** | **1.63 ± 0.18** |

## Discussion

In this Chapter I show how the flight behaviour of six procellariiform species varies with body size and local wind conditions. Because sample sizes were modest and most data were collected during the outbound section of the foraging trips, the behavioural patterns reported in this chapter are not necessarily representative of the population (or foraging trips of individual species) but provide context for the fine-scale behaviour of the individuals birds.

## Wind conditions

Much of the sub-Antarctic is dominated by westerly winds and most of the tracked birds flew in westerly winds (i.e. winds coming from the west) during outbound and inbound flights, but Wandering Albatrosses also flew with northerly winds on inbound flights. Wandering Albatrosses in the southwestern Indian Ocean typically perform anti-clockwise looping foraging trips where they leave their nests in favourable westerly winds and travel north into areas with prevailing easterly winds, allowing them to then travel back to their nests while constantly flying in favourable wind conditions (Weimerskirch et al. 2000). The same strategy can be followed by performing clockwise trips when travelling to the south (Weimerskirch et al. 2000) and this is what I observed for Grey-headed Albatrosses. Grey-headed Albatrosses performed clockwise looping foraging trips, constantly flying in cross winds, before returning to the colony with the prevailing westerly wind at their backs. Grey-headed Albatrosses seemed to favour flying with tail winds more often than the other species. Many of their foraging trips were directed flights with following winds, to a narrow band between the subtropical and sub-Antarctic fronts (Reisinger et al. 2018; Carpenter-Kling et al. 2020) where the birds spend several days foraging. This area is to the east of Marion Island and the birds had to make their way back against the wind, but maintained a cross wind orientation by tacking across the wind to gain ground against the wind (Weimerskirch et al. 2002; Nevitt et al. 2008; Richardson 2011; Sachs 2016). Wind conditions at the start of a foraging trip may influence the foraging strategy of seabirds (De Pascalis et al. 2020) and the birds may also have knowledge of the local wind fields (Ventura et al. 2020) allowing them to decide on the direction of their flight.

Only two of the three Sooty Albatrosses had partial GPS tracks (from Marion Island) and both birds headed east to south-east in northerly and northwesterly winds. More typically, Sooty Albatrosses travel north from Marion Island (Schoombie et al. 2017; Carpenter-Kling et al. 2020) and these two tracked birds were most likely driven southeast by the unusually northerly winds. Birds foraging in the south Atlantic flew in less windy conditions, most likely because the Atlantic breeders were only tracked relatively close to their breeding islands. The southwest Indian Ocean is distinctly windier than the south Atlantic (Young

1999) and mean wind speed increases with latitude in the Southern Ocean, with highest speeds between 50–60° S (Young 1999; Weimerskirch et al. 2012). However, Great Shearwaters from Gough Island have been tracked flying in high wind speeds covering extreme daily distances (Schoombie et al. 2018).

## Dynamic soaring behaviour

Video data showed that albatrosses occasionally roll at extreme angles, going beyond vertical (103°–114°) regardless of size, but the most extreme angle (114°) was from the smallest albatross sampled, the Sooty Albatross. Dynamic soaring procellariiforms are probably all capable of rolling at extreme angles, but larger birds might be limited when turning into the wind at high speeds when the forces on the wings would be highest (Richardson 2011). Previously albatrosses have been estimated to roll at angles up to 70° (Pennycuick 1982). Large albatrosses, such as Wandering Albatrosses, also have higher wing loading than smaller species, which are associated with increased flight speeds (Warham 1977; Shaffer et al. 2001b). Increased flight speeds result in increased centripetal acceleration and remote controlled gliders have been shown to record centripetal forces > 90 *g* during extreme high speed dynamic soaring flight (Richardson 2012). Dynamic soaring seabirds in the present study were often subjected to centripetal forces > 1 *g* (i.e. 1 *g* above the force of gravity), reaching up to 1.3 *g* in Wandering Albatrosses and ~2 *g* in Grey-headed Albatrosses. The physical strength (e.g. structural wing strength) may limit the rate at which birds are able to turn in varying wind conditions and birds may perform longer dynamic soaring cycles to reduce the aerodynamic forces on their wings (Richardson 2011). This is evident from Wandering Albatrosses which had the longest period for individual dynamic soaring cycles. Richardson (2011) argued that the theoretical airspeed that Wandering Albatrosses can achieve is much faster than what is seen in nature, which he attributed to the increased forces experienced at such speeds. Unfortunately, I did not have wing measurements or masses for the birds used in my study and could not accurately calculate wing loading for each individual. Future study could explore the potential physical limitations of flying seabirds in varying wind conditions.

Increased wind speeds resulted in larger roll angles in albatrosses, but the total roll angle (absolute difference of both upper and lower turn angles) seemed to be lower for Wandering Albatrosses. Wandering Albatrosses have the largest wingspan of extant birds, at approximately 3–4 m (Tickell 2000; Shaffer et al. 2001b), and consequently a high wing loading (Pennycuick 1982), which is associated with lower manoeuvrability and turning rates (Warham 1977). It seems possible that Wandering Albatrosses might be more limited in their response to local wind conditions than smaller species. When flying in strong winds, Wandering Albatrosses had larger roll angles when turning with the wind (upper turn of the dynamic soaring cycles) than when turning into the wind (lower turn). Smaller species are expected to have faster turning rates (Warham 1977), and this was supported by the seemingly shorter dynamic soaring cycles exhibited by the White-chinned Petrel and Great Shearwater. The Great Shearwater had the smallest roll angles and did not display regular dynamic soaring cycles. Shearwaters are varied in their flight ability, which may be compromised when species are adapted to dive in pursuit of prey (Kuroda 1953; Brown et al. 1978), such as Sooty Shearwaters *Ardenna griseus* able to dive to ~70 m (Shaffer et al. 2009). Great Shearwaters seem to be intermediate with regards to flying and diving ability within the shearwaters (Brown et al. 1978) and although I only obtained behavioural data from a foraging individual, Great Shearwaters have the ability to fly very fast in high wind speeds while commuting (Schoombie et al. 2018). During such flights they may display more regular dynamic soaring with extreme roll angles, but more data are needed to confirm this. The ability of dynamic soaring seabirds to vary their roll angles and consequently change the length of individual soaring cycles, may have consequences for their ability to adapt to changing wind conditions (see below).

## Flapping behaviour

The use of accelerometers to measure flapping behaviour in albatrosses has demonstrated a greater role of flapping flight in dynamic soaring than previously appreciated (Sato et al. 2009; Sakamoto et al. 2013). One of the striking results of my study was that Wandering Albatrosses did not seem to flap significantly less than smaller albatrosses. Indeed, Grey-headed Albatrosses flapped least off all the species studied. Flapping flight in procellariiforms is thought to scale allometrically, with large birds flapping less than small birds (Sato et al. 2009), but sample sizes remain low and more data are required to assess population level behaviour. It also has to be noted that Grey-headed Albatrosses were flying with tail-winds on many occasions, which could also explain why they seemingly flapped less. Wandering Albatrosses did have the lowest flapping intensity (VeDBA), which could be used as a measure of energy expenditure (Van Walsum et al. 2020). Chapter 5 reported how larger male Wandering Albatrosses flap more than females. Flapping intensity peaks during take-off, as opposed to routine flight and taking off is harder for males given their higher wing loading, especially at lower wind speeds (Clay et al. 2020, Chapter 5). Thus, there might be a trade-off for these larger birds in light winds where they might prefer to flap-glide rather than land, risking increased energy expenditure to take-off again or even getting stuck in a low wind area (Jouventin and Weimerskirch 1990; Alerstam et al. 1993).

In contrast, the smaller Great Shearwater flapped considerably more than any of the other birds in the present study and had the highest flapping intensity, which is expected for smaller bodies birds (Sato et al. 2009). Shearwaters have a different flight mode to dynamic soaring birds, where they soar close to the water in wave troughs with intermittent flapping (Spivey et al. 2014). Spear and Ainley (1997b) previously grouped Great Shearwaters and White-chinned Petrels together with flap-gliding seabirds, while "diving-type" shearwaters were grouped with glide-flappers. Recent studies have shown that both Great Shearwaters and White-chinned Petrels perform shallow dives, but may be capable of diving to depths of ~20 m (Ronconi et al. 2010; Rollinson et al. 2014). Unfortunately, I did not have tracking data for the White-chinned Petrel and the results are thus not comparable to the Great Shearwater as the behavioural state (forage or commute) and wind conditions for the White-chinned Petrel could not be inferred. The amount of flapping observed in albatrosses and petrels are most likely influenced by the winds they are flying in.

## Wind driven flight

Wind speed is a key factor underpinning dynamic soaring among procellariiform seabirds. Overall, birds foraging in the south Atlantic Ocean flapped more than birds foraging in the southwest Indian Ocean linked to the lighter winds in the south Atlantic (Young 1999). The Sooty Albatross tracked from Gough Island flapped almost twice as often as the two birds tracked from Marion Island. Atlantic and Indian Ocean birds might be adapted to fly in different wind conditions and may respond differently to changes in the Southern Ocean climate (Weimerskirch et al. 2012), but more data are required to better understand these observed differences. Grey-headed and Sooty Albatrosses show little overlap between different populations breeding on sub-Antarctic Islands in the Indian (Marion Island) and Atlantic Oceans (South Georgia and Tristan da Cunha; Nel et al. 2001; Clay et al. 2016; Schoombie et al. 2017). However Grey-headed Albatrosses range much further, sometimes performing circumnavigations during non-breeding periods (Clay et al. 2016). White-chinned Petrels breeding on Marion Island mainly stay within waters between Southern Africa and Antarctica (Rollinson et al. 2018), while Great Shearwaters are trans-equatorial migrants basically ranging the entire Atlantic Ocean but with their breeding restricted to the Tristan da Cunha archipelago (Ronconi et al. 2018; Schoombie et al. 2018). The Great Shearwater in the present study stayed close to its breeding island, flapping almost a third of the time, but these birds can also travel incredible distances while rearing chicks with one bird travelling ~14 000 km (possibly 17 000 km, see Chapter 3) in a single foraging trip (Schoombie et al. 2018). With such large ranges, Great Shearwaters are likely adapted to travel and forage in a range of wind conditions and might be well suited for a combination of soaring and flapping flight. Birds relying solely on flapping flight are expected to have smaller ranges, while soaring birds are expected to have larger ranges (Watanabe 2016).

Wind speed and direction seemed to influence the roll angles during dynamic soaring flight as well as the presence of flapping. When flying with cross winds, birds banked into the wind for longer periods and had more extreme roll angles as the wind speed increased. Albatrosses and petrels increase their airspeed when flying into the wind (Pennycuick 1982; Spear and Ainley 1997) and can achieve a net upwind displacement by continuously tacking across the wind (Sachs 2016). The tacking behaviour is necessary to avoid large lateral displacements associated with dynamic soaring (Sachs 2016). In strong winds albatrosses and petrels fly faster (Pennycuick 1982; Spear and Ainley 1997) and these lateral displacements may be larger. Thus the birds may have to adjust their body angles faster by rolling at more extreme angles to avoid large lateral displacements, as such wind drift may have energetic consequences (Tarroux et al. 2016). In light winds birds had smaller roll angles and intermittent flapping was observed. Alerstam et al. (1993) described how albatrosses flew with irregular flight paths in light winds while intermittently flapping, with most flapping seen in Yellow-nosed Albatrosses. Larger species of procellariiforms seem to only flap in light winds while smaller species tend to flap-glide (Pennycuick 1982). My results were similar to the above observations, where larger albatrosses flapped less than smaller birds and mostly in light winds but showed that flapping (or more likely wing morphing, see Chapter 5) may also be important during flight in high wind speeds.

## Conclusions

The flying behaviour of procellariiforms comprises a complex set of fine-scale manoeuvers in response to dynamic environmental conditions. The multitude of responses by different species are likely one of the factors allowing the large variation in species (and body sizes) to co-exist in the Southern Ocean. Although sample sizes were small for most species, my results highlight the value of a multisensor approach when studying the fine-scale behaviour of free-ranging seabirds. I show how dynamic soaring seabirds of varying sizes respond to local wind patterns, by adjusting their roll angles and supplementing soaring with flapping in unfavourable winds. This demonstrates how seabirds can alter their behaviour to access resources efficiently in a pelagic environment with patchy resource distribution (Weimerskirch 2007). Flapping generally scaled with body size, but wind speed also played a crucial role in the amount of flapping observed. These results also highlight the importance of sampling birds at different breeding locations because local conditions may expose birds to different challenges and threats. Breeding stage also likely influences fine-scale movement patterns, just as it does at much larger scales (through changes in trip duration and distance;

Oppel et al. 2018). I mostly sampled birds during the brood-guard period, when birds might prioritise feeding their chicks above energy efficient flying (Frankish et al. 2020). Future studies of birds at different breeding stages might yield slightly different results. My sample sizes were too small for comparison between sexes (and many sexes were unknown) and future studies could include these comparisons as it is expected that sexually dimorphic seabirds could have different behaviours (Shaffer et al. 2001b; Phillips et al. 2004; Weimerskirch et al. 2014), as was possibly the case for Marion Island Wandering Albatrosses. The use of a range of bio-logging devices, ever decreasing in size, creates exciting new opportunities for the study of free ranging seabirds not possible before.

# Chapter 7: Synthesis

The main aim of this thesis was to study how albatrosses and petrels of varying body sizes respond to changing winds by altering their fine-scale flight behaviour. To achieve this, I used advanced bio-logging technology and developed two novel methods to extract body angles from the bird-borne loggers. The at-sea behaviour of oceanic seabirds is difficult to study as these birds range far from land, limiting opportunities for direct observation. Advances in bio-logging technology have opened new avenues to study the behaviour of seabirds in the absence of human observers. Since the early 2000s, the use of GPS loggers to study seabird behaviour has increased dramatically. I show the limitations of low-cost GPS loggers and the effect of sampling interval on derived metrics (Chapter 3) and conclude that it is preferable to use specialized loggers that record infrasecond data to study fine-scale seabird movement patterns. In Chapter 4 I develop two new methods to use bird-borne video loggers and IMUs to study the fine-scale flight behaviour of dynamic soaring seabirds. These methods are then applied to a range of seabird species in Chapters 5 and 6, to show how the birds respond to wind conditions.

## Main results

I show that metrics derived from GPS loggers are affected by sampling rates, something that needs to be considered when analysing data or planning research. At short sampling intervals the loggers are subject to measurement error, which compounds over time, resulting in overestimates of distances travelled. As sampling intervals increase, points are subject to interpolation error resulting in distance travelled being underestimated by 10–40%, suggesting that trip distances may be up to 40% longer than those reported in the literature based on hourly sample intervals. Error in path length (the distance between individual points) increased steadily with increasing sampling intervals up to 5 km for straight flights and 15 km for sinuous flights at hourly intervals. The error in relative turning angle between successive GPS locations was highest at short intervals < 1 min, after which the error seemingly stabilized. This resulted in behavioural states (identified by path length and turning angles) being variable at shorter sampling intervals, stabilising at moderate intervals and steadily becoming more unstable as intervals increased. Seabird studies using multiple GPS data sets, with varying sampling intervals, usually use the coarsest sampling interval to allow comparison of the data (Johnson et al. 2017). This approach inevitably has consequences on the quality of the inferences that can be made, which has to be acknowledged when interpreting results. When data with varying sampling intervals are treated as separate populations (Clay et al. 2020), these might not be directly comparable and different results might be obtained if corrected for the interpolation error associated with infrequent sampling rates.

In Chapter 4, I show how back-mounted video loggers can be used to extract roll angles by estimating the horizon angle in video footage. Pelagic seabirds flying over the open ocean have the horizon in sight most of the time, and horizon angle can be extracted reliably using computer vision techniques to identify strong colour gradients (where the ocean meets the sky). Video loggers are power intensive and record large data files, resulting in relatively short recording times. Accordingly, I explored the use of IMUs to extract fine-scale body angles of seabirds for longer periods than is currently possible with video loggers (e.g. several days). Tri-axial accelerometers are often used to estimate animal posture, but the increased centripetal forces experienced by soaring seabirds precludes the use of accelerometers for such purposes. Tri-axial magnetometers are free from the effects of centripetal acceleration and I show how they can be used to estimate yaw and roll angles, if we assume that birds do not pitch significantly during routine flight.

Using these newly developed methods, in Chapter 5 I analysed the fine-scale flight behaviour of Wandering Albatrosses by coupling roll angles and flapping flight (as identified from accelerometer data). Both roll angles and flapping rates were influenced by wind speed, with increasing wind speed resulting in more extreme roll angles and reduced flapping. The albatrosses adjusted for wind drift by turning into the wind for longer periods and were able to fly in light winds by supplementing dynamic soaring with intermittent flapping, particularly at the upper turn of the dynamic soaring cycle. The birds flapped more than expected, with males flapping more often than females and males seemed to restrict their take-offs to favourable wind conditions. These factors likely contribute to the spatial segregation sometimes reported for this sexually dimorphic species.

Finally, in Chapter 6 I compared the flight behaviour of six procellariiform species across a range of body sizes. Although sample sizes were small, I showed how species employed different flight strategies despite largely experiencing similar wind conditions (i.e. westerly winds dominating the Southern Ocean). Birds breeding in the south Atlantic Ocean typically experienced slightly lower wind speeds and flapped more than birds breeding at a higher latitude in the southwestern Indian Ocean. All species increased their roll angles with increasing winds while spending less time flapping, except for the Great Shearwater, which had a different flight mode and had overall smaller roll angles and increased flapping activity.

## The problem of sampling rates and location estimates

The introduction of microprocessors in bio-logging technology in the 1980s started a revolution of new ways to study animals in their natural environment (Kooyman 2004; Wilson and Vandenabeele 2012). With the lower cost and increased reliability of GPS loggers, studies using these loggers have increased dramatically in the past decade, but questions have been raised around the efficacy of GPS loggers to study animal behaviour when only small sample sizes could be obtained (Hebblewhite and Haydon 2010). Now larger sample sizes are available (e.g. Weimerskirch et al. 2014) or studies resort to collaborations where tracking data from various sources are pooled to allow large-scale inferences (Reisinger et al. 2018; Hindell et al. 2020). However, one drawback of using pooled datasets is the lack of standardisation among bio-logging studies (Campbell et al. 2016; Williams et al. 2020b). When using GPS loggers to study animal movement, the chosen sampling rates are rarely justified, apart from maximising recording time.

My results show that it is very important to consider sampling rates of GPS loggers when studying seabird movement. For large-scale movements (distribution ranges), coarse sampling rates (i.e. hourly) are adequate, but estimates of distances travelled inevitably will be underestimated. The magnitude of this error depends on the flight style of the birds; distances travelled will be underestimated to a greater extent for birds flying with tortuous paths. Although sinuous flight paths often occur during foraging, responses to wind may also play a role. A bird flying in light winds may increase the duration of soaring cycles, resulting in longer turns and more sinuous flight paths. Likewise, a bird tacking into a headwind may also have a more sinuous flight path (Nevitt et al. 2008; Richardson 2011; Sachs 2016). This may be different between species where flight mode may result in larger deviations from the straight-line flight course (Alerstam et al. 1993) and species may respond differently to wind conditions depending on flight mode (Ainley et al. 2015).

When location estimates are used to infer behavioural states, the effect of sampling rates become more complex. Many studies of animal behaviour use a combination of path length and turning angle to segregate location estimates of a foraging trip into discrete states (Patterson et al. 2008). However, the ability to accurately infer states may vary considerably in relation to sampling intervals, which will be applicable to behaviour at different scales. Coarse sampling rates may result in behavioural states being smoothed over a long time period and because of error associated with path length, short foraging events will most likely be missed. Although moderate (10–30 min) sampling rates produced the most stable estimates of behavioural state, they are not necessarily the most accurate. Accuracy depends on the behaviour in question. Models used to identify states from tracking data have been validated on several occasions, but these are mostly done with sampling rates of 1–10 mins (Dean et al. 2013; Thiebault and Tremblay 2013; Bennison et al. 2017). These validation studies may not be applicable to data at coarse sampling rates. Coarse sampling rates can give information regarding "hotspot" areas that could be associated with foraging, but these areas are easily identified by using simple kernel density estimates, negating the need for complex modelling (Bennison et al. 2017).

A simple way to decide on sampling intervals is to use the Nyquist (or sampling) theorem, which posits that the sampling rate should be at least double that of behaviour in question (Williams et al. 2020b). For example, when studying the daily movement of an animal, a 12-hour sampling interval would be appropriate. When the aim is to describe a foraging event that lasts 10 mins, a sampling interval of 5 min is needed. Seabirds may also use "forage-in-flight" strategies (Weimerskirch et al. 1997) where they cover larger distances and not necessarily target a specific area. During these flights they could encounter prey sporadically and often land for short periods of time. These short foraging bouts are difficult to identify from GPS data, with coarse sampling rates likely missing these events. Where researchers are interested in the fine-scale movement of animals to infer behaviour, it might be necessary to use specialised loggers, such as IMUs, or specialised GPS loggers with higher sampling rates and accuracy. GPS loggers that can record raw GPS data can be post-processed to correct for errors associated with clock drift and interference in the ionosphere (Ranacher et al. 2016a). These loggers can be used to estimate position at decimetre accuracy while logging at up to 10 Hz and have been used to study the dynamic soaring cycle of albatrosses (Sachs 2016).

## Loggers beyond location

Observing animals in their natural environment through visual observation is still a very important aspect of animal behavioural studies and technological advances should not be used in such a manner that they remove biologists from the field (Hebblewhite and Haydon 2010). Visual observation is challenging when it comes to far-ranging or cryptic animals, where direct observation can have many logistical challenges. Many seabirds spend most of their time at sea, only coming to land to breed or find a mate. Since the early 1900s, ship-based observation of seabirds have been used to study seabird ecology (Jespersen 1924;

Tasker et al. 1984; Spear et al. 2004) and is still an important tool today (Raymond et al. 2010; Ryan et al. 2020). However, ship-based observations also have associated biases, especially if birds react to the presence of a ship, as is often the case for procellariiforms (Griffiths 1982; Pennycuick 1982; Tasker et al. 1984), resulting in observations that may not reflect their natural behaviour.

Since the introduction of GPS loggers in seabird behavioural studies in the early 2000s (Weimerskirch et al. 2002; Ryan et al. 2004), the technologies available to measure animal movement have increased substantially. IMUs (including accelerometers, magnetometers and gyroscopes) can record data at much higher rates (e.g. 300 Hz or even more) and have much lower power consumption than GPS loggers. With advances in solid-state technology (Wilson and Vandenabeele 2012), these loggers are now small enough to allow deployment on small birds for long periods of time (Liechti et al. 2013). The use of IMUs on flying birds has mainly been restricted to the study of flapping flight from accelerometers (Williams et al. 2015), with a large number of studies on cormorants where the relationship between dynamic movement and energy expenditure has been well described (Kato et al. 2006; Wilson et al. 2006; Gómez Laich et al. 2008; Sato et al. 2008; Halsey et al. 2009b). The potential uses of magnetometers to study animal behaviour have recently been highlighted (Williams et al. 2017; Chakravarty et al. 2019) and these loggers have been used to described the flight of large, thermal-soaring condors (Williams et al. 2018).

In this thesis, tri-axial magnetometers were particularly useful to study the flight of dynamic soaring seabirds as these data are not sensitive to centripetal acceleration. However, validation through visual observation using bird-borne cameras was vital for the development of this method. When using IMUs to infer behaviour, it is imperative that the conclusions make biological sense and visual observation (human observer or bird-borne camera) may be needed to confirm inferred behaviours (Williams et al. 2018, 2020b). IMU data also complimented video data in that the IMU data could be used to identify potentially interesting video sequences. Combing through many hours of video footage in search of interesting animal behaviour is a tedious task, and transient behaviours can easily be missed. Visual observation of IMU data traces can be used to rapidly identify periods of interest and relevant video sequences can then be isolated, reducing the amount of footage to look through. Recently, IMU data have even been used to control bird-borne cameras to only capture certain events (Korpela et al. 2020).

The magnetometer analyses described in Chapter 4 showed how yaw angles (heading) can be calculated from dynamic soaring seabirds. To my knowledge, this is the first study to do so, as estimates of heading from magnetometers usually depends on posture corrections from accelerometer data (Bidder et al. 2015), which is not possible for dynamic soaring birds (Williams et al. 2015). Accurate heading from soaring seabirds opens up exciting opportunities to study fine-scale flight of seabirds using dead-reckoning techniques (Bidder et al. 2015), but more work is needed on this topic as continual calibration of magnetometer loggers will be necessary as well as corrections for wind drift. Such dead-reckoned tracks can now be validated with decimetre-accurate GPS tracks at 10 Hz (see above).

## The flying behaviour of albatrosses and petrels

Seabirds forage in an environment where resources are sparsely distributed across a massive area (Weimerskirch 2007). However, while breeding, they are central place foragers, constrained to return to their nesting grounds to incubate eggs or feed chicks. This makes them an interesting group of birds to study as they all start at the same point, but do not necessarily target the same foraging areas (e.g. Reisinger et al. 2018; Carpenter-Kling et al. 2020). Yet regardless of size, breeding albatrosses and petrels can cover similar distances during foraging trips (see Figure 1.1). Migration ranges of migrating birds are influenced by flight mode where ranges scale allometrically for flapping birds, but is largely independent of body size for soaring birds (Watanabe 2016). It is likely similar for albatrosses and petrels, where their flight mode seems to influence their foraging distribution. I first briefly describe the flight modes and morphology of varying groups of albatrosses and petrels, before discussing how they may react to varying winds in the Southern Ocean.

## Flight mode and morphology

Southern Ocean seabirds have been divided into several broad groups based on their modes of flight (Warham 1977; Pennycuick 1982; Spear and Ainley 1997; Ainley et al. 2015). These include gliders (or dynamic soarers), which use dynamic soaring flight most of the time, only occasionally flapping; flappers, which spend most of their time flapping; and combination flap-gliders, which mostly glide with intermittent flapping, and glide-flappers, which mostly flap with intermittent gliding (Spear and Ainley 1997). Gliders include albatrosses and larger petrels, flap-gliders are surface feeding petrels and larger shearwaters, glide-flappers are diving-type shearwaters and storm petrels, while flappers are mostly Charadriiformes. Flight mode seems to be related to wing loading, and although wing area scales allometrically, there is variation in wing loading between similar-sized species (Warham 1977). Wing loading also varies as birds lose and gain weight (Warham 1977). For example, wing loading will be lower immediately after a long incubation shift and higher when returning to its nest with a full stomach. This may result in birds favouring flying in winds with a head wind component during outbound flights while favouring tail wind components during inbound flights (Alerstam et al. 2019), which may result in the looping nature of many large seabirds while breeding (Weimerskirch et al. 1997). Unfortunately, I could not test for differences in flight behaviour between outbound and inbound flights as most of my fine-scale data were from outbound flights. However, tracking data suggest that species may have different flight strategies during inbound and outbound flights. Wandering Albatrosses mainly flew with cross winds but occasionally flew with tail winds during inbound flights, while Grey-headed Albatrosses occasionally flew with tail winds during outbound flights and flew into the wind to get back to their nests with tacking flight. Changes in wing loading during a foraging trip may influence decisions on where birds forage in certain wind conditions, but birds may also be able to change their wing loading by altering their wing configurations (Pennycuick 1960). The effect of varying wing loading is likely more pronounced in birds that do not regularly use a dynamic soaring , such as glide-flappers (e.g. diving shearwaters), where the birds may favour flying at low altitudes in head winds during outbound flights and at higher altitudes assisted by following winds during inbound flights (Alerstam et al. 2019).

In general, procellariiforms can be grouped by body size such that larger birds have higher wing loading and flight speeds but are less manoeuvrable, whereas smaller birds have lower wing loading and flight speed but are more manoeuvrable, and medium-sized birds fall in between these groups (Warham 1977). However, similar sized species may have varying structural adaptations, often linked to diving behaviour (Wilson et al. 1992), that result in different flight modes (Kuroda 1953; Pennycuick 1982). Another factor to consider is that adaptations in wing shape results in varying flight speeds during gliding and flapping flight (Pennycuick 1987). The wide range of morphologies present in procellariiform seabirds may offer some explanation for how they are able to coexist (Warham 1977). As expected, amongst the birds that I studied, the smaller petrels flapped more than the larger albatrosses, but flapping flight varied among the albatrosses. Albatrosses breeding on Gough Island flapped more than albatrosses from Marion Island, and may be adapted to flying in lighter winds of sub-tropical waters. Grey-headed Albatrosses are known to reach very high ground speeds during flight (Catry et al. 2004) and spent the least amount of time flapping of all the albatrosses studied. The period of dynamic soaring cycles decreased with body size, with Wandering Albatrosses having the longest cycle (~10 s). Albatrosses have more sinuous flight paths than shearwaters as a result of their curved flight while dynamic soaring (Alerstam et al. 1993). Larger albatrosses might be limited by the rate at which they change their roll angles, whereas smaller petrels can rapidly change from one extreme angle to the next, reducing the duration of the dynamic soaring cycle. Such structural limitations may influence how seabirds are able to react to changing winds.

## Wind-driven flight

Wind is undoubtedly an important factor for seabird flight (Raymond et al. 2010; Weimerskirch et al. 2012). The flight behaviours of all study species were influenced by both wind speed and relative direction. In general, albatrosses are rarely observed flapping and this only occur in relatively calm conditions (Warham 1977; Pennycuick 1982; Richardson 2011), but even in calm conditions Wandering Albatrosses can glide over the waves without flapping (Pennycuick 1982). For flap-gliding to be efficient, birds have to achieve a flight speed through flapping that is similar to the optimal gliding speed (Pennycuick 1987; Alerstam et al. 1993). In lower wind speeds, Wandering Albatrosses flap-glide by flapping at the upper turn of the dynamic soaring cycle, likely in response to a reduction in flight speed when turning into the wind at low speeds (Pennycuick 1982).

All the tracked birds fitted with magnetometers reacted to the wind by altering their roll angles. In strong winds, albatrosses and petrels roll at more extreme angles than in lower winds. For albatrosses, relative wind direction affected the way they changed their roll angles, turning from left to right and *vice versa*. When flying in cross winds (which was the case for most flights) albatrosses had larger roll angles when turning with the wind and smaller roll angles when turning into the wind, but spent more time turning into the wind. This effect was more pronounced in Wandering Albatrosses; smaller albatrosses were seemingly able to roll with large angles when turning into stronger winds. When birds turn with the wind (at the upper turn of the dynamic soaring cycle), they pick up speed and rapidly change direction by following the wind, before turning into the wind again and restarting the cycle. The rate at which birds can change their roll angles at the lower turn of the dynamic soaring cycle may influence the amount of wind drift they experience.

Albatrosses mainly fly with cross winds in the Southern Ocean (Alerstam et al. 1993; Weimerskirch et al. 2000, 2012), which allows them to attain high flight speeds (Alerstam et al. 1993). The recent increase in westerly wind speeds in the Southern Ocean associated with global climate change seems to be benefiting albatrosses (Weimerskirch et al. 2012), but if wind speeds continue to increase, seabirds may be in trouble as they are limited in their responses (González-Solís et al. 2009; Weimerskirch et al. 2012). Larger albatrosses and petrels may be more dependent on stronger winds than smaller species that are able to alternate gliding and flapping flight. Kuroda (1955) noted that Northern Fulmars *Fulmarus glacialis* in the Pacific Ocean were seemingly able to fly wherever they wanted regardless of wind conditions. Wandering Albatross males are larger than females and males seem to be affected by wind conditions to a larger degree than females (Clay et al. 2020). Males flapped more often than females and seemed to limit their take-offs to favourable wind conditions; this result helps to explain why males often favour areas with higher wind speeds than females (Shaffer et al. 2001b). However, flying in stronger winds may increase wind drift, resulting in the typical looping trips of Wandering Albatrosses (Weimerskirch et al. 1997).

### Life at high *g*!

The dynamic soaring flight mode of albatrosses and petrels results in these birds being exposed to fluctuating centripetal forces (*g*-force) at regular intervals. All birds tracked in this study consistently experienced *g*-forces > 1 *g* (i.e. 1 *g* in addition to the force of gravity) at least once each hour of flight. The flight speed of seabirds may be limited by the *g*-force they are able to tolerate (Richardson 2011). The amount of *g*-force experienced did not seem to scale allometrically; rather, there appears to be a more complex relationship between *g*-force and flight mode, wing shape, and wing loading. Grey-headed Albatrosses experienced the highest maximum *g*-force (~2 *g*) and Wandering Albatrosses had the lowest (~1 *g*), despite the much larger sample size for the latter species. The White-chinned Petrel experienced similar forces to the smaller albatrosses. It would be interesting for future studies to look at the distribution of *g*-forces throughout a foraging trip to see if this changes as wing loading changes with increased weight while foraging (Warham 1977) and through varying wing configurations (Pennycuick 1960). The forces experienced by different birds in flight may also provide insights into the physical limitation of birds flying in different wind conditions, and may explain why larger seabirds have a tendon wing locking mechanism that is not present in smaller species (Pennycuick 1982).

## Limitations and precautions to consider for bio-logging

Bio-logging technology opens up exciting new avenues of animal behavioural research that was not previously possible (Wilmers et al. 2015). However, a considerable amount of work is still needed to establish guidelines for the use of these technologies (Williams et al. 2020b). I realised throughout my use of these various technologies that it is vital to understand the principles behind the working of individual loggers to be able to use them effectively. The devices I used for fine-scale data acquisition only lasted several days, resulting in most of the data being restricted to outbound foraging flights. Even worse, many loggers ran out of battery power before the birds even left their nests. To ensure that data were recorded during the foraging trip, many birds were equipped as they were relieved by their partners, but this required many hours (and a fair amount of luck) in the field, which is not always possible. Future studies would greatly benefit from loggers that can be programmed to only record when a bird leaves its nest or solar-powered loggers that only record specific events (Korpela et al. 2020).

## Timing

I used multiple independent loggers run by separate micro-processors. Accurate temporal matching of loggers was extremely important, but sometimes proved to be difficult, as the camera timestamps had a considerable amount of drift between individual video bins. This resulted in the video data slowly drifting in time relative to the IMU data, which had to be corrected through visual inspection. This was a time-consuming process but was essential to allow comparison between video and IMU data. Studies using bio-loggers with multiple sensors would benefit from loggers being controlled by the same micro-processor, to ensure temporal alignment.

## Accelerometers

The tri-axial accelerometers I used proved to be a valuable tool to isolate periods of flight or to identify flapping flight but were not useful to estimate bird posture during flight. Accelerometers are normally well suited to estimate posture (Shepard et al. 2008), but not when birds experience centripetal acceleration. Dynamic soaring birds are exposed to increased centripetal forces for large parts of their flight and thus estimating posture from accelerometer data was not possible. This is a very important aspect to consider as it means that the standard methods of pitch and roll correction of magnetometer data (Bidder et al. 2015) is not applicable unless additional data on posture is available (Williams et al. 2017).

## Magnetometers

Magnetometers are now being used to study animal behaviour in a similar way to accelerometers (Williams et al. 2017; Chakravarty et al. 2019). Because magnetometers are free from the effects of centripetal acceleration, they provide means to measure movement where accelerometer data are limited (see above). However, magnetometers are sensitive to interference in the magnetic field, which can be caused by ferrous or magnetic material (Bidder et al. 2015). Careful calibration of magnetometers is crucial for accurate values (Bidder et al. 2015; Williams et al. 2017). The Earth's magnetic field varies across the globe and becomes more varied closer to the magnetic poles, which needs to be considered when studying wide-ranging species where data are collected over long periods of time. Under these conditions, repeated calibration of the data might be necessary.

# Recommendations for future research

Bio-loggers are valuable tools to study the fine-scale behaviour of dynamic soaring seabirds, but currently most data are from breeding birds where complete foraging trips are rarely recorded (Fritz et al. 2003; Sato et al. 2009; Sachs et al. 2012; Sakamoto et al. 2013). Data from complete foraging trips are needed to further test the effect of sampling rates on behavioural states estimated from GPS locations and to see how flight behaviour changes throughout a foraging trip. Most of my data were also gathered during the brood-guard period; data from other breeding stages are needed to test how bird behaviour changes through the breeding cycle. More data are also needed for smaller species as I was only able to get IMU data from one Great Shearwater and one White-chinned Petrel.

There is a definite need for standardisation when it comes to the analysis of IMU data in animal behavioural studies (Campbell et al. 2016; Williams et al. 2020b). Future studies should compare ways of estimating flapping flight (Sato et al. 2009; Van Walsum et al. 2020; Williams et al. 2020a) to assess differences in reported metrics and possibly suggest appropriate methods for different species. Future studies would also benefit from adding gyroscopes to IMUs where animals have increased centripetal acceleration during locomotion (Wilson et al. 2013). These data can then be used to validate proposed methods to overcome challenges related to centripetal acceleration. Gyroscopes would also be useful to test the assumption made in Chapter 4, that dynamic soaring seabirds do not pitch significantly during routine flight.

A limitation of comparing fine-scale behavioural data to environmental variables is that the environmental data seldom match the resolution of the behavioural data. Accurate fine-scale environmental data are limited in the Southern Ocean and studies rely on remote-sensed data. Fine-scale tracking data have been used to estimate fine-scale wind speed and direction through analysis of changing ground speed and heading (Yonehara et al. 2016), but relating behaviour to such estimates might be counterintuitive. Future studies may benefit from using bird-borne cameras to estimate weather conditions. Wind speed may be estimated from wave crests and it might be possible to estimate wave height from such video footage.

The loggers I attached to the tail feathers of Wandering Albatrosses were not useful for estimating body angles. However, tail mounted IMU loggers could be used in conjunction with backwards-facing cameras to study how seabirds use their tails for steering (Gillies et al. 2011), and how this may differ between species and with varying wind conditions.

## Conclusions

Bio-logging devices are useful to study the fine-scale behaviour of flying seabirds, but sampling frequencies must be carefully considered during data acquisition and research planning. Such measurements can benefit greatly from validation through visual observation from bird-borne video loggers. Albatrosses and petrels varied their fine-scale flight behaviour in response to winds, by flapping less and rolling at more extreme angles in increased winds. The varied responses of albatrosses and petrels to the wind supports the idea that seabird movement and distribution is determined by flight mode and not by size alone. Birds of different sizes may have morphological adaptations that allow them to fly in specific conditions and this may ultimately drive their movement paths and large-scale distribution. In an environment where the wind is constantly changing it is important for us to understand how animals respond to the wind. Albatrosses and petrels are among the species most intimately linked with wind and continued study of their responses to wind is important for informed conservation decisions.

# References

Ainley DG, Porzig E, Zajanc D, Spear LB (2015) Seabird flight behavior and height in response to altered wind strength and direction. Mar Ornithol 43:25–36

Alerstam T, Bäckman J, Evans TJ (2019) Optimal central place foraging flights in relation to wind. J Ornithol 160:1065–1076

Alerstam T, Gudmundsson GA, Larsson B (1993) Flight tracks and speeds of Antarctic and Atlantic seabirds: radar and optical measurements. Philos Trans R Soc B Biol Sci 340:55–67

Bale R, Hao M, Bhalla APS, Patankar NA (2014) Energy efficiency and allometry of movement of swimming and flying animals. Proc Natl Acad Sci USA 111:7517–7521

Bennison A, Bearhop S, Bodey TW, Votier SC, Grecian WJ, Wakefield ED, Hamer KC, Jessopp M (2017) Search and foraging behaviors from movement data: A comparison of methods. Ecol Evol 8:13–24

Bezanson J, Edelman A, Karpinski S, Shah VB (2017) Julia: A fresh approach to numerical computing. SIAM Rev 59:65–98

Bidder OR, Walker JS, Jones MW, Holton MD, Urge P, Scantlebury DM, Marks NJ, Magowan EA, Maguire IE, Wilson RP (2015) Step by step: reconstruction of terrestrial animal movement paths by dead-reckoning. Mov Ecol 3:23

Birdlife International (2004) Tracking ocean wanderers: the global distribution of albatrosses and petrels. BirdLife International., Cambridge, UK

Bograd SJ, Block BA, Costa DP, Godley BJ (2010) Bio-logging technologies: New tools for conservation. Introduction. Endanger Species Res 10:1–7

Bouten W, Baaij EW, Shamoun-Baranes J, Camphuysen KCJ (2013) A flexible GPS tracking system for studying bird behaviour at multiple scales. J Ornithol 154:571–580

Boyd I, Wanless S, Camphuysen CJ (eds) (2006) Top predators in marine ecosystems: their role in monitoring and management. Cambridge University Press, Cambridge

Boyd IL, Kato A, Ropert-Coudert Y (2004) Bio-logging science: sensing beyond the boundaries. Mem Natl Inst Polar Res Spec issue 58:1–14

Bramanti M, Dall'Antonia L, Papi F (1988) A new technique to monitor the flight paths of birds. J Exp Biol 134:467–472

Brooke M d. L, Hanley S, Laughlin SB (1999) The scaling of eye size with body mass in birds. Proc R Soc B Biol Sci 266:405–412

Brown DD, Kays R, Wikelski M, Wilson R, Klimley AP (2013) Observing the unwatchable through acceleration logging of animal behavior. Anim Biotelemetry 1:1–16

Brown RGB, Bourne WRP, Wahl TR (1978) Diving by Shearwaters. Condor 80:123–125

Cagnacci F, Boitani L, Powell RA, Boyce MS (2010) Animal ecology meets GPS-based radiotelemetry: a perfect storm of opportunities and challenges. Philos Trans R Soc B Biol Sci 365:2157–2162

Calenge C (2006) The package "adehabitat" for the R software: A tool for the analysis of space and habitat use by animals. Ecol Modell 197:516–519

Campbell HA, Urbano F, Davidson S, Dettki H, Cagnacci F (2016) A plea for standards in reporting data collected by animal-borne electronic devices. Anim Biotelemetry 4:1–4

Canny J (1986) A Computational Approach to Edge Detection. IEEE Trans Pattern Anal Mach Intell PAMI-8:679–698

Carneiro APB, Pearmain EJ, Oppel S, Clay TA, Phillips RA, Bonnet-Lebrun AS, Wanless RM, Abraham E, Richard Y, Rice J, et al (2020) A framework for mapping the distribution of seabirds by integrating tracking, demography and phenology. J Appl Ecol 57:514–525

Carpenter-Kling T, Reisinger RR, Orgeret F, Connan M, Stevens KL, Ryan PG, Makhado A, Pistorius PA (2020) Foraging in a dynamic environment: Response of four sympatric sub-Antarctic albatross species to interannual environmental variability. Ecol Evol 10:11277–11295

Catry P, Phillips RA, Croxall JP (2004) Sustained fast travel by a Gray-headed Albatross (*Thalassarche chrysostoma*) riding an Antarctic storm. Auk 121:1208–1213

Chakravarty P, Maalberg M, Cozzi G, Ozgul A, Aminian K (2019) Behavioural compass: Animal behaviour recognition using magnetometers. Mov Ecol 7:1–13

Clay TA, Joo R, Weimerskirch H, Phillips RA, den Ouden O, Basille M, Clusella-Trullas S, Assink JD, Patrick SC (2020) Sex-specific effects of wind on the flight decisions of a sexually dimorphic soaring bird. J Anim Ecol 89:1811–1823

Clay TA, Manica A, Ryan PG, Silk JRD, Croxall JP, Ireland L, Phillips RA (2016) Proximate drivers of spatial segregation in non-breeding albatrosses. Sci Rep 6:1–13

Clay TA, Oppel S, Lavers JL, Phillips RA, Brooke M de L (2019) Divergent foraging strategies during incubation of an unusually wide-ranging seabird, the Murphy's petrel. Mar Biol 166:1–14

Cleeland JB, Lea M-A, Hindell MA (2014) Use of the Southern Ocean by breeding Short-tailed Shearwaters (*Puffinus tenuirostris*). J Exp Mar Bio Ecol 450:109–117

Collins PM, Green JA, Warwick-Evans V, Dodd S, Shaw PJA, Arnould JPY, Halsey LG (2015) Interpreting behaviors from accelerometry: A method combining simplicity and objectivity. Ecol Evol 5:4642–4654

Cooke SJ (2008) Biotelemetry and bio-logging in endangered species research and animal conservation: relevance to regional, national, and IUCN Red List threat assessments. Endanger Species Res 4:165–185

Cooke SJ, Hinch SG, Wikelski M, Andrews RD, Kuchel LJ, Wolcott TG, Butler PJ (2004) Biotelemetry: A mechanistic approach to ecology. Trends Ecol. Evol. 19:334–343

Cox SL, Orgeret F, Gesta M, Rodde C, Heizer I, Weimerskirch H, Guinet C (2018) Processing of acceleration and dive data on-board satellite relay tags to investigate diving and foraging behaviour in free-ranging marine predators. Methods Ecol Evol 9:64–77

Dall'Antonia L, Dall'Antonia P, Benvenuti S, Ioale P, Massa B, Bonadonna F (1995) The homing behaviour of Cory's shearwaters (*Calonectris diomedea*) studied by means of a direction recorder. J Exp Biol 198:359–362

Davis RW, Fuiman LA, Williams TM, Collier SO, Hagey WP, Kanatous SB, Kohin S, Horning M (1999) Hunting behavior of a marine mammal beneath the Antarctic fast ice. Science 283:993–996

De Pascalis F, Imperio S, Benvenuti A, Catoni C, Rubolini D, Cecere JG (2020) Sex-specific foraging behaviour is affected by wind conditions in a sexually size dimorphic seabird. Anim Behav 166:207–218

Dean B, Freeman R, Kirk H, Leonard K, Phillips RA, Perrins CM, Guilford T (2013) Behavioural mapping of a pelagic seabird: Combining multiple sensors and a hidden

Markov model reveals the distribution of at-sea behaviour. J R Soc Interface 10:20120570

Dell'Ariccia G, Benhamou S, Dias MP, Granadeiro JP, Sudre J, Catry P, Bonadonna F (2018) Flexible migratory choices of Cory's shearwaters are not driven by shifts in prevailing air currents. Sci Rep 8:1–9

Dewhirst OP, Evans HK, Roskilly K, Harvey RJ, Hubel TY, Wilson AM (2016) Improving the accuracy of estimates of animal path and travel distance using GPS drift-corrected dead reckoning. Ecol Evol 6:6210–6222

Dial KP, Greene E, Irschick DJ (2008) Allometry of behavior. Trends Ecol Evol 23:394–401

Dias MP, Oppel S, Bond AL, Carneiro APB, Cuthbert RJ, González-Solís J, Wanless RM, Glass T, Lascelles B, Small C, et al (2017) Using globally threatened pelagic birds to identify priority sites for marine conservation in the South Atlantic Ocean. Biol Conserv 211:76–84

Duda RO, Hart PE (1972) Use of the Hough transformation to detect lines and curves in pictures. Commun ACM 15:11–15

Duriez O, Kato A, Tromp C, Dell'Omo G, Vyssotski AL, Sarrazin F, Ropert-Coudert Y (2014) How cheap is soaring flight in raptors? A preliminary investigation in freely-flying vultures. PLoS One 9:

Dusha D, Boles W, Walker R (2007) Attitude estimation for a fixed-wing aircraft using horizon detection and optical flow. Proc - Digit Image Comput Tech Appl 9th Bienn Conf Aust Pattern Recognit Soc DICTA 2007 485–492

Einoder LD, Page B, Goldsworthy SD, De Little SC, Bradshaw CJA (2011) Exploitation of distant Antarctic waters and close neritic waters by short-tailed shearwaters breeding in South Australia. Austral Ecol 36:461–475

Elliott KH, Chivers LS, Bessey L, Gaston AJ, Hatch SA, Kato A, Osborne O, Ropert-Coudert Y, Speakman JR, Hare JF (2014) Windscapes shape seabird instantaneous energy costs but adult behavior buffers impact on offspring. Mov Ecol 2:1–15

Ettinger SM, Nechyba MC, Ifju PG, Waszak M (2002) Towards flight autonomy: Vision-based horizon detection for micro air vehicles. Proc Florida Conf Recent Adv Robot 7:617–640

Fauchald P, Erikstad KE, Skarsfjord H (2000) Scale-dependent predator-prey interactions: The hierarchical spatial distribution of seabirds and prey. Ecology 81:773–783

Fernández P, Anderson DJ, Sievert PR, Huyvaert KP (2001) Foraging destinations of three low-latitude albatross (*Phoebastria*) species. J Zool 254:391–404

Forin-Wiart MA, Hubert P, Sirguey P, Poulle ML (2015) Performance and accuracy of lightweight and low-cost GPS data loggers according to antenna positions, fix intervals, habitats and animal movements. PLoS One 10:1–21

Frankish CK, Phillips RA, Clay TA, Somveille M, Manica A (2020) Environmental drivers of movement in a threatened seabird: insights from a mechanistic model and implications for conservation. Divers Distrib 26:1315–1329

Fritsch FN, Carlson RE (1980) Monotone piecewise cubic interpolation. SIAM J Numer Anal 17:238–246

Fritz H, Said S, Weimerskirch H (2003) Scale-dependent hierarchical adjustments of movement patterns in a long-range foraging seabird. Proc R Soc B Biol Sci 270:1143–1148

Gershikov E, Libe T, Kosolapov S (2013) Horizon line detection in marine images: which method to choose? Int J Adv Intell Syst 6:79–84

Gibb R, Shoji A, Fayet AL, Perrins CM, Guilford T, Freeman R (2017) Remotely sensed wind speed predicts soaring behaviour in a wide-ranging pelagic seabird. J R Soc Interface 14:20170262

Gillies JA, Thomas ALR, Taylor GK (2011) Soaring and manoeuvring flight of a steppe eagle *Aquila nipalensis*. J Avian Biol 42:377–386

Gomez-Marin A, Partoune N, Stephens GJ, Louis M (2012) Automated tracking of animal posture and movement during exploration and sensory orientation behaviors. PLoS One 7:e41642

Gómez Laich A, Wilson RP, Quintana F, Shepard ELC (2008) Identification of imperial cormorant *Phalacrocorax atriceps* behaviour using accelerometers. Endanger Species Res 10:29–37

González-Solís J, Felicísimo A, Fox JW, Afanasyev V, Kolbeinsson Y, Muñoz J (2009) Influence of sea surface winds on shearwater migration detours. Mar Ecol Prog Ser

391:221–230

Goto Y, Yoda K, Sato K (2017) Asymmetry hidden in birds' tracks reveals wind, heading, and orientation ability over the ocean. Sci Adv 3:1–10

Gould SJ (1966) Allometry and size in ontogeny and phylogeny. Biol Rev 41:587–638

Griffiths AM (1982) Reactions of some seabirds to a ship in the Southern Ocean. Ostrich 53:228–235

Halsey LG, Green JA, Wilson R, Frappell PB (2009a) Accelerometry to estimate energy expenditure during activity: best practice with data loggers. Physiol Biochem Zool 82:396–404

Halsey LG, Shepard ELC, Quintana F, Gomez Laich A, Green JA, Wilson RP (2009b) The relationship between oxygen consumption and body acceleration in a range of species. Comp Biochem Physiol - A Mol Integr Physiol 152:197–202

Handley JM, Pistorius P (2016) Kleptoparasitism in foraging gentoo penguins *Pygoscelis papua*. Polar Biol 39:391–395

Harvey C, Baliga VB, Lavoie P, Altshuler DL (2019) Wing morphing allows gulls to modulate static pitch stability during gliding. J R Soc Interface 16:20180641

Hebblewhite M, Haydon DT (2010) Distinguishing technology from biology: a critical review of the use of GPS telemetry data in ecology. Philos Trans R Soc B Biol Sci 365:2303–2312

Hedd A, Pollet IL, Mauck RA, Burke CM, Mallory ML, McFarlane Tranquilla LA, Montevecchi WA, Robertson GJ, Ronconi RA, Shutler D, et al (2018) Foraging areas, offshore habitat use, and colony overlap by incubating Leach's storm-petrels *Oceanodroma leucorhoa* in the Northwest Atlantic. PLoS One 13:e0194389

Hersbach H, Bell B, Berrisford P, Biavati G, Horányi A, Muñoz Sabater, J, Nicolas J, Peubey C, Radu R, Rozum I, Schepers D, et al (2018) ERA5 hourly data on pressure levels from 1979 to present. In: Copernicus Clim. Chang. Serv. Clim. Data Store (CDS).

Hicks O, Burthe S, Daunt F, Butler A, Bishop C, Green JA (2017) Validating accelerometry estimates of energy expenditure across behaviours using heart rate data in a free-living seabird. J Exp Biol 220:1875–1881

Hindell MA, Reisinger RR, Ropert-Coudert Y, Hückstädt LA, Trathan PN, Bornemann H, Charrassin JB, Chown SL, Costa DP, Danis B, et al (2020) Tracking of marine predators to protect Southern Ocean ecosystems. Nature 580:87–92

Hooker SK, Whitehead H, Gowans S, Baird RW (2002) Fluctuations in distribution and patterns of individual range use of northern bottlenose whales. Mar Ecol Prog Ser 225:287–297

Hurford A (2009) GPS measurement error gives rise to spurious 180° turning angles and strong directional biases in animal movement data. PLoS One 4:e5632

Jespersen P (1924) The frequency of birds over the high atlantic ocean. Nature 114:281–283

Johnson DD, Ganskopp DC (2008) GPS collar sampling frequency: Effects on measures of resource use. Rangel Ecol Manag 61:226–231

Johnson LR, Boersch-Supan PH, Phillips RA, Ryan SJ (2017) Changing measurements or changing movements? Sampling scale and movement model identifiability across generations of bio-logging technology. Ecol Evol 7:9257–9266

Jouventin P, Weimerskirch H (1990) Satellite tracking of Wandering albatrosses. Nature 343:746–748

Kato A, Ropert-Coudert Y, Grémillet D, Cannell B (2006) Locomotion and foraging strategy in foot-propelled and wing-propelled shallow-diving seabirds. Mar Ecol Prog Ser 308:293–301

Kie JG (2013) A rule-based ad hoc method for selecting a bandwidth in kernel home-range analyses. Anim Biotelemetry 1:13

Kogure Y, Sato K, Watanuki Y, Wanless S, Daunt F (2016) European shags optimize their flight behavior according to wind conditions. J Exp Biol 219:311–318

Kooyman GL (2004) Genesis and evolution of bio-logging devices: 1963 – 2002. Mem Natl Inst Polar Res Spec Issue 58:15–22

Korpela J, Suzuki H, Matsumoto S, Mizutani Y, Samejima M, Maekawa T, Nakai J, Yoda K (2020) Machine learning enables improved runtime and precision for bio-loggers on seabirds. Commun Biol 3:1–9

Kroeger CE, Crocker DE, Orben RA, Thompson DR, Torres LG, Sagar PM, Sztukowski LA, Andriese T, Costa DP, Shaffer SA (2020) Similar foraging energetics of two sympatric albatrosses despite contrasting life histories and wind-mediated foraging strategies. J Exp Biol 223:jeb228585

Kuroda N (1953) On the skeletons of *Puffinus nativitatis* and *Pagodroma nivea*. Japanese J Ornithol 13:50–68

Kuroda N (1955) Observations on pelagic birds of the northwest Pacific. Condor 57:290–300

Leos-Barajas V, Photopoulou T, Langrock R, Patterson TA, Watanabe YY, Murgatroyd M, Papastamatiou YP (2017) Analysis of animal accelerometer data using hidden Markov models. Methods Ecol Evol 8:161–173

Liechti F, Witvliet W, Weber R, Bächler E (2013) First evidence of a 200-day non-stop flight in a bird. Nat Commun 4:1–7

Lipschutz I, Gershikov E, Milgrom B (2013) New methods for horizon line detection in infrared and visible sea images. Int J Comput Eng Res 3:226–233

Lotz SI, Clilverd M (2019) Demonstrating the use of a class of min-max smoothers for D region event detection in narrow band VLF phase. Radio Sci 54:233–244

Mackley EK, Phillips RA, Silk JRD, Wakefield ED, Afanasyev V, Fox JW, Furness RW (2010) Free as a bird? Activity patterns of albatrosses during the nonbreeding period. Mar Ecol Prog Ser 406:291–303

Marshall GJ (1998) Crittercam: An animal-borne imaging and data logging system. Mar Technol Soc Mar Technol Soc J 32:11–17

Mitani Y, Sato K, Ito S, Cameron MF, Siniff DB, Naito Y (2003) A method for reconstructing three-dimensional dive profiles of marine mammals using geomagnetic intensity data: results from two lactating Weddell seals. Polar Biol 26:311–317

Mitchell LJ, White PCL, Arnold KE (2019) The trade-off between fix rate and tracking duration on estimates of home range size and habitat selection for small vertebrates. PLoS One 14:e0219357

Moll RJ, Millspaugh JJ, Beringer J, Sartwell J, He Z (2007) A new “view” of ecology and conservation through animal-borne video systems. Trends Ecol Evol 22:660–668

Morris G, Conner LM (2017) Assessment of accuracy, fix success rate, and use of estimated horizontal position error (EHPE) to filter inaccurate data collected by a common commercially available GPS logger. PLoS One 12:1–12

Naito Y (2004) New steps in bio-logging science. Mem Natl Inst Polar Res Spec Issue 58:50–57

NCEI Geomagnetic Modeling Team and British Geological Survey (2019) World Magnetic Model 2020. NOAA Natl Centers Environ Inf

Nel DC, Lutjeharms JRE, Pakhomov EA, Ansorge IJ, Ryan PG, Klages NTW (2001) Exploitation of mesoscale oceanographic features by grey-headed albatross *Thalassarche chrysostoma* in the southern Indian Ocean. Mar Ecol Prog Ser 217:15–26

Nevitt GA, Losekoot M, Weimerskirch H (2008) Evidence for olfactory search in wandering albatross, *Diomedea exulans*. Proc Natl Acad Sci USA 105:4576–4581

Noda T, Kawabata Y, Arai N, Mitamura H, Watanabe S (2014) Animal-mounted gyroscope/accelerometer/magnetometer: In situ measurement of the movement performance of fast-start behaviour in fish. J Exp Mar Bio Ecol 451:55–68

Oppel S, Bolton M, Carneiro APB, Dias MP, Green JA, Masello JF, Phillips RA, Owen E, Quillfeldt P, Beard A, et al (2018) Spatial scales of marine conservation management for breeding seabirds. Mar Policy 98:37–46

Orben RA, O'Connor AJ, Suryan RM, Ozaki K, Sato F, Deguchi T (2018) Ontogenetic changes in at-sea distributions of immature short-tailed albatrosses *Phoebastria albatrus*. Endanger Species Res 35:23–37

Pagano AM, Rode KD, Cutting A, Owen MA, Jensen S, Ware JV, Robbins CT, Durner GM, Atwood TC, Obbard ME, et al (2017) Using tri-axial accelerometers to identify wild polar bear behaviors. Endanger Species Res 32:19–33

Patterson TA, Thomas L, Wilcox C, Ovaskainen O, Matthiopoulos J (2008) State-space models of individual animal movement. Trends Ecol Evol 23:87–94

Pennycuick CJ (1982) The flight of petrels and albatrosses (Procellariiformes), observed in South Georgia and its vicinity. Philos Trans R Soc B Biol Sci 300:75–106

Pennycuick CJ (1983) Thermal soaring compared in three dissimilar tropical bird species, *Fregata magnificens*, *Pelecanus occidentals* and *Coragyps atratus*. J Exp Biol 102:307–326

Pennycuick CJ (1987) Flight of auks (Alcidae) and other northern seabirds compared with southern procellariiformes: ornithodolite observations. J Exp Biol 128:335–347

Pennycuick CJ (1960) Gliding flight of the Fulmar Petrel. J Exp Biol 37:330–338

Pereira JM, Paiva VH, Phillips RA, Xavier JC (2018) The devil is in the detail: small-scale sexual segregation despite large-scale spatial overlap in the wandering albatross. Mar Biol 165:55

Phalan B, Phillips RA, Silk JR, Afanasyev V, Fukuda A, Fox JW, Catry P, Higuchi H, Croxall JP (2007) Foraging behaviour of four albatrosses species by night and day. Mar Ecol Prog Ser 340:271–286

Phillips RA, Croxall JP, Silk JRD, Briggs DR (2008) Foraging ecology of albatrosses and petrels from South Georgia: two decades of insights from tracking technologies. Aquat Conserv Mar Freshw Ecosyst 17:S6–S21

Phillips RA, Silk JRD, Croxall JP, Afanasyev V (2006) Year-round distribution of white-chinned petrels from South Georgia: Relationships with oceanography and fisheries. Biol Conserv 129:336–347

Phillips RA, Silk JRD, Phalan B, Catry P, Croxall JP (2004) Seasonal sexual segregation in two *Thalassarche* albatross species: competitive exclusion, reproductive role specialization or foraging niche divergence? Proc R Soc B Biol Sci 271:1283–1291

Phillips RA, Xavier JC, Croxall JP (2003) Effects of satellite transmitters on albatrosses and petrels. Auk 120:1082–1090

Ponganis PJ (2007) Bio-logging of physiological parameters in higher marine vertebrates. Deep Res II Top Stud Oceanogr 54:183–192

Postlethwaite CM, Dennis TE (2013) Effects of temporal resolution on an inferential model of animal movement. PLoS One 8:e57640

Praczyk T (2018) A quick algorithm for horizon line detection in marine images. J Mar Sci Technol 23:164–177

Qasem L, Cardew A, Wilson A, Griffiths I, Halsey LG, Shepard ELC, Gleiss AC, Wilson R (2012) Tri-axial dynamic acceleration as a proxy for animal energy expenditure; should we be summing values or calculating the vector? PLoS One 7:e31187

R Development Core Team (2018) R: A language and environment for statistical computing. R Foundation for Statistical Computing, Vienna

Ranacher P, Brunauer R, Trutschnig W, Van der Spek S, Reich S (2016a) Why GPS makes distances bigger than they are. Int J Geogr Inf Sci 30:316–333

Ranacher P, Brunauer R, Van Der Spek S, Reich S (2016b) What is an appropriate temporal sampling rate to record floating car data with a GPS? ISPRS Int J Geo-Information 5:1–17

Raymond B, Shaffer SA, Sokolov S, Woehler EJ, Costa DP, Einoder L, Hindell M, Hosie G, Pinkerton M, Sagar PM, et al (2010) Shearwater foraging in the Southern Ocean: The roles of prey availability and winds. PLoS One 5:e10960

Reisinger RR, Raymond B, Hindell MA, Bester MN, Crawford RJM, Davies D, de Bruyn PJN, Dilley BJ, Kirkman SP, Makhado AB, et al (2018) Habitat modelling of tracking data from multiple marine predators identifies important areas in the Southern Indian Ocean. Divers Distrib 24:535–550

Richardson PL (2011) How do albatrosses fly around the world without flapping their wings? Prog Oceanogr 88:46–58

Richardson PL (2015) Upwind dynamic soaring of albatrosses and UAVs. Prog Oceanogr 130:146–156

Richardson PL (2012) High-Speed Dynamic Soaring. R/C Soar Dig 29:36–49

Richardson PL, Wakefield ED, Phillips RA (2018) Flight speed and performance of the wandering albatross with respect to wind. Mov Ecol 6:1–15

Rollinson DP, Dilley BJ, Davies D, Ryan PG (2018) Year-round movements of white-chinned petrels from Marion Island, south-western Indian Ocean. Antarct Sci 30:183–195

Rollinson DP, Dilley BJ, Ryan PG (2014) Diving behaviour of white-chinned petrels and its relevance for mitigating longline bycatch. Polar Biol 37:1301–1308

Ronconi RA, Ryan PG, Ropert-Coudert Y (2010) Diving of great shearwaters (*Puffinus gravis*) in cold and warm water regions of the South Atlantic Ocean. PLoS One 5:e15508

Ronconi RA, Schoombie S, Westgate AJ, Wong SNP, Koopman HN, Ryan PG (2018) Effects of age, sex, colony and breeding phase on marine space use by Great Shearwaters *Ardenna gravis* in the South Atlantic. Mar Biol 165:58

Ropert-Coudert Y, Grémillet D, Kato A, Ryan PG, Naito Y, Le Maho Y (2004) A fine-scale time budget of Cape gannets provides insights into the foraging strategies of coastal seabirds. Anim Behav 67:985–992

Ropert-Coudert Y, Van de Putte AP, Reisinger RR, Bornemann H, Charrassin JB, Costa DP, Danis B, Hückstädt LA, Jonsen ID, Lea MA, et al (2020) The retrospective analysis of Antarctic tracking data project. Sci Data 7:1–11

Ropert-Coudert Y, Wilson RP (2005) Trends and perspectives in animal-attached remote sensing. Front Ecol Environ 3:437–444

Rutz C, Bluff LA, Weir AAS, Kacelnik A (2007) Video Cameras on Wild Birds. Science 318:765

Rutz C, Hays GC (2009) New frontiers in bio-logging science. Biol Lett 5:289–292

Rutz C, Troscianko J (2013) Programmable, miniature video-loggers for deployment on wild birds and other wildlife. Methods Ecol Evol 4:114–122

Ryan PG, Lee JR, Bouard F Le (2020) Moult intensity in blue petrels and a key moult site off West Antarctica. Antarct Sci 32:1–9

Ryan PG, Petersen SL, Peters G, Grémillet D (2004) GPS tracking a marine predator: the effects of precision, resolution and sampling rate on foraging tracks of African Penguins. Mar Biol 145:215–223

Sachs G (2005) Minimum shear wind strength required for dynamic soaring of albatrosses. Ibis 147:1–10

Sachs G (2016) In-flight measurement of upwind dynamic soaring in albatrosses. Prog Oceanogr 142:47–57

Sachs G, Traugott J, Nesterova AP, Bonadonna F (2013) Experimental verification of dynamic soaring in albatrosses. J Exp Biol 216:4222–4232

Sachs G, Traugott J, Nesterova AP, Dell'Omo G, Kümmeth F, Heidrich W, Vyssotski AL, Bonadonna F (2012) Flying at no mechanical energy cost: disclosing the secret of wandering albatrosses. PLoS One 7:e41449

Safi K, Kranstauber B, Weinzierl R, Griffin L, Rees EC, Cabot D, Cruz S, Proaño C, Takekawa JY, Newman SH, et al (2013) Flying with the wind: Scale dependency of speed and direction measurements in modelling wind support in avian flight. Mov Ecol 1:1–13

Sakamoto KQ, Takahashi A, Iwata T, Yamamoto T, Yamamoto M, Trathan PN (2013) Heart rate and estimated energy expenditure of flapping and gliding in black-browed albatrosses. J Exp Biol 216:3175–3182

Sato K, Daunt F, Watanuki Y, Takahashi A, Wanless S (2008) A new method to quantify prey acquisition in diving seabirds using wing stroke frequency. J Exp Biol 211:58–65

Sato K, Sakamoto KQ, Watanuki Y, Takahashi A, Katsumata N, Bost C-A, Weimerskirch H (2009) Scaling of soaring seabirds and implications for flight abilities of giant pterosaurs. PLoS One 4:e5400

Schoombie S, Dilley BJ, Davies D, Glass T, Ryan PG (2017) The distribution of breeding Sooty Albatrosses from the three most important breeding sites: Gough, Tristan and the Prince Edward Islands. Emu 117:160–169

Schoombie S, Dilley BJ, Davies D, Ryan PG (2018) The foraging range of Great Shearwaters (*Ardenna gravis*) breeding on Gough Island. Polar Biol 41:2451–2458

Shaffer A, Weimerskirch H, Scott D, Pinaud D, Thompson DR, Sagar PM, Moller H, Taylor GA, Foley DG, Tremblay Y, et al (2009) Spatiotemporal habitat use by breeding sooty shearwaters *Puffinus griseus* . Mar Ecol Prog Ser 391:209–220

Shaffer SA, Costa DP, Weimerskirch H (2001a) Behavioural factors affecting foraging effort of breeding wandering albatrosses. J Anim Ecol 70:864–874

Shaffer SA, Weimerskirch H, Costa DP (2001b) Functional significance of sexual dimorphism in Wandering Albatrosses, *Diomedea exulans*. Funct Ecol 15:203–210

Shepard ELC, Wilson RP, Quintana F, Gómez Laich A, Liebsch N, Albareda DA, Halsey LG, Gleiss A, Morgan DT, Myers AE, et al (2008) Identification of animal movement patterns using tri-axial accelerometry. Endanger Species Res 10:47–60

Sherub S, Fiedler W, Duriez O, Wikelski M (2017) Bio-logging, new technologies to study conservation physiology on the move: a case study on annual survival of Himalayan vultures. J Comp Physiol A 203:531–542

Shiomi K, Yoda K, Katsumata N, Sato K (2012) Temporal tuning of homeward flights in seabirds. Anim Behav 83:355–359

Spear LB, Ainley DG (1997) Flight speed of seabirds in relation to wind speed and direction. Ibis 139:234–251

Spear LB, Ainley DG, Hardesty BD, Howell SNG, Webb SW (2004) Reducing biases affecting at-sea surveys of seabirds: Use of multiple observer teams. Mar Ornithol 32:147–157

Spivey RJ, Stansfield S, Bishop CM (2014) Analysing the intermittent flapping flight of a Manx Shearwater, *Puffinus puffinus*, and its sporadic use of a wave-meandering wing-sailing flight strategy. Prog Oceanogr 125:62–73

Suryan RM, Anderson DJ, Shaffer SA, Roby DD, Tremblay Y, Costa DP, Sievert PR, Sato F, Ozaki K, Balogh GR, et al (2008) Wind, waves, and wing loading: Morphological specialization may limit range expansion of endangered albatrosses. PLoS One 3:e4016

Tarroux A, Weimerskirch H, Wang SH, Bromwich DH, Cherel Y, Kato A, Ropert-Coudert Y, Varpe Ø, Yoccoz NG, Descamps S (2016) Flexible flight response to challenging wind conditions in a commuting Antarctic seabird: do you catch the drift? Anim Behav 113:99–112

Tasker ML, Jones PH, Dixon T, Blake BF (1984) Counting seabirds at sea from ships: a review of methods employed and a suggestion for a standardized apporach. Auk 101:567–577

Thiebault A, Tremblay Y (2013) Splitting animal trajectories into fine-scale behaviorally consistent movement units: Breaking points relate to external stimuli in a foraging seabird. Behav Ecol Sociobiol 67:1013–1026

Thiebot JB, Arnould JPY, Gómez-Laich A, Ito K, Kato A, Mattern T, Mitamura H, Noda T, Poupart T, Quintana F, et al (2017) Jellyfish and other gelata as food for four penguin species-insights from predator-borne videos. Front Ecol Environ 15:1–5

Tickell WLN (2000) Albatrosses. Pica Press, Sussex

Tomkiewicz SM, Fuller MR, Kie JG, Bates KK (2010) Global positioning system and associated technologies in animal behaviour and ecological research. Philos Trans R Soc B Biol Sci 365:2163–2176

Torres LG, Thompson DR, Bearhop S, Votier S, Taylor GA, Sagar PM, Robertson BC (2011) White-capped albatrosses alter fine-scale foraging behavior patterns when associated with fishing vessels. Mar Ecol Prog Ser 428:289–301

Townshend AD, Worringham CJ, Stewart IB (2008) Assessment of speed and position during human locomotion using nondifferential GPS. Med Sci Sports Exerc 40:124–132

Tremblay Y, Bertrand S, Henry RW, Kappes MA, Costa DP, Shaffer SA (2009) Analytical approaches to investigating seabird-environment interactions: A review. Mar Ecol Prog Ser 391:153–163

Tremblay Y, Shaffer SA, Fowler SL, Kuhn CE, McDonald BI, Weise MJ, Bost CA, Weimerskirch H, Crocker DE, Goebel ME, et al (2006) Interpolation of animal tracking data in a fluid environment. J Exp Biol 209:128–140

Tremblay Y, Thiebault A, Mullers R, Pistorius P (2014) Bird-borne video-cameras show that seabird movement patterns relate to previously unrevealed proximate environment, not prey. PLoS One 9:e88424

Van Walsum TA, Perna A, Bishop CM, Murn CP, Collins PM, Wilson RP, Halsey LG (2020) Exploring the relationship between flapping behaviour and accelerometer signal during ascending flight, and a new approach to calibration. Ibis 162:13–26

Vazquez-Prokopec GM, Stoddard ST, Paz-Soldan V, Morrison AC, Elder JP, Kochel TJ, Scott TW, Kitron U (2009) Usefulness of commercially available GPS data-loggers for tracking human movement and exposure to dengue virus. Int J Health Geogr 8:1–11

Ventura F, Granadeiro JP, Padget O, Catry P (2020) Gadfly petrels use knowledge of the windscape, not memorized foraging patches, to optimize foraging trips on ocean-wide scales. Proc R Soc B Biol Sci 287:20191775

Visser I, Speekenbrink M (2010) depmixS4: An R package for hidden markov models. J Stat Softw 36:1–21

Wakefield ED, Phillips RA, Jason M, Akira F, Hiroyoshi H, Marshall GJ, Trathan PN (2009) Wind field and sex constrain the flight speeds of central-place foraging albatrosses. Ecol Monogr 79:663–679

Walker JS, Jones MW, Laramee RS, Holton MD, Shepard ELC, Williams HJ, Scantlebury DM, Marks NJ, Magowan EA, Maguire IE, et al (2015) Prying into the intimate secrets of animal lives; software beyond hardware for comprehensive annotation in “Daily Diary” tags. Mov Ecol 3:1–16

Wang Y, Liao Z, Guo H, Liu T, Yang Y (2009) An approach for horizon extraction in ocean observation. Proc 2009 2nd Int Congr Image Signal Process CISP'09 1–5

Warham J (1977) Wing loadings, wing shapes, and flight capabilities of procellariiformes. New Zeal J Zool 4:73–83

Watanabe YY (2016) Flight mode affects allometry of migration range in birds. Ecol Lett 19:907–914

Watanabe YY, Takahashi A (2013) Linking animal-borne video to accelerometers reveals prey capture variability. Proc Natl Acad Sci USA 110:2199–2204

Weimerskirch H (1998) How can a pelagic seabird provision its chick when relying on a distant food resource? Cyclic attendance at the colony, foraging decision and body condition in sooty shearwaters. J Anim Ecol 67:99–109

Weimerskirch H (2007) Are seabirds foraging for unpredictable resources? Deep Res Part II Top Stud Oceanogr 54:211–223

Weimerskirch H, Bishop C, Jeanniard-du-Dot T, Prudor A, Sachs G (2016) Frigate birds track atmospheric conditions over months-long transoceanic flights. Science 353:74–78

Weimerskirch H, Bonadonna F, Bailleul F, Mabille G, Dell'Omo G, Lipp HP (2002) GPS tracking of foraging albatrosses. Science 295:1259

Weimerskirch H, Cherel Y, Delord K, Jaeger A, Patrick SC, Riotte-Lambert L (2014) Lifetime foraging patterns of the wandering albatross: Life on the move! J Exp Mar Bio Ecol 450:68–78

Weimerskirch H, Collet J, Corbeau A, Pajot A, Hoarau F, Marteau C, Filippi D, Patrick SC (2020) Ocean sentinel albatrosses locate illegal vessels and provide the first estimate of the extent of nondeclared fishing. Proc Natl Acad Sci 117:3006–3014

Weimerskirch H, Guionnet T, Martin J, Shaffer SA, Costa DP (2000) Fast and fuel efficient? Optimal use of wind by flying albatrosses. Proc R Soc B Biol Sci 267:1869–1874

Weimerskirch H, Le Corre M, Ropert-Coudert Y, Kato A, Marsac F (2005) The three-dimensional flight of red-footed boobies: adaptations to foraging in a tropical environment? Proc R Soc B Biol Sci 272:53–61

Weimerskirch H, Louzao M, De Grissac S, Delord K (2012) Changes in wind pattern alter albatross distribution and life-history traits. Science 335:211–214

Weimerskirch H, Pinaud D, Pawlowski F, Bost C-A (2007) Does prey capture induce area-restricted search? A fine-scale study using GPS in a marine predator, the Wandering Albatross. Am Nat 170:734–743

Weimerskirch H, Wilson RP (2000) Oceanic respite for wandering albatrosses. Nature 406:955–956

Weimerskirch H, Wilson RP, Lys P (1997) Activity pattern of foraging in the wandering albatross: a marine predator with two modes of prey searching. Mar Ecol Ser 151:245–254

Wensveen PJ, Thomas L, Miller PJO (2015) A path reconstruction method integrating dead-reckoning and position fixes applied to humpback whales. Mov Ecol 3:31

Williams HJ, Duriez O, Holton MD, Dell'Omo G, Wilson RP, Shepard ELC (2018) Vultures respond to challenges of near-ground thermal soaring by varying bank angle. J Exp Biol 221:jeb.174995

Williams HJ, Holton MD, Shepard ELC, Largey N, Norman B, Ryan PG, Duriez O, Scantlebury M, Quintana F, Magowan EA, et al (2017) Identification of animal movement patterns using tri-axial magnetometry. Mov Ecol 5:6

Williams HJ, Shepard ELC, Duriez O, Lambertucci SA (2015) Can accelerometry be used to distinguish between flight types in soaring birds? Anim Biotelemetry 3:1–11

Williams HJ, Shepard ELC, Holton MD, Alarcón PAE, Wilson RP, Lambertucci SA (2020a) Physical limits of flight performance in the heaviest soaring bird. Proc Natl Acad Sci U S A 117:17884–17890

Williams HJ, Taylor LA, Benhamou S, Bijleveld AI, Clay TA, de Grissac S, Demšar U, English HM, Franconi N, Gómez-Laich A, et al (2020b) Optimizing the use of bio-loggers for movement ecology research. J Anim Ecol 89:186–206

Wilmers CC, Nickel B, Bryce CM, Smith JA, Wheat RE, Yovovich V (2015) The golden age of bio-logging: How animal-borne sensors are advancing the frontiers of ecology. Ecology 96:1741–1753

Wilson AM, Lowe JC, Roskilly K, Hudson PE, Golabek KA, McNutt JW (2013) Locomotion dynamics of hunting in wild cheetahs. Nature 498:185–189

Wilson RP (2001) Beyond rings on birds for determination of movements: Wither the archival tag? Ardea 89:231–240

Wilson RP, Hustler K, Ryan PG, Burger AE, Noldeke EC (1992) Diving birds in cold water: do Archimedes and Boyle determine energetic costs? Am Nat 140:179–200

Wilson RP, Liebsch N, Davies IM, Quintana F, Weimerskirch H, Storch S, Lucke K, Siebert U, Zankl S, Müller G, et al (2007) All at sea with animal tracks; methodological and analytical solutions for the resolution of movement. Deep Res Part II Top Stud Oceanogr 54:193–210

Wilson RP, Pütz K, Peters G, Culik BM, Scolaro JA, Charrassin J-B, Ropert-Coudert Y (1997) Long-term attachment of transmitting and recording devices to penguins and other seabirds. Wildl Soc Bull 25:101–106

Wilson RP, Quintana F, Hobson VJ (2012) Construction of energy landscapes can clarify the movement and distribution of foraging animals. Proc R Soc B Biol Sci 279:975–980

Wilson RP, Shepard ELC, Liebsch N (2008) Prying into the intimate details of animal lives: Use of a daily diary on animals. Endanger Species Res 4:123–137

Wilson RP, Vandenabeele SP (2012) Technological innovation in archival tags used in seabird research. Mar Ecol Prog Ser 451:245–262

Wilson RP, White CR, Quintana F, Halsey LG, Liebsch N, Martin GR, Butler PJ (2006) Moving towards acceleration for estimates of activity-specific metabolic rate in free-living animals: the case of the cormorant. J Anim Ecol 75:1081–1090

Wood S (2011) Fast stable restricted maximum likelihood and marginal likelihood estimation of semiparametric generalized linear models. J R Stat Soc B 73:3–36

Yamamoto T, Kohno H, Mizutani A, Sato H, Yamagishi H, Fujii Y, Murakoshi M, Yoda K (2017) Effect of wind on the flight of brown booby fledglings. Ornithol Sci 16:17–22

Yoda K (2019) Advances in bio-logging techniques and their application to study navigation in wild seabirds. Adv Robot 33:108–117

Yoda K, Naito Y, Sato K, Takahashi A, Nishikawa J, Ropert-Coudert Y, Kurita M, Le Maho Y (2001) A new technique for monitoring the behaviour of free-ranging Adélie penguins. J Exp Biol 204:685–690

Yoda K, Sato K, Niizuma Y, Kurita M, Bost C-A, Le Maho Y, Naito Y (1999) Precise monitoring of porpoising behaviour of Adélie penguins determined using acceleration data loggers. J Exp Biol 202:3121–3126

Yonehara Y, Goto Y, Yoda K, Watanuki Y, Young LC, Weimerskirch H, Bost C-A, Sato K (2016) Flight paths of seabirds soaring over the ocean surface enable measurement of fine-scale wind speed and direction. Proc Natl Acad Sci 113:9039–9044

Young IR (1999) Seasonal variability of the global ocean wind and wave climate. Int J Climatol 19:931–950